Virginia Commonwealth University
VCU Scholars Compass

Theses and Dissertations | Graduate School

2018

Utilizing Voltage-gated Calcium Channels to Assess the Activity of Cathinone Derivatives at Human Monoamine Transporters

Brian A. Ruiz
Virginia Commonwealth University

Follow this and additional works at: https://scholarscompass.vcu.edu/etd

Part of the Cellular and Molecular Physiology Commons

© The Author

Downloaded from
https://scholarscompass.vcu.edu/etd/5547

This Thesis is brought to you for free and open access by the Graduate School at VCU Scholars Compass. It has been accepted for inclusion in Theses and Dissertations by an authorized administrator of VCU Scholars Compass. For more information, please contact libcompass@vcu.edu.

©Brian A. Ruiz 2018
All Rights Reserved

Utilizing Voltage-gated Calcium Channels to Assess the Activity of Cathinone Derivatives at Human Monoamine Transporters

A thesis submitted in partial fulfillment of the requirements for degree of Master of Physiology and Biophysics at Virginia Commonwealth University.

by

Brian A. Ruiz
Bachelor of Science in Biology, University of Virginia, 2008
Pre-medical Graduate Health Sciences Certificate, Virginia Commonwealth University, 2017

Director: José-Miguel Eltit, Ph.D, Assistant Professor,
Department of Physiology and Biophysics

Virginia Commonwealth University
Richmond, Virginia
July, 2018

Acknowledgement

I would like to thank my advisor, Dr. José-Miguel Eltit, for all of his guidance, wisdom, and mentorship during this journey. I thank Dr. Steve Negus for his support and advice, and for motivating me to be always be inquisitive about the science and rationale behind research. I thank Dr. Charles Anderson for the advice and positive encouragement throughout my time at VCU. I thank Iwona Ruchala for her insight and for assisting me in learning mammalian cell transfection. I thank Tyler Steele for all of his assistance in training me in various lab techniques. I thank Dr. Richard Glennon and Rachel Davies for providing me with novel cathinone derivatives to test in the calcium assay. I would like to thank my parents for the love and support they have provided my entire life. Lastly, I thank my wife, Katie, for all of her love, motivation, and support as I work through graduate school.

Table of Contents

Abstract……... v

Background and Introduction……..….1

Dopaminergic Pathways of the Brain Are Key Contributors to Drug Addiction..... 1

Psychostimulants Elicit Their Effects at the Monoamine Transporters……..... 3

Characterizing and Evaluating Psychostimulants……..... 9

Monoamine Transporters Conduct Substrate-induced Currents……..……10

Voltage-gated Calcium Channels Interact with Other Proteins……..……..14

Psychostimulant Effects Can Be Measured by Calcium Transients in HEK Cells.17

Specific Aims……19

Methods and Data Analysis……..…….....22

Epifluorescence Calcium Imaging Microscopy……... 22

hDAT_Flp In and hSERT_Flp In Cell Culture……. 22

$Ca_v1.2$ Transfection for Calcium Imaging……22

Calcium Imaging…….23

Fluorescence Resonance Energy Transfer (FRET) Experiments……27

Cloning of hDAT Tetra-cysteine Tagged Mutants…..……27

FRET Photobleaching……. 28

APP+ Uptake…….....33

Immunostaining, Fluorescent Microscopy, and Confocal Microscopy……....34

Results and Figures……37

Discussion……76

List of References……..85

Abstract

Utilizing Voltage-gated Calcium Channels to Assess the Activity of Cathinone Derivatives at Human Monoamine Transporters

By Brian A Ruiz, B.S.

A thesis submitted in partial fulfilment of the requirements for the degree of Master of Science in Physiology and Biophysics at Virginia Commonwealth University.

Virginia Commonwealth University, 2018

Director: Dr. José-Miguel Eltit, Ph.D., Assistant Professor,
Department of Physiology and Biophysics

Cathinones are psychostimulant compounds heavily implicated as drugs of abuse. They exert their physiological actions at the monoamine transporters, which are responsible for maintaining synaptic neurotransmitter homeostasis. Monoamine transporters produce currents during transport and have been shown to depolarize cell membranes and activate voltage-gated calcium channels in mammalian expression systems. This phenomenon is harnessed in an assay which measures these induced calcium transients, allowing for quantification of pharmacodynamic effects of compounds at monoamine transporters. It is unknown if this electrical coupling occurs in neurons, but the implications if it does are significant. In the current work, fluorescent resonance energy transfer studies of HEK cells expressing hDAT suggest that a subpopulation of monoamine transporters and calcium channels may be interacting

directly. Additionally, this work presents calcium assay data comparing several novel methcathinone analogs. Of the compounds tested, a single α-methyl substituent at the α-carbon yields the greatest potency at hDAT. The implications of these results shed light on future psychostimulant studies and further define the physiological relationship of the components of a system used to study these compounds.

BACKGROUND AND INTRODUCTION

Dopaminergic Pathways of the Brain Are Key Contributors to Drug Addiction

The neurological circuitry underlying psychostimulant addiction is complex and involves recruitment of multiple systems responsible for motivation/reward, memory/learning, compulsivity, and stress regulation. Transition from initial use of a psychostimulant to habitual drug-seeking is the result of progressive neuroplasticity and feedback among these systems. At the crux of this process is the mesolimbic dopamine system, which is essential for processing salient stimuli and acute rewarding effects (Crow, 1973, Wise, 1978) and encouraging goal-associated activities (Salamone, Correa et al., 2007). Dopaminergic afferents arising from the ventral tegmental area synapse at the nucleus accumbens and release dopamine, which is a key contribution to the abuse of drugs. Well-known psychostimulants increase the extracellular levels of DA in the NAc when injected systemically, moreover this type of drug promotes self-administration when injected locally at the NAc in experimental animals (Hoebel, Monaco et al., 1983). Additionally, lesions of the mesolimbic dopamine system restrict acute reinforcement effects of amphetamine and cocaine (McGregor & Roberts, 1993). In human brain imaging studies, drugs of abuse are shown to evoke increases of dopamine in the ventral striatum, which houses the nucleus accumbens, hijacking the pathway for processing salient stimuli (Volkow, Wang et al., 1996) and even altering reward thresholds (Volkow, Fowler et al., 2004). These studies and others suggest that

the initial rewarding drug effect of psychostimulants depends on release of dopamine in the nucleus accumbens.

The predominant theory of psychostimulant addiction begins with changes in dopaminergic firing in parts of the mesolimbic system as described above, which feeds into and induces neuroplasticity of the nucleus accumbens, followed by the dorsal striatum, prefrontal cortex, and the central nucleus of the amygdala (Koob & Volkow, 2010). The dorsal striatum is thought to be involved in compulsivity and habit learning (Ito, Dalley et al., 2002, Yin, Ostlund et al., 2005). Areas of the prefrontal cortex have been implicated in inhibitory self-control and craving and were shown to be activated in addicts both upon direct drug administration (Volkow, Wang et al., 2005) and exposure to conditioned cues (McClernon, Kozink et al., 2009). Based on PET scan studies, the prefrontal cortex has been shown to control reward valuation by regulating dopaminergic activity within the nucleus accumbens. However, in drug-addicted individuals, this regulation is lost (Volkow, Wang et al., 2007). Further, during acute withdrawal of drugs of abuse, studies have shown that brain stress systems are activated and corticotropin-releasing factor (CRF) is increased in the amygdala, producing anxiety and other stress-related effects (Koob & Kreek, 2007, Koob, 2008). These negative effects serve to reinforce addiction. Interestingly, anxiety and increased drug intake was abolished in animal studies utilizing CRF antagonists (Koob, 2008). Based on the functions of the systems described above, it is clear how neuroplastic changes induced by psychostimulants can lead to dysregulation of brain systems and an addictive state.

Psychostimulants Elicit Their Effects at the Monoamine Transporters

Psychostimulants are compounds which induce increased central nervous system activity, feelings of euphoria, and/or increased motor activity. Their primary method of action occurs at the monoamine transporters of neurons as either substrates (releasers) or blockers (reuptake inhibitors). Drugs that are considered substrates are actively transported into the neuron, while those classified as reuptake inhibitors occupy the transporter binding site but do not cross the cell membrane. In both scenarios, the compounds compete with neurotransmitter reuptake, leading to an increase in the extracellular concentration of the neurotransmitter, which can alter downstream neuronal signaling. Additionally, substrates have been shown to promote efflux of endogenous neurotransmitters, and as such are also termed releasers.

Amphetamine is one of the most well-known and historically significant psychostimulants. Originally synthesized as a less expensive alternative to ephedrine, which is a naturally-occurring stimulant, amphetamine was soon marketed for treating depression, narcolepsy, and attention deficit/hyperactivity disorder, among other conditions (Bett, 1946, Guttmann & Sargant, 1937). Amphetamine's stimulant properties and ability to improve focus and cognition became readily apparent, and users of the drug for these effects ranged from students to physicians and even to the Allied Troops during World War II (Guttmann & Sargant, 1937). By the 1950s, widespread abuse of amphetamine had been reported. Over time, changing formulations of prescribed amphetamine and the synthesis and popularity of other amphetamine derivates, such as methamphetamine, have shifted abuse concerns from amphetamine to more potent and dangerous compounds (Heal, Smith et al., 2012). Still, as one of the original

representatives of this class of drugs, amphetamine studies have significantly contributed to the understanding of psychostimulant action.

From a structural standpoint, amphetamine is a member of the beta-phenylethylamine class and consists of a primary amino group connected to a benzene ring via an ethyl alkyl chain containing an alpha-methyl group. The structure and composition of amphetamine are strikingly similar to that of the monoamines, which confers the bioactivity of amphetamine as a competitive substrate for the human dopamine transporter (hDAT), norepinephrine transporter (hNET), and serotonin transporter (hSERT).

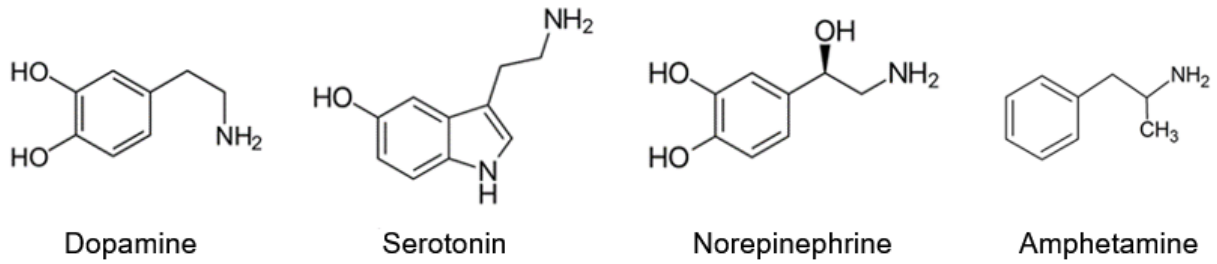

Figure 1: Structure of the monoamine neurotransmitters, dopamine, serotonin, and norepinephrine. Amphetamine included for comparison. Images from the Public Domain.

While amphetamines tend to be active at all three monoamine transporters, they are typically more potent at hDAT and hNET. In addition to being a competitive substrate at the monoamine transporters, amphetamines have been shown to interact with the vesicular monoamine transporter, VMAT2 (Teng, Crooks et al., 1998). It is hypothesized that this action abolishes the vesicular proton gradient and disrupts the internal stores of neurotransmitter, increasing the cytosolic concentration of said neurotransmitter (Sulzer, Chen et al., 1995), and promoting occupation at the internal binding site (Scholze,

Zwach et al., 2000), which encourages the reverse transport of the neurotransmitter through the plasma membrane monoamine transporter into the extracellular space (Robertson, Matthies et al., 2009). It may be expected that the increased concentration of cytosolic monoamines would be held in check and limited through mitochondrial monoamine oxidase (MAO) activity, however amphetamine has been shown to inhibit this enzyme (Mantle, Tipton et al., 1976, Miller, Shore et al., 1980, Robinson, 1985). Amphetamine is known to interact with other targets, including trace amine receptors and LGC-55 (an amine-gated chloride channel). However, studies have shown that blocking VMAT increased cytosolic dopamine but did not promote dopamine release in neurons deficient in DAT, suggesting that the monoamine transporters are the primary mode of action in eliciting psychostimulant effects (Jones, Gainetdinov et al., 1998b). While reverse transport of monoamines is known to occur, the exact mechanism and regulation is not well understood, and recently it has been hypothesized that protein kinase cell signaling pathways may be involved, further complicating the potential mechanism (Fog, Khoshbouei et al., 2006, Seidel, Singer et al., 2005, Steinkellner, Yang et al., 2012). In any event, reverse transport is believed to be the major factor of amphetamine's psychostimulant effects, with substrate competition playing a lesser, although still significant, role.

Supporting the above-mentioned mechanism are *in vitro* studies which look at monoamine release from synaptosomes and brain slices. Initial work shows that both S and R-isomers of amphetamine release radiolabeled dopamine from preloaded rat brain synaptosomes, although S(+)amphetamine is around four times more potent than

R(-)amphetamine as a releaser at DAT (Heikkila, Orlansky et al., 1975). Similar results were obtained in uptake inhibition assays utilizing HEK-293 cells engineered to express hDAT (Sitte, Huck et al., 1998). *In vivo* studies utilizing microdialysis have shown that dopamine is increased in the striatum in a dose-dependent manner in response to both isomers of amphetamine, further supporting the previous *in vitro* studies (Heal, Smith et al., 2013).

There exists a multitude of compounds that are considered substituted amphetamines, which contain a wide range of different functional groups built upon the amphetamine backbone. Common examples include methamphetamine, ephedrine, methylenedioxymethamphetamine (MDMA), and cathinones. Significantly, cathinone derivatives are synthesized illicitly throughout the world and abused for their amphetamine-like effects.

Cathinone is a naturally occurring psychostimulant found in Catha edulis, also known as the khat shrub, which is native to the Arabian Peninsula and the Horn of Africa (Krikorian, 1984). In the early part of the 20th Century, a related compound, cathine, was isolated and shown to have a similar chemical structure to two previously synthesized psychostimulants, methcathinone and 4-methylmethcathinone (Hyde et al., 1928). Later investigations identified an additional compound found in khat leaves, cathinone, as a much stronger psychostimulant than cathine (UN Document, 1975). Similarities in structure to amphetamine encouraged research and development of these related compounds as potential medical therapies, and indeed methcathinone was used pharmaceutically as an anti-depressant in the USSR. In the later stages of the 20th Century, methcathinone abuse became apparent based on reports from the USA

and USSR. Cathine, cathinone, and methcathinone were subsequently legally restricted as Schedule 1 drugs under the UN Convention on Psychotropic Substances (DeRuiter et al., 1994). However, beginning in the early 2000s, clandestine laboratories throughout the world were synthesizing cathinone derivatives, such as methylone, mephedrone, MDPV, and alpha-pyrrolidinophenones, collectively known as “bath salts”, which offered a low cost “legal high” (Madras, 2017). There is now a seemingly perpetual cycle among new cathinone derivative synthesis, abuse and health concerns in the public, and responsive government regulation of these new compounds.

Cathinone is a member of a class of compounds known as beta-phenylethylamines. Upon the phenylethylamine backbone, cathinone adds an alpha-methyl group and a beta-keto group. Various substituents added to this cathinone template yield the aforementioned cathinone derivatives. For example, N-methylation of cathinone yields methcathinone, and fluorination of the phenyl group forms derivatives such as flephedrone. A subpopulation of known cathinone analogs contains a pyrrolidinyl group at the nitrogen of the cathinone backbone, the most structurally basic being alpha-PPP and one of the most well-known being MDPV.

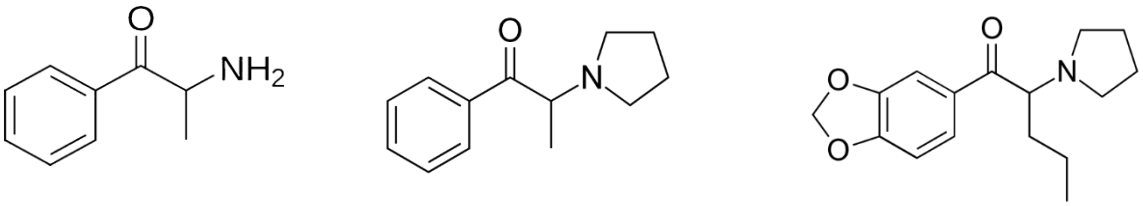

Cathinone α-PPP MDPV

Figure 2: Cathinone and synthetic cathinone derivatives, α-pyrrolidinopropiophenone (α-PPP) and methylenedioxypyrovalerone (MDPV). Images obtained from the Public Domain.

Many of these compounds have amphetamine analogs, and, in general, the cathinone tends to have stronger potency at the monoamine transporters than its amphetamine relative; although, interestingly, users tend to require higher doses of the cathinones due to the decreased lipophilicity imparted by the carbonyl group (Krikorian, 1984). Generally, cathinones which act as substrates have been shown to disrupt vesicular stores of dopamine and norepinephrine and induce reverse transport in a more potent fashion than structurally similar amphetamines (Rothman, Vu et al., 2003). Prior research also shows that for cathinones, similar to amphetamines, the S enantiomer typically is the more potent isomer. For example, in rodents, S(-) methcathinone was more effective in promoting locomotor activity when compared to the R(+) enantiomer (Banjaw, Miczek et al., 2006, Gugelmann, von Allmen et al., 1985).

Cathinones, just like amphetamines, target the monoamine transporters and alter reuptake and/or release of neurotransmitters. For example, methcathinone is a known releasing agent at hDAT, hNET, and hSERT with selectivity for hDAT and hNET over hSERT. Release assays, in which rat synaptosomes are preloaded with radioactive dopamine, have demonstrated that methcathinone is a potent releaser at DAT (EC50 = 12.5nM) and a weaker releaser at SERT (EC50 = 3,860nM) (Bonano, Banks et al., 2015). In comparison, S(+)methamphetamine was found to have an EC50 of 24.5nM at DAT and an EC50 of 736nM at SERT (Rothman, Baumann et al., 2001).

MDPV is another well-known cathinone and was one of the first compounds identified in bath salts. MDPV contains a pyrrolidine ring, a group that was shown to promote uptake inhibition at DAT and NET (Baumann, Partilla et al., 2013). Following a ban placed on MDPV, a new set of similar compounds arose, including α-PPP and α-

PVP. Uptake studies describe α-PVP as a potent uptake inhibitor similar to MDPV (IC50 at hDAT = 4.1nM and 12.8nM respectively) (Marusich, Antonazzo et al., 2014). Comparatively, α-PPP is weaker at hDAT uptake inhibition with an IC50 of 196.7nM (Marusich et al., 2014) but is still more potent than cocaine at hDAT inhibition (211nM) (Marusich et al., 2014). α-PPP has a similar structure to other compounds such as bupropion (anti-depressant), cathinone (drug of abuse), and amfepramone (appetite suppressant). These examples exhibit amphetamine-like physiology as dopaminergic and noradrenergic stimulants (Springer, Fritschi et al., 2003), so it is to be expected that α-PPP reflects a similar profile. All of the above pyrrolidine cathinones in comparison are weak at SERT, ranging in IC50 from 3000nM to more than 10,000nM. These compounds are thus shown to be selective for catecholamine inhibition, and, as such, produce stimulant effects as exhibited by locomotor activity studies in rats (Marusich et al., 2014).

Characterizing and Evaluating Psychostimulants

Many psychostimulants have been characterized utilizing structure-activity relationship studies. This approach essentially crafts comparisons of compounds where the differences between structures are often single atoms or functional groups. Such information allows for the prediction of activity of newer compounds and serves as a guide for selecting compounds to study in various characterization assays. Studies of synthetic cathinones as releasing agents or reuptake inhibitors have yielded several trends. Releasing agents tend to have a primary amine group or a small secondary amine group, and these generally prefer DAT over SERT. Substitutions on the phenyl

group alters the selectivity of the compound for certain transporters, i.e. adding substituents at the para-position of the ring increases affinity for SERT (Sakloth, Kolanos et al., 2015). Important to note in this case is that functional groups with low steric hinderance still maintain significant activity at hDAT, while in contrast, groups with large steric hinderance shift selectivity towards hSERT (Bonano et al., 2015). Tertiary amines, bulky secondary amines, and/or extended side chains at the α-carbon tend to confer reuptake inhibition at the monoamine transporters. (Baumann et al., 2013, Cameron, Kolanos et al., 2013, Kolanos, Sakloth et al., 2015). Additionally, from a stereochemical perspective, the S isomer is usually more potent than the R isomer. (Glennon et al., 2017). There are multiple avenues in which to study the effects of these compounds including use of rat synaptosomes and animal behavior models. The following sections lay the foundation to describe a more recent approach being utilized to characterize psychostimulants.

Monoamine Transporters Conduct Substrate-induced Currents

The nervous system contains a plethora of neurotransmitters which vary in functionality and serve to influence the electrical excitability of their target neurons directly by altering ion conductance or indirectly through metabotropic receptor activation. Glutamate is utilized in the majority of excitatory pathways of the CNS, while GABA is the primary inhibitory neurotransmitter. Modulating these fast-acting pathways are various other neurotransmitters, including the monoamines: dopamine and norepinephrine (also referred to as catecholamines) and serotonin. Dopaminergic neurons project from the ventral tegmental area to areas such as the amygdala,

hippocampus, ventral striatum, and prefrontal cortex, among others (Bjorklund & Dunnett, 2007). The circuits are complex and integrate to affect reward seeking/aversion, cognition/memory, mood, and positive reinforcement. They are also found in projections emanating from the substantia nigra pars compacta which synapse at the dorsal striatum (Bjorklund & Dunnett, 2007). Serotonergic neurons arise from the raphe nuclei and project to multiple areas regulating emotion/mood, circadian rhythm, body temperature, feeding, and hormone release (Jacobs & Azmitia, 1992). Norepinephrinergic neurons primarily project from the locus coeruleus of the brainstem and influence functions such as stress response, emotions, cognition/memory, and arousal (Benarroch, 2009). Additionally, norepinephrine mediates the activity of the sympathetic nervous system, which explains many of the peripheral effects seen in psychostimulant abuse (i.e. hypertension and tachycardia). The monoamines clearly have significant, widespread modulatory effects and are regulated by reuptake through the monoamine transporters.

Neurotransmission begins with the propagation of an action potential along the length of the neuron. Upon reaching the axon terminal of the presynaptic neuron, the depolarization produced by the action potential activates voltage-gated calcium channels ($Ca_v2.1$, $Ca_v2.2$ and/or $Ca_v2.3$). This calcium influx initiates the fusion of docked vesicles containing neurotransmitter to the plasma membrane, and subsequently, release of neurotransmitter into the synaptic cleft. The neurotransmitter is then free to diffuse and act on receptors on the postsynaptic neuron, thus propagating a signal. Proper control of the neurotransmitter's actions is crucial to maintaining normal, healthy physiological function of neurons. Microdialysis studies in DAT knockout mice

have shown a 5-fold increase in extracellular dopamine in the striatum (Giros, Jaber et al., 1996), and cyclic voltammetry in striatal slices identified that dopamine remains in the extracellular space 300 times longer than in wild-type DAT mice. This clearance rate is similar to simple diffusion, suggesting that DAT is the primary effector in clearing dopamine (Giros et al., 1996, Jones, Gainetdinov et al., 1998a). By clearing monoamines from the synaptic cleft, monoamine transporters have the ability to regulate the concentration of neurotransmitter available to act on their cognate receptors and modulate downstream neuronal signaling. Additionally, DAT-KO mice were shown to have a 95% reduction in total dopamine content and 75% reduction in dopamine release, implying that reuptake through DAT recycles and replenishes the monoamine stores of the presynaptic neuron at a rate that dopamine synthesis cannot achieve (Jones et al., 1998a).

The monoamine transporters, hDAT, hNET, and hSERT belong to the solute carrier 6 (SLC6) gene family, also classified as Na^+/Cl^- symporters. These 12-transmembrane integral membrane proteins are found perisynaptically and extrasynaptically on neurons (Hersch, Yi et al., 1997). Crystallization of the SLC6 prokaryotic homolog, LeuT, (Yamashita, Singh et al., 2005) has provided the framework for assessing ligand binding sites, intra- and extracellular gating structures, and possible conformational rearrangements that occur during transport. The reuptake of monoamines is a secondary active transport process, utilizing the energy of the Na+ gradient across the cell membrane to move monoamines into the cell against their concentration gradient (Broer, 2006, Chen, Reith et al., 2004, Hoglund, Adzic et al., 2005). Early work in transporters led to the formation of the “alternating access” model,

in which transporters switch between outward and inward facing conformations based on binding of substrate and/or various ions (Jardetzky, 1966). Fixed-stoichiometric calculations based on the “alternating access” model predicted the following ionic components to monoamine transport: SERT = 1 substrate : $1Na^+$: $1Cl^-$: $1K^+$ (out), DAT = 1 substrate : $2Na^+$: 1 Cl^-, and NET = 1 substrate : $1Na^+$: $1Cl^-$. By this model’s predictions, DAT and NET transport are electrogenic (Gu, Wall et al., 1994), while SERT transport is electroneutral (Rudnick & Nelson, 1978).

Interestingly, experiments have demonstrated substrate-induced currents that are larger than the expected ionic stoichiometric values. Uptake and electrophysiology studies at DAT and NET have shown that transport and the produced current are not only dependent on voltage, but also larger than the calculations predicted by the alternating access model (Galli, Blakely et al., 1996, Galli, DeFelice et al., 1995, Sonders, Zhu et al., 1997). Another proposed model which accounts for this increased current is “channel-like mode”, in which substrate and ions pass through the channel in a similar fashion as the mechanism of ion channels (DeFelice, Adams et al., 2001). While the debate of monoamine transporter mechanism is unsettled, it is clear that changes in current through the transporter lead to changes in membrane potential as evidenced by substrate-induced depolarization studies in neurons (Branch & Beckstead, 2012, Ingram, Prasad et al., 2002). This depolarization can influence nearby voltage-sensitive proteins, meaning it is possible for activity of the transporter to affect more than just neurotransmitter reuptake. Importantly to this study, this phenomenon has been harnessed in developing a technique to characterize drug activity at the monoamine transporters.

Voltage-gated Calcium Channels Can Form Complexes with Other Proteins

Voltage-gated calcium channels exist in multiple isoforms and are significant regulators of neurotransmitter and hormone release, excitation-contraction coupling in muscle cells, and a multitude of cell-signaling pathways. These channels regulate calcium influx through a response to depolarization stimuli, i.e. changes in membrane electrical potential, and thus are instrumental in transducing an electrical signal into a chemical signal (Catterall, 2011). Within the cytosol, the concentration of calcium is held in the nanomolar range (100nM) (Dong, Jiang et al., 2006) via tight regulation of the plasma membrane Ca^{2+} ATPase (PMCA), a high-affinity, low-capacity pump, and the plasmalemmal sodium-calcium exchanger (NCX), a low-affinity, high capacity pump. Additionally, calcium is buffered by various calcium-binding molecules and sequestered within internal stores via the mitochondria and sarco-/endoplasmic reticulum Ca^{2+} ATPase (SERCA) pumps on the endoplasmic reticulum (Clapham, 2007). The extracellular concentration is approximately 1-2mM, and in conjunction with a negative membrane potential, creates a large electrochemical gradient. This gradient, coupled with strict intracellular calcium regulation, enables transient increases in intracellular calcium via voltage-gated channels upon activation (Berridge, Lipp et al., 2000), producing an ideal switch for cellular processes that require strict control due to significant downstream biological impact and/or high energy costs.

Initial purification studies in skeletal muscle have shown that calcium channels are complexes comprised of α1, α2, β3, γ, and δ subunits (Curtis & Catterall, 1984, Curtis & Catterall, 1986), while immunoprecipitation studies in neurons revealed channels containing all the above subunits excluding γ (Ahlijanian, Westenbroek et al.,

1990). The α1 monomer contains four domains, each of which is comprised of 6 transmembrane helices, labeled S1 through S6. S4 confers the voltage-sensing ability of the channel, and, upon exposure to an activating potential, induces conformational changes which open the pore. S5 and S6 are connected by a membrane-associated loop and not only form the pore, but also contain the calcium ion selectivity filter of the channel. Interestingly, experiments show that the α1 subunit alone forms a functioning channel, although expression level is low and channel kinetics and voltage requirements are abnormal (Perez-Reyes, Kim et al., 1989). The remaining subunits and their isoforms serve to modulate surface expression, voltage sensitivity, and proper gating of the calcium channel (Catterall, 2011, Catterall, Perez-Reyes et al., 2005, Ertel, Campbell et al., 2000).

There exist a multitude of calcium channels defined by specific types of calcium currents, which differ in activation potential, channel conductance, inactivation and deactivation times, and response to pharmaceutical compounds such as Ca^{2+} channel blockers. The current work focuses on L-type calcium channels, which are so termed due to the fact that their inward currents have slow voltage-dependent inactivation and thus are *long-lasting* compared to other calcium channels (Reuter, 1979, Tsien, Lipscombe et al., 1988). Coded within the human genome are four known L-type α1 subunits: $Ca_v1.1$, $Ca_v1.2$, $Ca_v1.3$ and $Ca_v1.4$. $Ca_v1.1$ and $Ca_v1.4$ are almost exclusively expressed in skeletal muscle and retinal cells, respectively. In comparison, $Ca_v1.2$ and $Ca_v1.3$ are more promiscuous and are both expressed in excitable cells such as neurons, chromaffin cells, and cardiomyocytes. With respect to neurons, $Ca_v1.2$ and $Ca_v1.3$ are typically found on the dendrites and soma (Di Biase, Obermair et al., 2008),

and have been shown to modulate neuronal action potentials and calcium-induced cell signaling pathways regulating gene transcription (Ma, Cohen et al., 2012). In this regard, $Ca_v1.2$ and $Ca_v1.3$ have been implicated in learning and memory, fear response formation, drug addiction, and development (Striessnig, Pinggera et al., 2014).

It has previously been shown that voltage-gated calcium channels interact with a multitude of proteins. For example, $Ca_v2.1$ and $Ca_v2.2$ channels are known to interact directly with the SNARE protein complex at the axon terminal. The specific binding site of the calcium channel was localized to part of the intracellular loop between domains II and III (Rettig, Sheng et al., 1996, Sheng, Rettig et al., 1994). Further, administration of peptides which block SNAREs from binding calcium channels abolished synaptic transmission (Mochida, Sheng et al., 1996, Rettig, Heinemann et al., 1997). This tight coordination of proteins with the calcium channel allows for the formation of microdomains in which the concentration of calcium can reach 30-50µM (Wadel, Neher et al., 2007), which is necessary to promote certain mechanisms as evidenced by SNAREs . Given that these protein-protein relationships are known to occur, it is reasonable to hypothesize that monoamine transporters and calcium channels may form a similar type of relationship in the plasma membrane

Electrophysiological studies in dopaminergic neurons have further defined the relationship between monoamine transporters and calcium channels. It has been demonstrated through whole-cell patch clamp that DAT substrates produce inward currents and increase excitability in neurons (Ingram et al., 2002). Additionally, the spontaneous activity of dopaminergic neurons in the ventral tegmental area was shown to be dependent on $Ca_v1.3$ (Liu, Harding et al., 2014). As such, it may be possible for

coupling to occur between hDAT currents and $Ca_V1.3$ activation in neurons. Indeed, this has been demonstrated by studies in which substrate-induced transporter-mediated currents activate voltage-gated calcium channels in HEK cells (Cameron, Solis et al., 2015, Ruchala, Cabra et al., 2014).

Psychostimulant Effects Can Be Measured by Calcium Transients in HEK Cells

Of recent significance is the development of a biotechnical sensor which allows for comparison of compounds that interact at monoamine transporters. As monoamine transporters are known to produce a current during transport activity, the idea arose that this activity could in fact activate channels sensitive to voltage. Studies addressing this have confirmed that the monoamine transporters in HEK-293 cells can activate calcium channels via substrate-induced currents, specifically Cav1.2 and Cav1.3 (Cameron et al., 2015, Ruchala et al., 2014). Upon activation, calcium enters the cell, and utilizing a calcium-sensing dye, such as Fura-2, can serve to report changes in calcium concentrations via fluorescence. These changes in fluorescence produce a dose vs. response curve for compounds that interact at the monoamine transporters (see Methods for a detailed description of this calcium assay). Further, neurotransmitter release and reuptake inhibition data from rat synaptosomes are strongly correlated with the substrate and blocker studies of the calcium assay, providing validation of the technique to quantitatively measure drug potency (Solis, Partilla et al., 2017). This technique thus can allow for rapid screening of compounds and help to define structural-activity relationships.

In summary, monoamine transporters can elicit membrane depolarization through substrate-induced currents. This has been described in neurons (Branch & Beckstead, 2012) and in cell expression systems. Muscle cells engineered to express hSERT were able to produce calcium signals upon exposure to serotonin and S(+)MDMA, and experiments showed that these signals were mediated by hSERT currents activating the L-type calcium channel, $Ca_v1.1$ (Ruchala et al., 2014). Further, HEK cells expressing hDAT and L-type calcium channels are known to generate calcium signals in response to amphetamine and dopamine in a dose-dependent manner (Cameron et al., 2015). Interestingly, these studies suggest that a minimum depolarization of around 20 mV (assuming HEK cell resting membrane potential is approximately -50mV) is needed to evoke current through $Ca_v1.2$. In comparison, saturating concentrations of amphetamine and dopamine activated $Ca_v1.2$, but did not activate $Ca_v2.2$, which begins to conduct current at around -15mV. This suggests that in the calcium assay a range of depolarizations leads to a range of $Ca_v1.2$-mediated calcium currents, as supported by I-V curve data (Cameron et al., 2015), which may correlate with the ability of the calcium assay to produce dose versus response data based on substrate-induce depolarizations at monoamine transporters. Multiple factors play a role in the function of voltage-gated calcium channels, such as voltage-sensitivity and inactivation kinetics, and it is possible that localization of the calcium channels with monoamine transporters is an important factor in electrical coupling.

SPECIFIC AIMS

1) It is known that substrate-induced current in monoamine transporters depolarizes the cell membrane and can activate voltage-sensitive calcium channels. Previous super resolution studies have established that hDAT and $Ca_V1.2$ localize at the plasma membrane with some colocalization. Specific aim 1 is to further characterize the interaction between hDAT and $Ca_V1.2$ and localization in live cells utilizing FRET analysis to determine if interactions occur in the <10nm range.
2) Specific aim 2 is to evaluate the pharmacological effects on hDAT and hSERT of a series of S(-)methcathinone analogs with a structural-activity relationship approach. The series includes comparisons among methyl-substitutions at the α-carbon and introduction of a pyrrolidine group, mirroring α-PPP, another synthetic cathinone.

As previously described, the electrical coupling of monoamine transporters and voltage-gated calcium channels has proven to be a useful tool in quantifying effects of psychostimulants at the monoamine transporters. In the calcium assay, there is clearly a functional relationship between these transporters and $Ca_V1.2$, although this is not fully understood. Prior super resolution studies have suggested that hDAT and $Ca_V1.2$ exhibit some strong colocalization at the plasma membrane (Harris, 2016). To further define this relationship, a series of experiments were performed utilizing fluorescent

resonance energy transfer (FRET – see Methods for a full description). This technique can suggest if two proteins are found to exist in proximities of 10nm or less.

Further, the functional coupling between transporters and channels was used as a method to pharmacologically quantify several cathinone analogs. The compounds under study are pictured below.

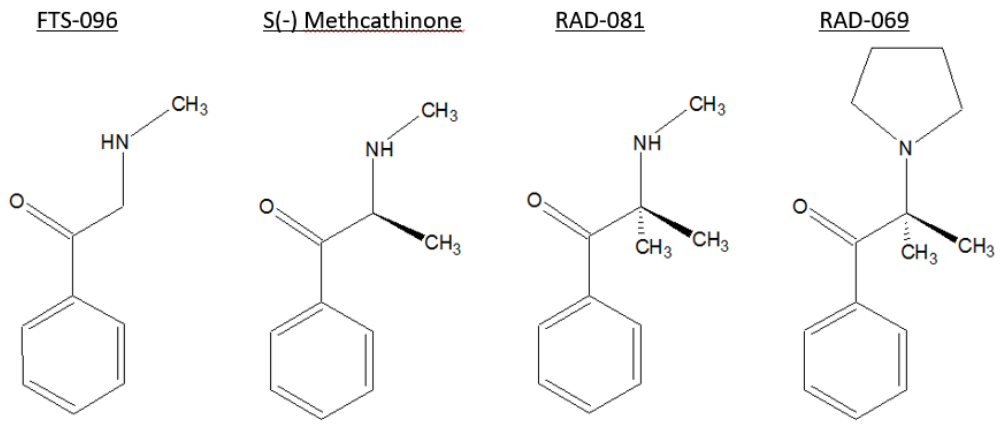

Figure 3: Compounds for testing. From left to right: α-desmethyl methcathinone, S(-)methcathinone, α-methyl methcathinone, and α-methyl α-PPP. Laboratory-specific distinctions utilized throughout paper for brevity.

The current study takes a structural-activity relationship approach in investigating hDAT and hSERT activity of novel compounds related to S(-)methcathinone in which methyl substituents present at the α-carbon are varied, followed by the transition to a pyrrolidinophenone. The final compound in the series introduces a pyrrolidine group, which imparts character similar to MDPV, α-PPP, and α-PVP. As previously mentioned, these compounds elicit similar CNS effects as (S+)methamphetamine, a well-known drug of abuse with an estimated economic burden of $16.2 billion to $48.3 billion in the United States as of 2005 (Nicosia et al., 2009). Compounds with similar effects appear to have a grip on the illicit market, and new compounds are continually being

synthesized to serve this market. By comparing the above three test compounds with S(-)methcathinone, it will first determine if there exists potential abuse liability for these drugs. Further, if potency is maintained with the removal of the chiral center, additional compounds containing different groups extended off the β-carbon can be synthesized and studied at a quicker rate by eliminating the need to study multiple stereoisomers.

METHODS AND DATA ANALYSIS

Epifluorescence Calcium Imaging Microscopy

hDAT-Flp In and hSERT-Flp In Cell Culture

Flip-In 293 T-Rex permanent cell lines expressing either human dopamine transporter (hDAT) or human serotonin transporter (hSERT) were previously constructed and stored in liquid nitrogen (Cameron et al., 2015, Ruchala et al., 2014). For experimental studies, these cells are thawed and maintained in Dulbecco Modified Eagle Medium (DMEM) containing 10% Hyclone fetal bovine serum and 1% penicillin/streptomycin, and 1.6µg/mL hygromycin at 37 degrees Celsius. Cells are passaged approximately every three days and for no more than 10 passages.

$Ca_V1.2$ Transfection for Calcium Imaging

Four days prior to experimentation, permanent cell lines expressing hDAT or hSERT are plated with DMEM onto 36 wells of a 96-well imaging plate precoated with Matrigel to ensure sufficient cell adhesion. These cells are then maintained at 37 degrees Celsius for 24 hours prior to transfection. On the day of transfection, a transfection mix is prepared consisting of 440µL of DMEM, 8µL of FuGENE 6 and the following coding plasmids: 0.8µg of $Ca_V1.2$ alpha subunit, 0.5µg of β_3 subunit, 1.0µg of $\alpha_2\delta$ subunit and 0.25µg EGFP as a transfection marker. Each of the 36 wells receives

12µL of the transfection mixture, after which the imaging plate is placed in 37 degrees Celsius incubation for 4 hours. The media is then replaced with media containing 1µg/mL doxycycline to induce hDAT or hSERT expression. The cells are then incubated for three days prior to calcium imaging.

Calcium Imaging

On the day of calcium imaging, 4µL of fura-2AM, previously dissolved in Pluronic F-127 (10%) in DMSO, is combined with 2mL of Imaging Solution (IS) yielding a final concentration of 3.4µM fura-2AM. The Imaging Solution is prepared in advance and contains 130mM NaCl, 4mM KCl, 2mM $CaCl_2$, 1mM $MgCl_2$, 10mM Hepes, and 10mM glucose brought to pH = 7.35. The DMEM from each well of the imaging plate is removed and replaced with 50µL of the 3.4µM fura-2AM. The cells are then placed in 37 degrees Celsius incubation for 15 minutes, followed by 25 minutes at room temperature. The Fura-2 solution is removed and replaced with IS. The cells are then stored at room temperature for 20 minutes prior to imaging. Compounds for testing in the calcium imaging assay are dissolved in water to a stock concentration of 10mM. Serial dilutions of the compounds are then made from this stock for testing with hDAT-Flip In or hSERT-Flip In cells. Dopamine or serotonin solutions are made at a concentration of 10µM.

Microscopy is performed utilizing an Olympus IX70 microscope and a 20x 0.80NA objective set up with an Horiba Scientific sCMOS Lightning Camera (PCO edge 4.2 LT) and PTI EasyRatioPro Imaging system equipped with a monochromator for fast switching of emission wavelengths (Horiba Scientific). Cells are perfused using a

pressurized system (Automate Scientific) and solutions are heated to ~35 degrees Celsius using Temp Clamp-1 (Automate scientific). The perfusion is under automatic control utilizing MDX Analytical Technologies' Clampex 10.2.0.12 software and live recordings are made utilizing PTI's EasyRatio Pro software.

Cells are selected based on EGFP expression, which is a marker of successful transfection. Ideally, the field of view contains cells with a varied range of EGFP transfection. Additionally, cells must be 60-80% confluent which reflects a monolayer of cells, but also leaves space for determining background subtraction during analysis. Cells must also possess the typical HEK cell shape. Cells that are small and spherical are not utilized as this may be indicative of cell death, and populations containing these cells are avoided. Prior to recording, cells are perfused with 35 degrees Celsius IS. Upon recording initialization, 10 seconds of IS is perfused, establishing a baseline signal. Next, a control pulse of 10μM dopamine (in the case of testing hDAT) or serotonin (in the case of testing hSERT) is applied for 5 seconds, inducing a transporter-mediated current which activates the transfected $Ca_v1.2$ channels. Calcium enters the cell upon channel activation and binds Fura-2AM (Figure 4), producing a fluorescent shift which is measured as a calcium signal. This is followed by a 30 second washout with IS to restore baseline conditions. For a known substrate, the test compound is perfused for 5 seconds producing a second calcium signal, followed by a 30 seconds washout with IS. For a known blocker, the test compound is perfused for 30 seconds followed by a 5 second pulse of the same concentration of compound competing 10μM dopamine or serotonin, finishing with a 30 second washout with IS. The preincubation with test compound in the case of blockers ensures that kinetic

factors are removed in comparing inhibition effects. The changes in Fura-2AM fluorescence based on varied drug concentrations allow for analysis to elicit a dose-response curve.

Fura-2AM is a calcium-sensing dye which is excited at two wavelengths, 340nm and 380nm, and emits at 510nm. AM refers to the fact that the carboxylic acid groups are modified with acetoxymethyl (AM) esters, which render the dye uncharged allowing it to pass through cell membranes. Within the cell, these ester groups are cleaved by esterases, producing a charged form of the dye which becomes trapped in the cytosol (Figure 4).

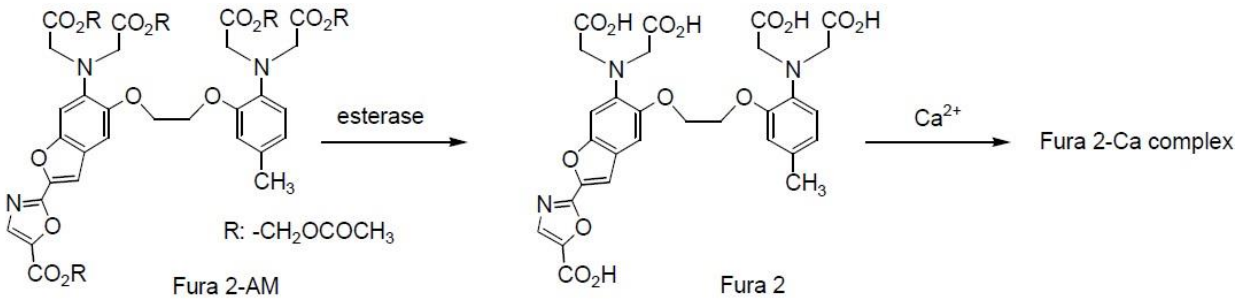

Figure 4: Fura-2AM undergoing hydrolysis, generating the calcium-binding form. Adapted from Dojindo Molecular Technologies, Inc., 2018

In the calcium assay, calcium concentration within the cell changes based on substrate-induced currents at the transporters, which lead to plasma membrane depolarization and $Ca_v1.2$ activation. The emission intensity of Fura-2 changes for both 340nm and 380nm excitation wavelengths based on the amount of calcium-bound Fura-2. Calculating the ratio of fluorescence generated by 340nm to 380nm excitation thus correlates to the intracellular concentration of calcium as previously determined (Grynkiewicz, Poenie et al., 1985). Further, since the ratio of emission intensities is

being measured, Fura-2 controls for variations in excitation intensity, cell thickness, and uneven dye loading (Grynkiewicz et al., 1985). Thus, fluorescent signals obtained in this manner accurately reflect changes in calcium concentration.

Analysis of calcium assay data begins with selecting cells that exhibit a rapid and strong response to the initial monoamine neurotransmitter control. The background-subtracted ratio of fluorescence at 340nm/380nm is exported to Microsoft Excel. Within Excel, all values are divided by baseline fluorescence, which is defined by the signal exhibited during the experiment for the first 10 seconds, i.e. prior to administration of the neurotransmitter control. The maximum values of the control peak and the experimental peak are calculated for each cell, and the experimental peak is divided by the control peak. The ratio of experimental peak maximum to control peak maximum is averaged for all cells for each drug concentration. These values are entered into Prism and non-linear regression is run to determine the dose versus response curve. From this curve, EC50 and IC50 values are derived. At least 30 cells are utilized for most concentrations, although for non-responsive and saturating concentrations at least 18 cells are selected.

To depict cumulative calcium traces, signals are baseline subtracted and normalized to the control neurotransmitter peak. Following these calculations, all initial neurotransmitter control peaks reach a maximum value of one, and the experimental peaks can be viewed together in comparison to the neurotransmitter control.

FRET Photobleaching Experiments

Cloning of hDAT tetra-cysteine tagged mutants

Oligonucleotides are designed to generate two tetra-cysteine (CCPGCC) tagged hDAT mutants via restriction enzyme digestion and ligation of the CCPGCC inserts into 3Z_hDAT plasmids. One version inserts CCPGCC into intracellular loop 4 of hDAT (hereafter referred to as hDAT_PolyC1). The other inserts CCPGCC into the C-terminus of hDAT (hereafter referred to as hDAT_PolyC2). Oligonucleotides are pictured below in Figure 5.

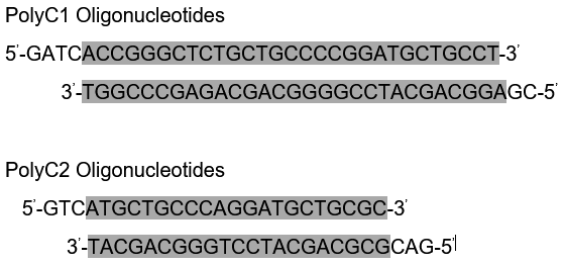

Figure 5: PolyC1 and PolyC2 oligonucleotides. Grey sequences indicate alignments after annealing process. Overhang sequences bind to cut 3Z vector during ligation.

10µg of each of the PolyC1 oligonucleotides are placed in 50mM NaCl and incubated at 100 degrees Celsius for several minutes to promote the annealing process, followed by a slow cooldown to room temperature. The DNA is then extracted from the salt solution utilizing silica and resuspended in autoclaved water. Meanwhile, the 3Z_hDAT plasmid is restriction digested with Blc1 and Cla1, followed by silica extraction, and resuspension in autoclaved water. Ligation of the cut 3Z_hDAT plasmid with the annealed DNA insert is performed, and the product is sent out for sequence confirmation. Upon positive sequencing, hDAT_PolyC1 is cut from the 3Z vector and ligated into a pcDNA5/FRT/TO expression vector. This plasmid is then used to generate permanent cell lines utilizing the Flp-In™ TREX™ 293 system as defined by Invitrogen's

previously established protocol (Life Technologies). The above process is repeated to generate the hDAT_PolyC2 cell line, although PpuM1 is used in the restriction digest step. Refer to figure 9 for sequence alignments of hDAT, hDAT_PolyC1, and hDAT_PolyC2.

mVenus_hDAT_PolyC1 is synthesized by cutting hDAT_PolyC1 from 3Z_hDAT_PolyC1 via Kpn1 and Xba1 restriction digestion. Next, the same restriction enzymes are used to cut the vector, mVenus_C1 (Addgene #27794). The vector and insert are ligated, forming a plasmid in which mVenus is attached the N-terminus of hDAT_PolyC1. This plasmid is transformed and selected by kanamycin resistance in E.coli, and the DNA is extracted for future use.

FRET Photobleaching

HEK, hDAT, and the two varieties of tetra-cysteine tagged hDAT mutant cell lines are thawed and cultured as previously described. Cells are plated on 96-well imaging plates 4 days prior to experimentation. 24 hours after plating, cells are transfected as follows: HEK cells, used as positive controls, are transfected with 12µL per well of the following mixture; 1.0µg mVenus_hDAT_polyC1 plasmid and 3 uL Fugene 6 in 440 ul of DMEM. Cells expressing hDAT (negative control) and polyC variants (test conditions) are transfected with 12µL per well of the following transfection mixture:1.0µg mVenus-$Ca_V1.2$ alpha subunit, 0.5µg β3 subunit, and 1.0µg α2δ subunit coding plasmids mixed in 440µL DMEM. mVenus is a variant of yellow fluorescent protein (YFP) used as the energy donor in the FRET studies. After four hours of incubation at 37 degrees Celsius,

the media is exchanged for 1µg/mL doxycycline to induce transporter expression. After 3 additional days of incubation, experimentation begins.

On the day of the experiment, resorufin arsenical hairpin binder (ReAsH) and British anti-Lewisite (BAL) aliquots are prepared. Stock solutions are diluted in IS to concentrations of 1.5µM and 250µM for ReAsH and BAL, respectively. ReAsH targets the C-C-P-G-C-C amino acid motif and upon binding forms its fluorescent complex (Figure 6). BAL serves to wash and remove any unbound ReAsH from the cells and reduce non-specific labeling. Media is aspirated from the cells and each well receives 50µL of ReAsH solution, followed by incubation at room temperature for 30 minutes. The ReAsH solution is removed and 100µL of BAL solution is placed into each well, which again is followed by incubation at room temperature for 30 minutes. Afterwards, the BAL wash is removed and replaced with IS, and the cells acclimate for 20 minutes prior to experimentation.

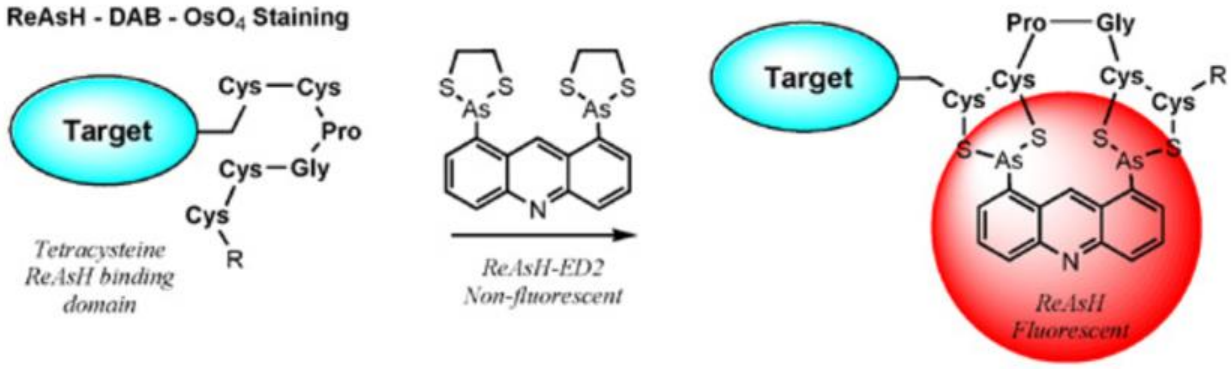

Figure 6: Schematic of ReAsH binding a C-C-P-G-C-C motif. Adapted from Nanoprobes, Inc. 2018.

Microscopy is performed with an Olympus IX70 microscope, utilizing a Polychrome V light source, 20x 0.75NA objective lens, and a Luca S digital camera. Till Photonic's Live Acquisition software is utilized to control the light parameters and record

experimental images. Cells are selected based on proper expression of mVenus-$Ca_V1.2$, which is defined by visualization of distinct membrane fluorescence (Figures 18-21) and cells showing excessive expression accompanied by altered cellular shape (usually rounded cells) are excluded from the analysis. It is paramount that cells are selected quickly via the objective lens and the light source turned off immediately upon identification to minimize bleaching effects on the mVenus fluorescent protein. First, the cells are imaged at 490nm, which is within the excitation wavelength of mVenus, and 25 pictures are taken at 20 frames per second. Next, the cells are imaged at 590nm, which is within the excitation spectra of ReAsH, and 25 pictures are taken at 20 frames per second. Afterwards, the ReAsH molecule is photo-bleached utilizing 100% intensity, 590nm light for 3 minutes. After bleaching, the cells are imaged for 25 pictures at 590nm (20 frames per second) to confirm the bleaching effect occurred. Lastly, the cells are exposed to 490nm light and 25 pictures are recorded at 20 frames per second. This is repeated until all wells have been imaged. All parameters for image acquisition are kept constant among experiments (exposure time, bandwidth of the excitation light, light intensity and EM gain of the camera).

ReAsH dye has two primary parameters for staining optimization. First, concentration of ReAsH can be varied, ranging from 1µM to 10µM. In our experimental set-up, 1.5µM gave the best difference in fluorescence over background. During trials utilizing 2.0µM, there was significant background and/or nonspecific fluorescence, confirmed by comparing hDAT wild type cells, which should not retain ReAsH, to the hDAT_PolyC mutants. It was also seen that 1µM staining did not provide a fluorescent signal much higher than the background. As such, 1.5µM was determined to be the

optimal concentration in this study's experimental setups. The second variable concerning ReAsH staining is incubation time. The manufacturer suggests testing a range of ReAsH incubation from 30 minutes to 1 hour during optimization trials. In testing a range of timeframes, there was no significantly detectable difference in fluorescence.

FRET is a phenomenon in which energy transfer occurs between electron orbitals of donor and acceptor molecules. The emission spectra of the donor must overlap the excitation spectra of the acceptor. Ideal molecules for FRET coupling do not overlap in any other part of their spectra. FRET only occurs in a range of 10nm or less; outside of this range, excitation of the donor will produce only the donor's emission wavelengths when viewed through microscopy. Within the 10nm range, excitation of the donor leads to its emission energy being absorbed by the acceptor (Figure 7) quenching the donor's photon emission. As this absorbed energy falls within its excitation spectra, the acceptor is excited and emits energy at a different wavelength. 490nm light excites mVenus-Ca_V1.2, and importantly does not directly excite ReAsH. mVenus' emission spectra overlaps ReAsH excitation, donating energy to ReAsH only if within FRET distance. 590nm light excites ReAsH but does not excite mVenus. Due the appropriate spectral overlap of mVenus and ReAsH, the photoacceptor (ReAsH) in the current study can be selectively bleached upon exposure to high intensity 590 nm excitation light as previously described without affecting mVenus fluorescence. If FRET has occurred, the result should reflect increased emission fluorescence of the donor (mVenus) as compared to pre-bleach conditions.

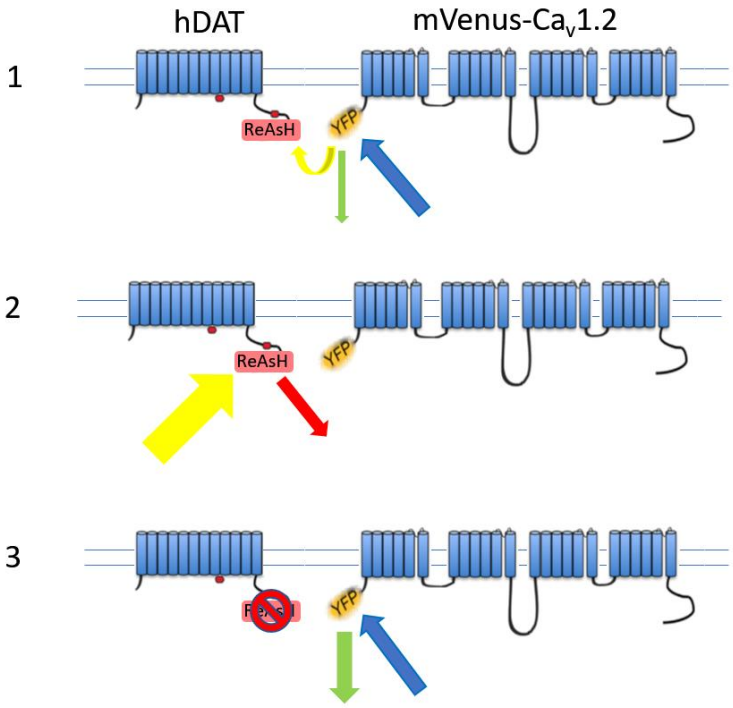

Figure 7: Steps in FRET photobleaching experiment: YFP(mVenus) = donor and ReAsH = acceptor. Small red ovals refer to the CCPGCC tags added to hDAT. (1) 490nm (blue arrow) excites mVenus. FRET indicated by yellow arrow. Energy not overlapping in FRET is emitted and measured (green arrow) (2) ReAsH is selectively bleached at 590nm (yellow arrow). (3) 490nm (blue arrow) excites mVenus and fluorescence (green arrow) is measured. This value is larger if FRET does in fact occur.

Analysis of FRET data is performed utilizing ImageJ. Each data file is a compilation of 25 images taken for a given experimental condition. These images are averaged, at which point whole cells are selected and intensity values are measured, including background intensity. After this is performed for a given well for both the 490nm pre-bleaching and post-bleaching conditions, the background is subtracted from the experimental values, and the percentage change from the pre-bleach to post-bleach conditions is calculated. Once all values of the percent change in intensity are calculated, these are averaged. This process is performed for all four cell populations under study.

APP+ Uptake

HEK cells expressing hDAT, hDAT_PolyC1, and hDAT_Polyc2 are grown in DMEM containing hygromycin at standard mammalian cell culture conditions as previously stated. Cells are plated in a 96-well imaging plate and incubated as previously described for 24 hours. The DMEM is then replaced with DMEM containing 1µL/mL doxycycline to induce transporter expression, and the cells incubate for an additional 3 days. On the day of the experiment, solutions of 3µM, 10µM, and 30µM 4-(4(Dimethylamino)phenyl)-1-methylpyridinium (APP+) are made utilizing IS as solvent. Additionally, 0.5µM solutions of 2 beta-carbomethoxy-3 beta-(4-iodophenyl)tropane (β-CIT) are made, including combination solutions of 3µM, 10µM, and 30µM APP+ with 0.5µM β-CIT. APP+ was shown to be a fluorescent substrate at hSERT (Solis, Zdravkovic et al., 2012), and is also a substrate at hDAT and hNET (Karpowicz, Dunn et al., 2013). β-CIT is a cocaine analog and is used at a saturating concentration as a monoamine transporter blocker in this assay to discern specific versus non-specific uptake of APP+.

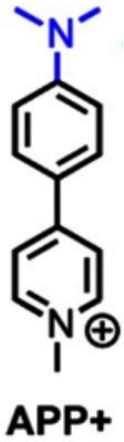

Figure 8: Structure of APP+, a fluorescent substrate at monoamine transporters. Removal of the tertiary amine group in blue yields MPP+, a well-known neurotoxin. Adapted from Karpowicz, Dunn, Sulzer, and Sames, 2013.

Epifluorescent microscopy is performed utilizing an Olympus IX70 microscope, set up with a Luca S digital camera and a Polychrome V light source. Images are obtained, and perfusion is automatically controlled utilizing Till Photonic's Live Acquisition software. For recording, the excitation wavelength is set to 460nm and images are taken at 10 frames per second with an exposure time of 50ms. Media is removed from cells and replaced with IS. Cells are allowed to acclimate to the new solution for 20 minutes. In the case of measuring overall APP+ uptake, cells are exposed to 40 seconds of IS perfusion to establish a baseline signal. Subsequently, cells are perfused with APP+ for 60 seconds, and a fluorescent signal is obtained as APP+ enters the cells. In determining transporter-specific uptake, cells are perfused for 10 seconds with IS, followed by 30 seconds of 0.5μM β-CIT. Subsequently, the cells are exposed to a solution containing APP+ and 0.5μM β-CIT for 60 seconds. By blocking the monoamine transporter with β-CIT, any fluorescent signal obtained reflects non-specific uptake, perhaps through other transporters and/or passive diffusion. In analysis, this data is subtracted from the APP+ only trials in order to obtain specific uptake performed by the monoamine transporter.

Immunostaining, Fluorescent Microscopy and Confocal Microscopy

HEK, hDAT-Flp In, hDAT_PolyC1-Flp In and hDAT_PolyC2-Flp In cells are plated on cover slips in DMEM for hDAT antibody immunostaining and visualization with fluorescent microscopy. Incubation proceeds for 24 hours at 37 degrees Celsius, after which the media is replaced with media containing 1μL/mL doxycycline which promotes expression of hDAT in Flp In-TREx cells. These cells are then incubated in standard cell

culture conditions for 3 days. Cover slips are removed from the media and cells are fixed in approximately 3mL of -20 degrees Celsius methanol in 6-well plates. The cells are immediately washed with 1X phosphate-buffered saline (PBS), and then washed twice more with PBS for 15 minutes per wash.

Subsequently, the primary antibody solution is prepared utilizing a dilution of 1µL of rat monoclonal anti-DAT into 500µL 1X PBS + 1% bovine serum albumin (BSA). 50µL of the diluted antibody are placed onto Parafilm-wrapped plastic dishes, and the cover slips are placed cells facing downward on this solution. These dishes are placed into 100mm culture dishes containing double-deionized water-soaked Kimwipes for humidity control and are stored in 4 degrees Celsius overnight. The next day, cover slips are washed in 1X PBS + 1%BSA 3 times for 15 minutes per wash. Next, the secondary antibody solution is prepared utilizing a dilution of 1µL Alexa Fluor 555 goat anti-rat IgG into 800µL 1X PBS + 1%BSA. The cover slips are placed cells facing upward on fresh Parafilm-wrapped dishes and covered with 75µL of the antibody dilution. The cells are stored away from light and incubated at room temperature for 1.5 hours. Next, the cells are washed with 1X PBS + 1%BSA, then washed again with 1X PBS +1%BSA containing DAPI for nuclear staining. After one final wash with 1X PBS +1%BSA, the cover slips are mounted onto glass slides with Prolong Diamond anti-fade mounting media. The slides are stored away from light for at least 24-48 hours prior to fluorescent microscopy. Epifluorescent microscopy is performed utilizing an Olympus IX70 microscope using a 20x 0.75NA objective, set up with a Luca S digital camera and a Polychrome V light source. Images were obtained utilizing Till Photonic's Live Acquisition software.

The slides for confocal microscopy are prepared in the same manner as described above, however the cell lines utilized are only hDAT, hDAT_PolyC1 Flip-In, and hDAT_PolyC2 Flip-In. These cells are then also transfected with mVenus-$Ca_V1.2$ using the same transfection technique as previously described. After four hours of incubation at 37 degrees Celsius, the media is replaced with media containing 1µL/mL doxycycline for induction of hDAT expression. Confocal imaging studies are performed with a Zeiss confocal microscope utilizing a 60x lens.

RESULTS AND FIGURES

AIM 1

Immunostaining studies utilizing Alexa Fluor 555 goat anti-rat IgG allowed for the quantification of relative expression of hDAT and the two tetracysteine-tagged hDAT mutants in HEK293 cells (Figure 10). Whole cell fluorescence was measured utilizing ImageJ. Average background-subtracted fluorescence per cell line is graphed compared to HEK cells (Figure 11). Wild-type hDAT cells exhibited the most expression with an average fluorescence of 4,624 ± 147.1 (n=80) arbitrary units (a.u.). hDAT_PolyC1 expression was slightly lower than hDAT, having an average fluorescence of 4,366 ± 105.1 (n=80) a.u. hDAT_PolyC2 had the lowest expression of the three transporters with an average fluorescence of 3,168 ± 127.0 (n=65) a.u ($P<0.0001$, One-way ANOVA vs hDAT and hDAT_PolyC1). HEK-293 cells that did not express hDAT were utilized as a control and experiments yielded an average fluorescence of 67.91 ± 2.664 (n=70) a.u. The fluorescence of the negative control can perhaps be attributed to non-specific staining of the hDAT antibody or autofluorescence of the cell, although the value obtained is minimal compared to hDAT, hDAT_PolyC1, and hDAT_PolyC2 fluorescence.

Confocal studies were performed to determine localization of antibody-tagged hDAT, hDAT_PolyC1, and hDAT_PolyC2. hDAT images show localization at the cell membrane (Figure 12). hDAT_PolyC1 images show almost no localization at the

membrane. Staining in this case occurs within the cell in a scattered manner, suggesting hDAT_PolyC1 is trapped in the endoplasmic reticulum (Figure 13). hDAT_PolyC2 staining shows localization at the plasma membrane, however there is some reticular staining within the cell (Figure 14). The hDAT_PolyC1 construct appears to prevent plasma membrane localization, while hDAT_PolyC2 maintains some membrane localization. A previously unpublished super resolution image of hDAT-Flp In cells transfected with mVenus-Ca_v1.2 (Figure 15) is included for comparison (Harris, 2016). This image and prior studies show that hDAT and Ca_v1.2 occupy the plasma membrane in distinct regions but do colocalize on occasion (Harris, 2016). As previously mentioned, the resolution of this type of microscopy is approximately 100nm, and the size of proteins and their interactions occur below this value. These super resolution images suggest that there may be some protein-protein interaction, which will be further addressed in this study's FRET data.

Functional studies of hDAT, hDAT_PolyC1, and hDAT_PolyC2 were performed to compare substrate transport utilizing APP+. This compound is a substrate at hDAT that fluoresces upon integration with intracellular components of cells. Dose responses of 3uM, 10uM, and 30uM APP+ are seen in Figure 17. An example of the time course of APP+ uptake is shown for hDAT wild type in Figure 16. As seen in previous APP+ uptake studies, there are two noticeable rates of substrate uptake. The first, fast rate occurs at the onset of APP+ application, followed by a slower, steady-state rate. In this experiment, the final fluorescence values are compared, which is a measure of the cumulative APP+ uptake in one minute. Non-specific uptake was determined utilizing β-CIT, a known hDAT reuptake inhibitor, at saturating concentration to prevent hDAT

activity. These values were subtracted from the fluorescence values obtained from the APP+ only measurements to obtain APP+ transport specific to hDAT.

The fluorescence values measured at 60 seconds after the initialization of APP+ perfusion are graphed for all three cell lines with all three APP+ concentrations in Figure 17. APP+ uptake in wild-type hDAT yielded an EC50 of 3.80 ± 0.622 (n=16) uM, while hDAT_PolyC2 APP+ uptake yielded an EC50 of 8.74 ± 1.22 (n=16) uM. Additionally, in trials with 30uM APP+, the maximal fluorescence achieved in wild-type hDAT was measured at 7719 ± 733.7161 (n=16) a.u, while in comparison the maximal fluorescence measured in hDAT_PolyC2 was 3279 ± 285.6423 (n=16) a.u. These values reflect that APP+ is 2.3 times less potent and 2.4 times less efficacious at hDAT_PolyC2 than at wild-type hDAT. hDAT_PolyC1 does not appear to significantly transport APP+, which may be an issue of surface expression as seen in the confocal imaging studies described above, but impairment of the transport activity as result of the polyC tag insertion at hDAT cannot be ruled out.

Representative images of HEK, hDAT, hDAT_PolyC1, and hDAT_PolyC2 cells utilized for FRET studies are seen in Figures 18-21. Analysis of results is performed in ImageJ. Cells were selected based on mVenus-Ca_v1.2 expression. The criteria of inclusion for analysis was the proper expression of this protein in the plasma membrane; cells showing excessive expression of mVenus-Ca_v1.2 were rejected from the analysis. Images were background subtracted and regions of interest including the whole cell were drawn to quantify the total mVenus fluorescence intensity for each cell (Figure 22). After photo-bleaching ReAsH, the FRET acceptor, fluorescence increased by 2.00 ± 0.041% (n=66) in the positive control: HEK cells transfected with

mVenus_hDAT_PolyC1. hDAT_PolyC1 and hDAT_PolyC2 cells transfected with $Ca_v1.2$-mVenus increased in fluorescence by 1.92 ± 0.0287% (n=62) and 2.07± 0.0575% (n=38), respectively. Wild type hDAT cells transfected with $Ca_v1.2$-mVenus increased in fluorescence by 0.36 ± 0.0318% (n=56). One-way ANOVA analysis showed a statistical difference ($p<0.0001$) between the value obtained for wild type hDAT and the three hDAT mutants. No statistical difference was seen among the three hDAT mutants.

AIM 2

The pharmacological characterization of new cathinone variants at hDAT and hSERT was performed using the electrical coupling between monoamine transporters and Ca^{2+} channels as a detecting tool. In this method, substrates of monoamine transporters generate a Ca^{2+} signal in cells co-expressing these two proteins. Drug dose responses and their respective calcium assay traces are seen in Figures 23-38. Figure 23 shows the dose versus response curve of S(-)methcathinone at hDAT. The EC50 of S(-)methcathinone is measured at 289nM ± 19nM with a Hill slope of 1.7, and a maximum efficacy of 0.933. The calcium signals as a result of the exposure to different concentrations of S(-)methcathinone are depicted in Figure 24.

Figure 25 represents the dose versus response curve of FTS-096 at hDAT. The EC50 is measured at 3.13µM ± 0.29µM with a Hill slope of 1.7, and a maximum efficacy of 0.880. Each individual response is shown in Figure 26. Comparing EC50 values to S(-)methcathinone, FTS-096 is approximately 10.8 times less potent at hDAT and does not achieve the same efficacy.

RAD-081 dose response data at hDAT are shown in Figure 27. The EC50 is found to be 1.04μM ± 0.06μM with a Hill slope of 1.915, and a maximum efficacy of 0.967. The calcium traces at hDAT for each RAD-081 concentration are seen in Figure 28. Compared to the EC50 value of S(-)methcathinone, RAD-081 is approximately 3.6 times less potent than S(-)methcathinone and achieves similar efficacy. RAD-069 dose response data at hDAT is shown in Figure 29. As this compound did not elicit a calcium signal as a substrate, blocker protocol was utilized, meaning the data shown represents competition of the drug with saturating (10μM) dopamine. As can be seen there is no appreciable change in dopamine-induced calcium signals across drug concentrations up to 50μM. Testing was halted as these high concentrations are not physiologically relevant, and RAD-069 was deemed inactive at hDAT in this assay. Cumulative calcium traces for RAD-69 at hDAT are seen in Figure 30.

To compare differences in activity of these compounds at other transporters, the cathinone analogs were also tested in hSERT. Figure 31 depicts S(-)methcathinone dose versus response data at hSERT. The EC50 was found to be 14.3μM ± 1.9μM with a Hill slope of 2.00, and a maximum efficacy of 0.748. Figure 32 represents the calcium assay traces for S(-)methcathinone at hSERT. Although a substrate at hSERT, S(-)methcathinone is less potent and less efficacious at hSERT than at hDAT. FTS-096 data is shown in Figure 33. As no calcium signal was elicited by the compound itself, the blocker protocol was utilized to compete FTS-096 with 10μM dopamine. No dose versus response curve could be fit to these points, which occur in a flat, linear fashion. Calcium traces are shown in Figure 34. Interestingly, 1μM FTS-096 competing 10μM serotonin yielded 0.8312 efficacy, while all higher concentrations yielded efficacies

ranging from 0.6778 to 0.7733. Perhaps some blocking effect is occurring at concentrations above 1µM and the compound is not fully efficacious. More than likely, however, the variations seen relate to differences across experimental days such as calcium channel transfection or Fura-2AM loading. In prior studies utilizing the blocker protocol, it has been noted that rundown of the second neurotransmitter control signal can occur, possibly attributed to bleaching of Fura-2AM or transporter internalization. As there is no significant change in signal comparing high concentrations to the dopamine control, this compound is deemed inactive in this assay.

RAD-081 hSERT data are seen in Figures 35 and 36. The EC50 is found to be 16.6µM ± 10µM with a Hill slope of 0.8751, and a maximum efficacy of 0.559. As a substrate in hSERT, RAD-081 is slightly less potent and less efficacious than S(-)methcathinone. Compared as a substrate in hDAT, RAD-081 is approximately 16 times less potent in hSERT, and less efficacious as well. Figure 37 depicts the dose versus response data for RAD-069 at hSERT. Calcium traces for these trials are seen in Figure 38. As there was no calcium signal produced from application of the drug itself, RAD-069 was tested as a blocker in competition with 10µM serotonin. Placed on the dose versus response graph for comparison, the experimental control is marked at log [RAD069] equal to -7. This point represents the value of a second application of serotonin as a percentage of the first application of serotonin (no test compound included in the trial). In this way, it is shown that the first two concentrations tested do not have much of an effect on serotonin transport. Most likely, in this blocker setup there is once again some rundown of the calcium signal. At 50µM, there is a decrease in calcium signal, which may reflect the onset of blocker activity at high concentrations or

variability within the assay itself. Nevertheless, the concentration tested is not physiologically relevant and as such is deemed inactive in this assay. In order to gauge potential abuse liability, DAT selectivity is calculated as the hSERT EC50 divided by the hDAT EC50, which is listed in Table 3. DAT selectivity for FTS-096, S(-)methcathinone, and RAD-081 are 31.95, 47.67, and 15.96, respectively.

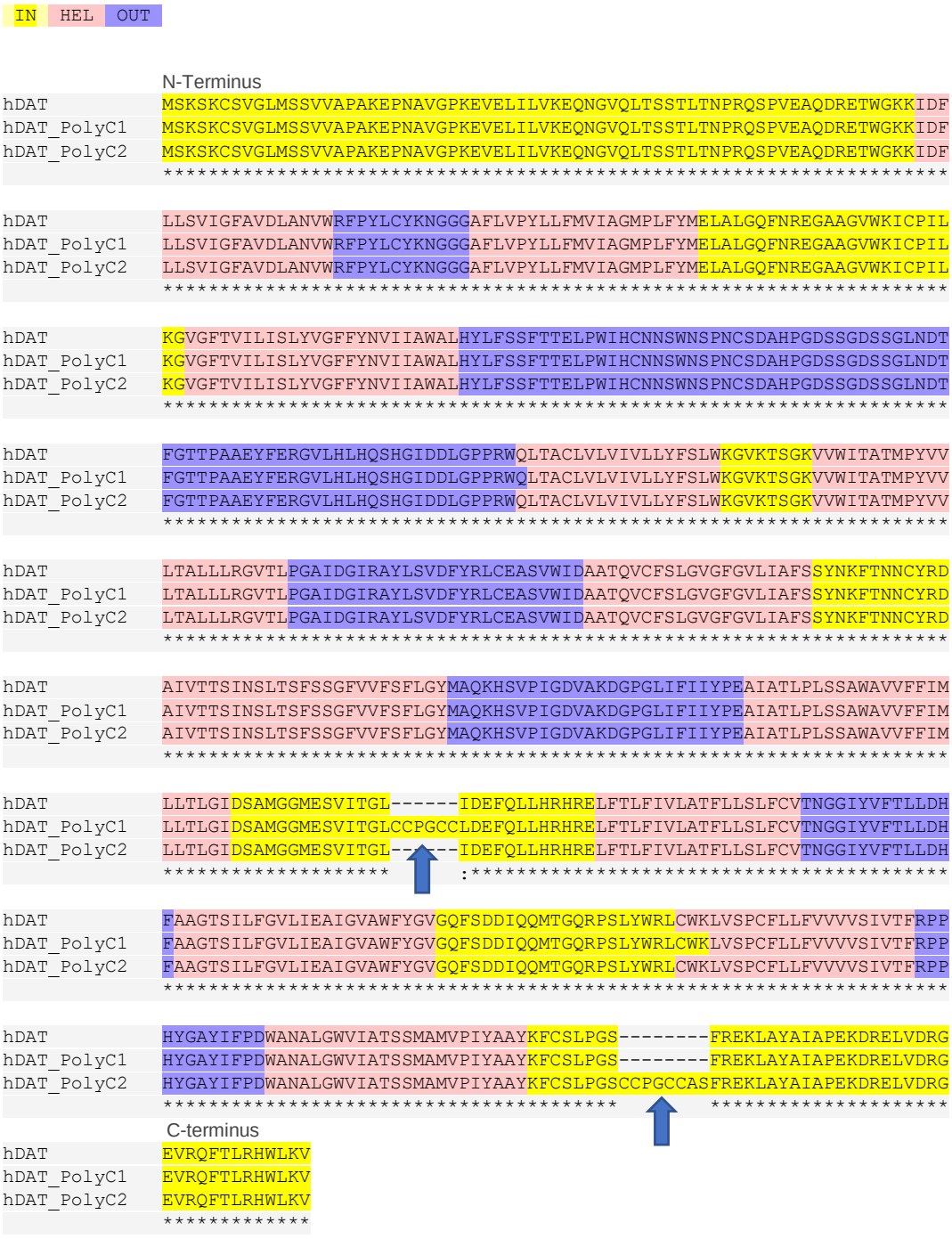

Figure 9: Amino acid sequence alignment of hDAT, hDAT_PolyC1, and hDAT_PolyC2. Colors in the sequence refer to location of that amino acid segment: yellow = intracellular, pink = transmembrane, and purple = extracellular. Blue arrows indicate location of tetra-cysteine motifs (CCPGCC). mVenus_hDAT_PolyC1 not shown. Tetracysteine tag for this protein occurs in same location as in hDAT_PolyC1. mVenus protein is attached to the N-terminus as described in the methods. Alignment performed utilizing PSI-Coffee (Chang, Di Tommaso et al., 2012)

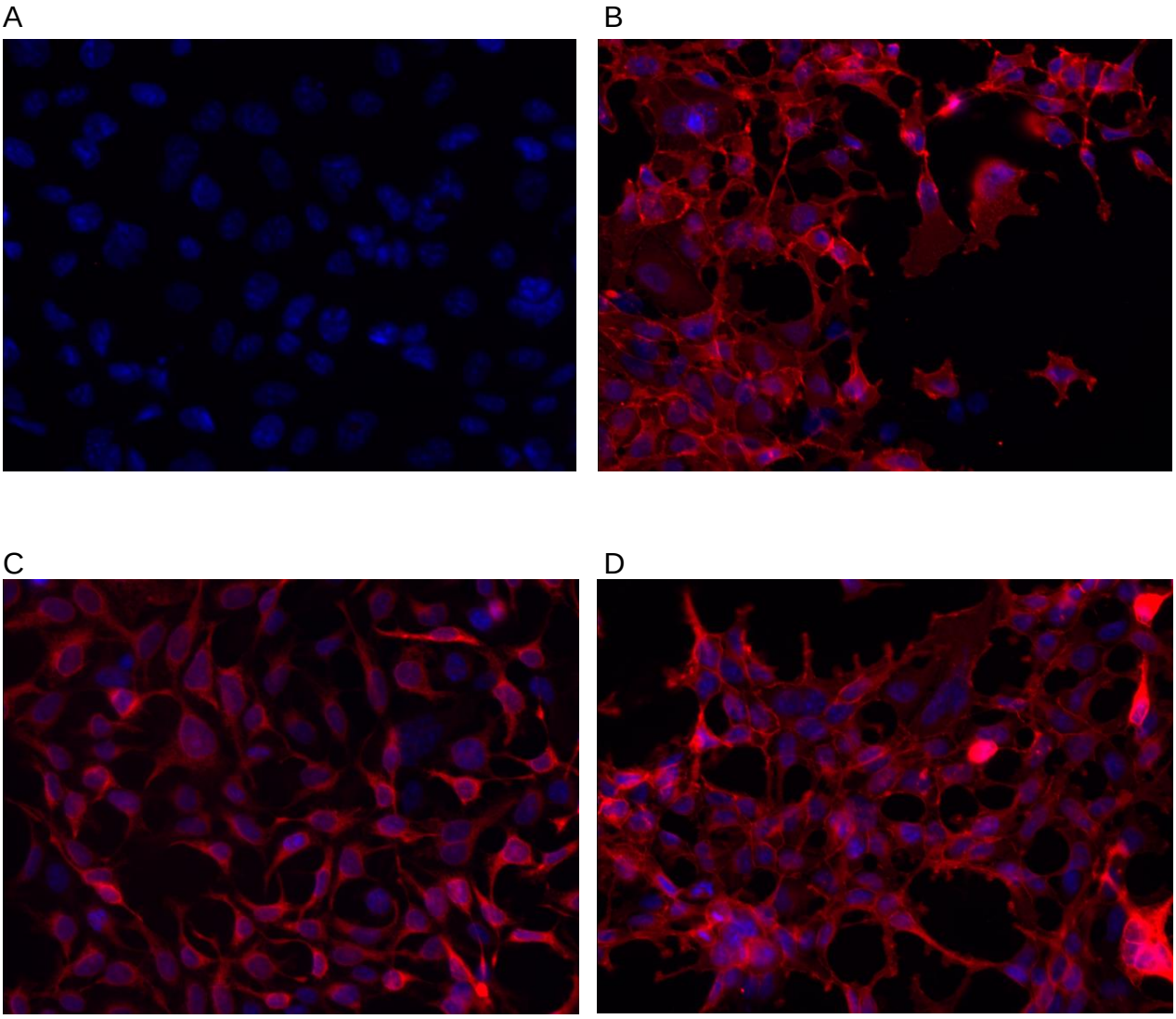

Figure 10: Representative images of immunostaining of hDAT with Alexa Fluor 555 goat anti-rat IgG (red stain) at (A) HEK-293 cells, (B) hDAT-Flip In cells, (C) hDAT_PolyC1-Flip In cells, and (D) hDAT_PolyC2-Flip in cells. Nuclei are stained with DAPI.

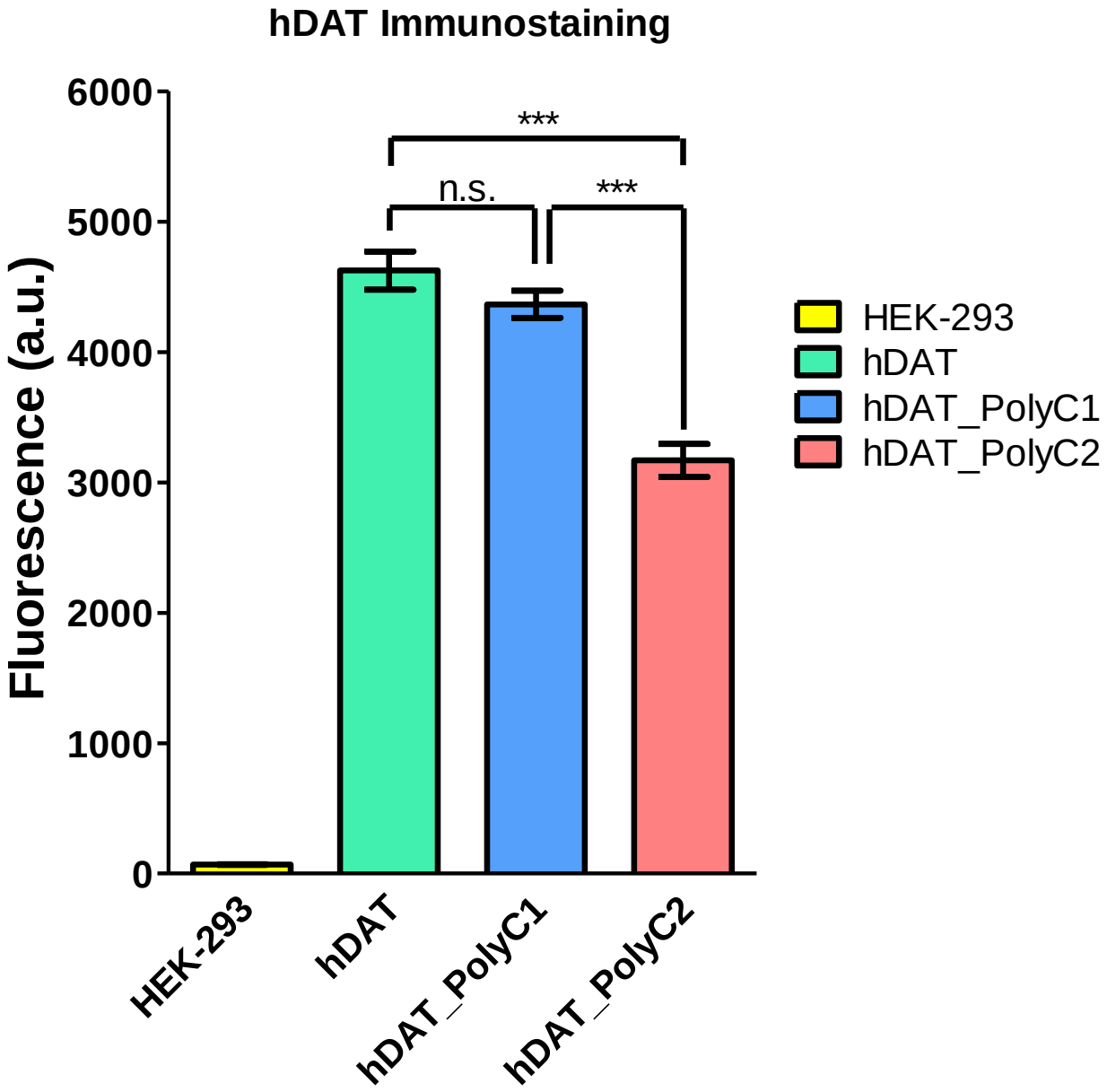

Figure 11: Average Alexa Fluor 555 goat-anti-rat IgG fluorescence per cell line. Overall fluorescence is indicative of relative protein expression. Brackets indicate ± s.e.m. N = 65-80 cells per cell line.*** hDAT_PolyC2 is statistically different from hDAT and hDAT_PolyC1 ($P<0.0001$,One-way Anova). hDAT and hDAT_PolyC1 are not statistically different (n.s.). All three hDAT cell lines are statistically different from HEK-293 ($P<0.0001$, One-way Anova).

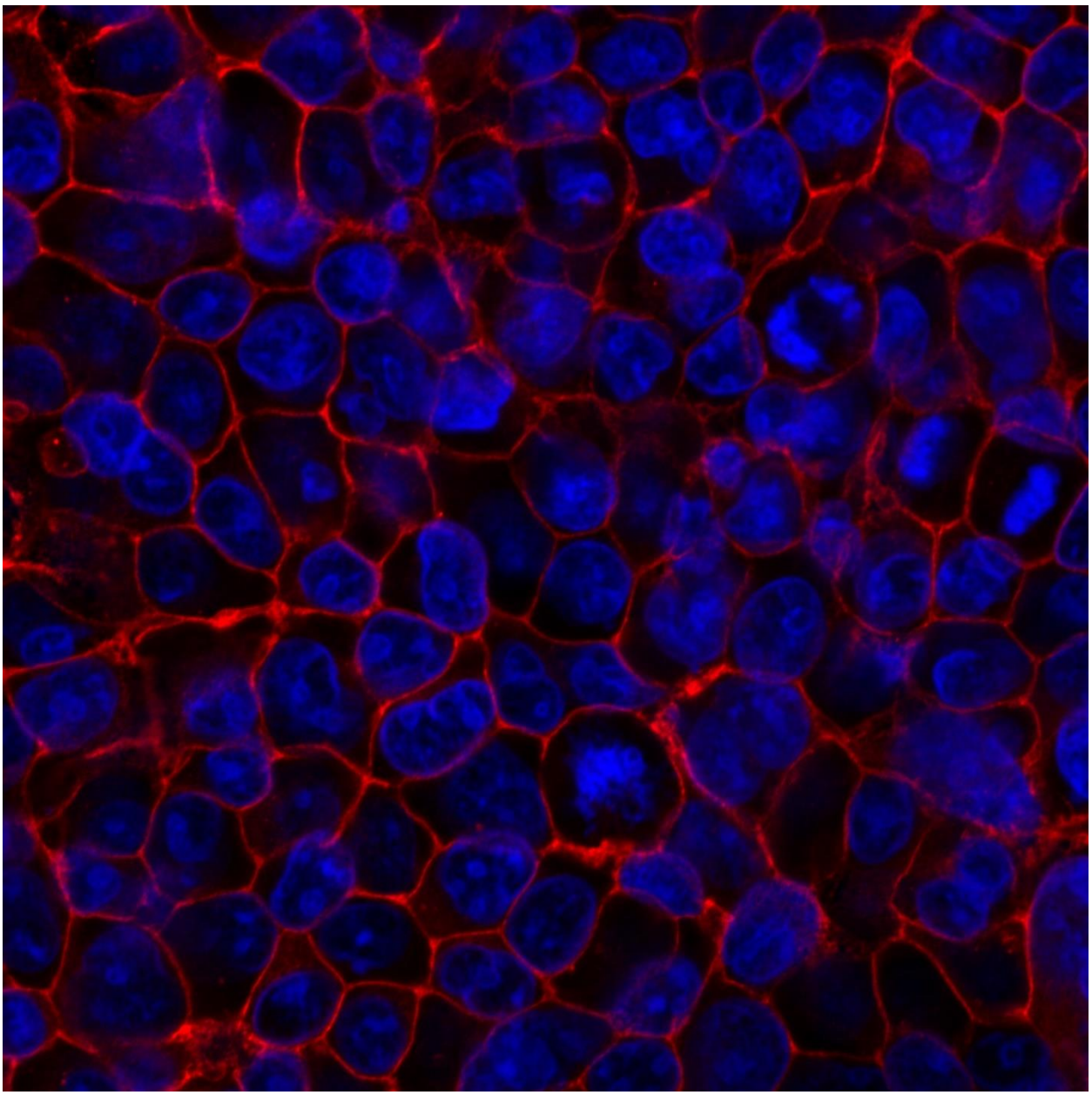

Figure 12: Confocal image of hDAT-Flip In cells stained with Alexa Fluor 555 goat-anti-rat IgG (red stain). hDAT is visualized primarily at the plasma membrane. Nuclei are stained with DAPI.

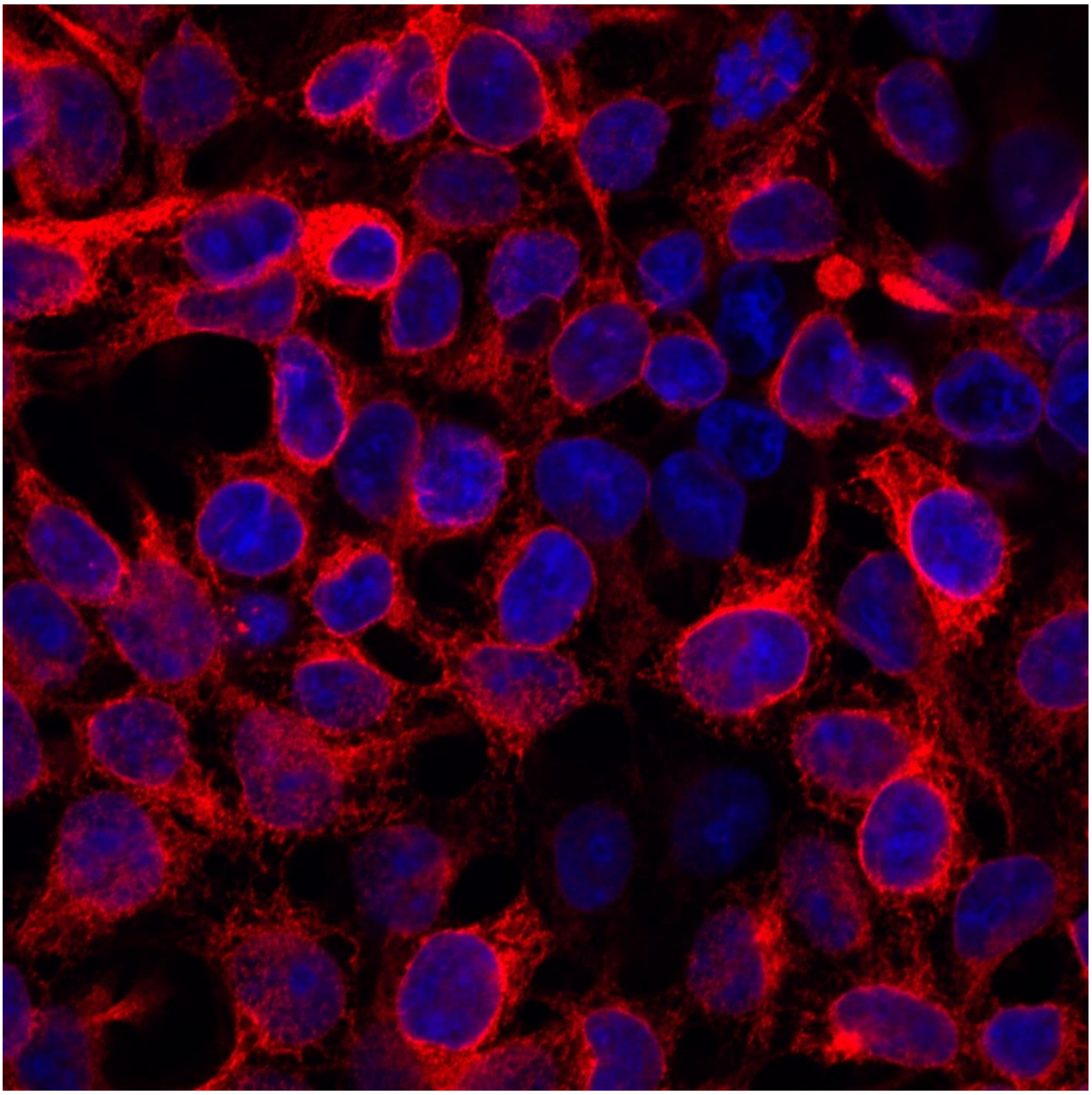

Figure 13: Confocal image of hDAT_PolyC1-Flip In cells stained with Alexa Fluor 555 goat-anti-rat IgG (red stain). hDAT_PolyC1 is primarily visualized within the cell as indicated by the reticular pattern, indicative of ER staining. Nuclei are stained with DAPI.

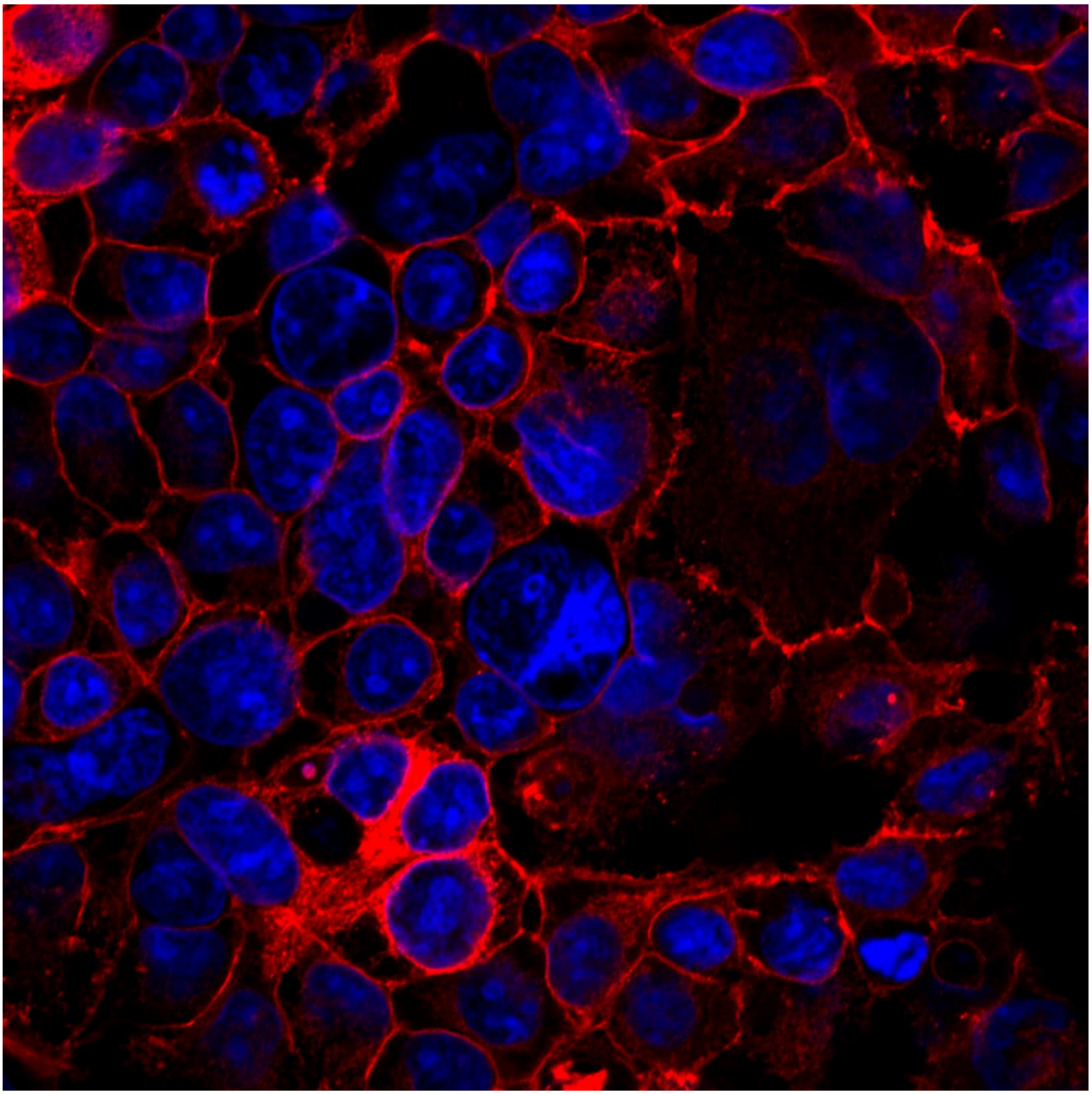

Figure 14: Confocal image of hDAT_PolyC2-Flip In cells stained with Alexa Fluor 555 goat-anti-rat IgG (red stain). hDAT_PolyC2 is visualized at the plasma membrane and internally as indicated by the reticular patterns. Nuclei are stained with DAPI.

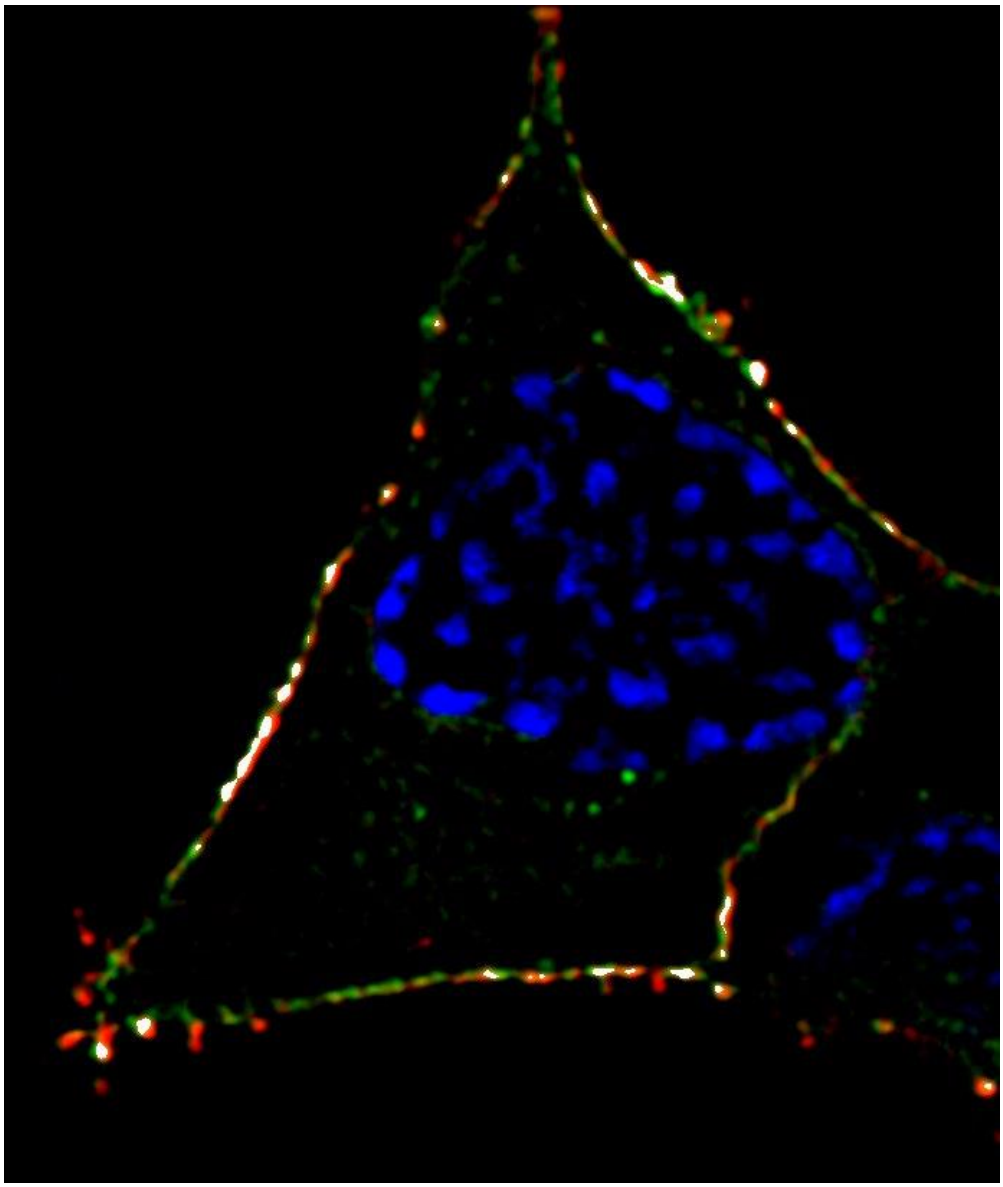

Figure 15: N-SIM super-resolution image of hDAT (red) HEK cell transfected with mVenus-$Ca_V1.2$ (green). Colocalization determined utilizing ImageJ (white). Previously unpublished image courtesy of Alan Harris (Harris, 2016).

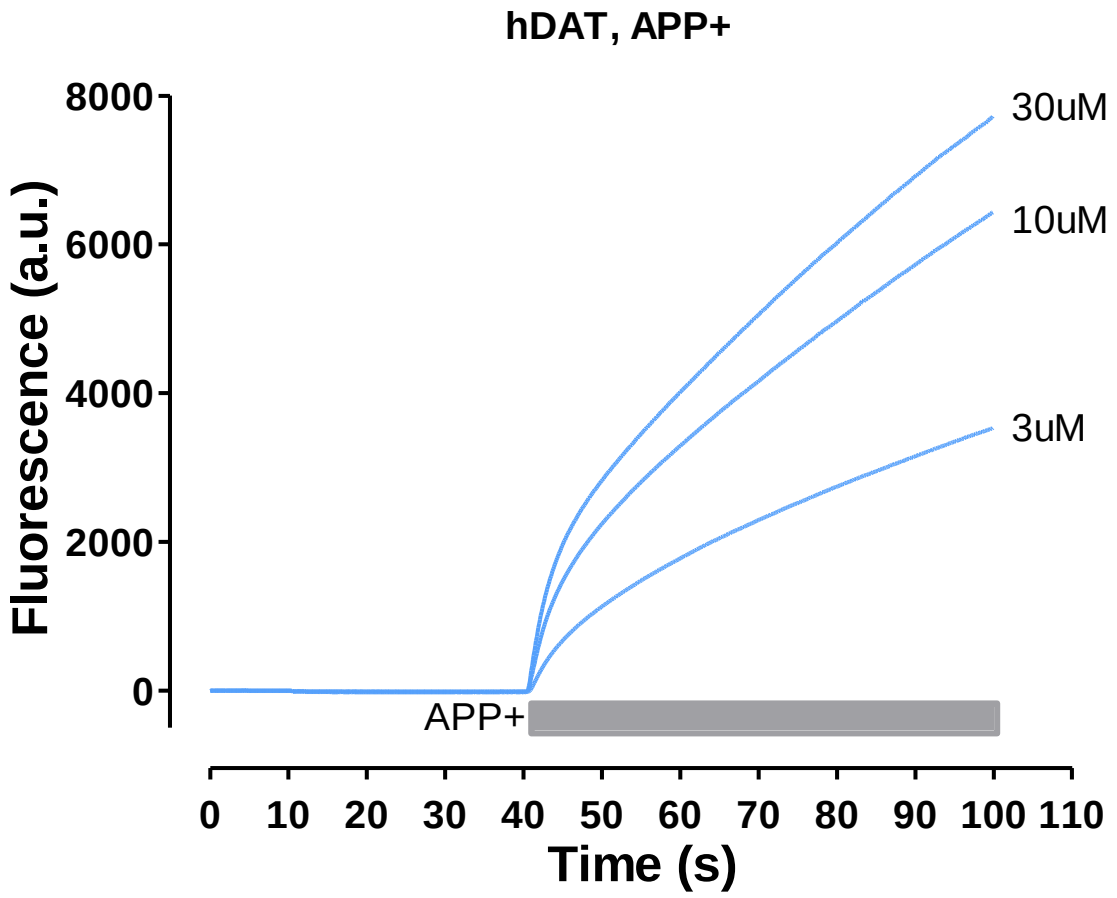

Figure 16: Representative trace plotting fluorescence versus time for the APP+ uptake protocol. Average traces for 3uM, 10uM, and 30uM are shown for APP+ uptake studies in hDAT. The final fluorescent values for each concentration are used to plot a steady-state dose response in Figure 17.

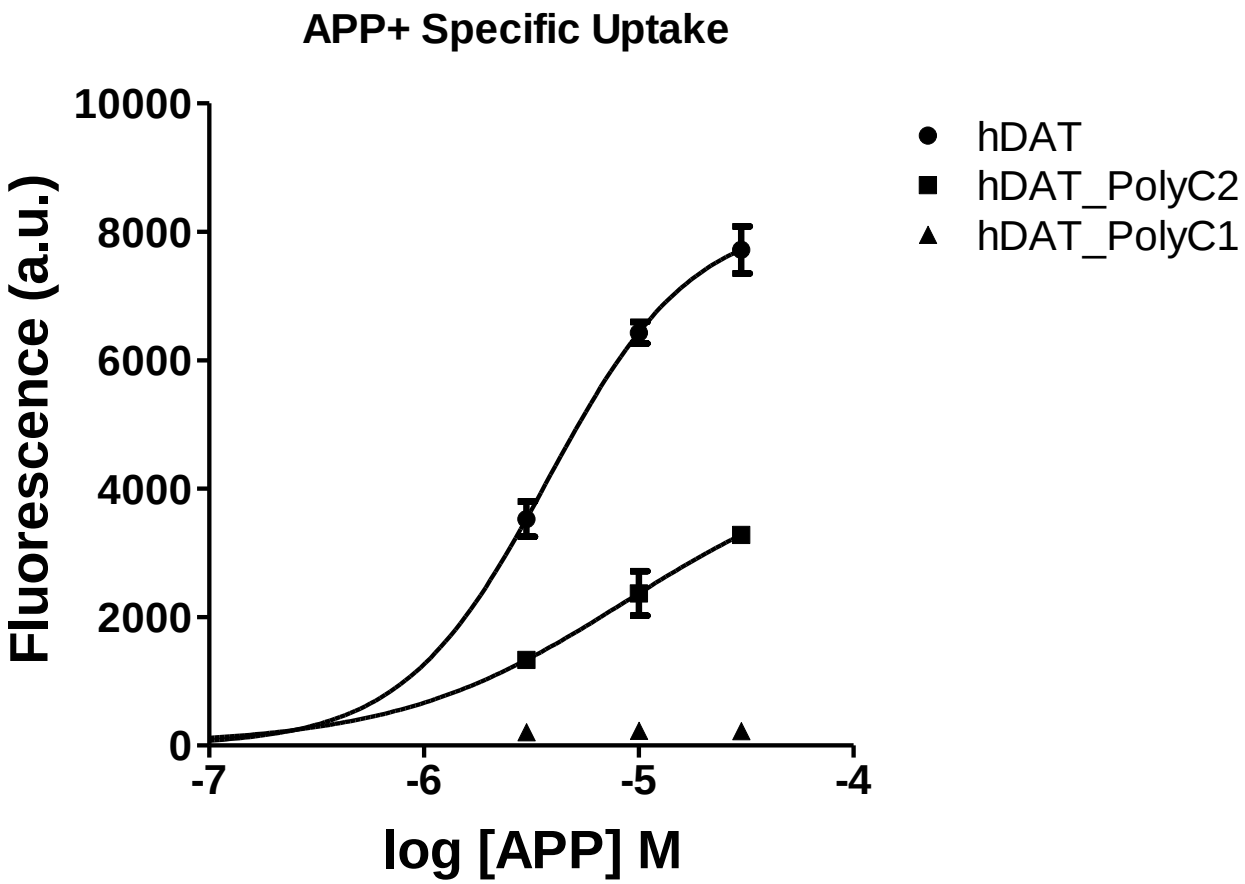

Figure 17: APP+ dose versus response curve for hDAT, hDAT_PolyC1, and hDAT_PolyC2. Each point is calculated by subtracting non-specific uptake from overall uptake. Non-specific uptake is determined by competing APP+ with 0.5uM β-CIT after a 30 second application of 0.5uM β-CIT alone. All points reflect fluorescent values obtained after 60 seconds of APP+ perfusion. Brackets indicate ± s.e.m. N = 4-6 imaging plate wells, 35-55 cells chosen per well.

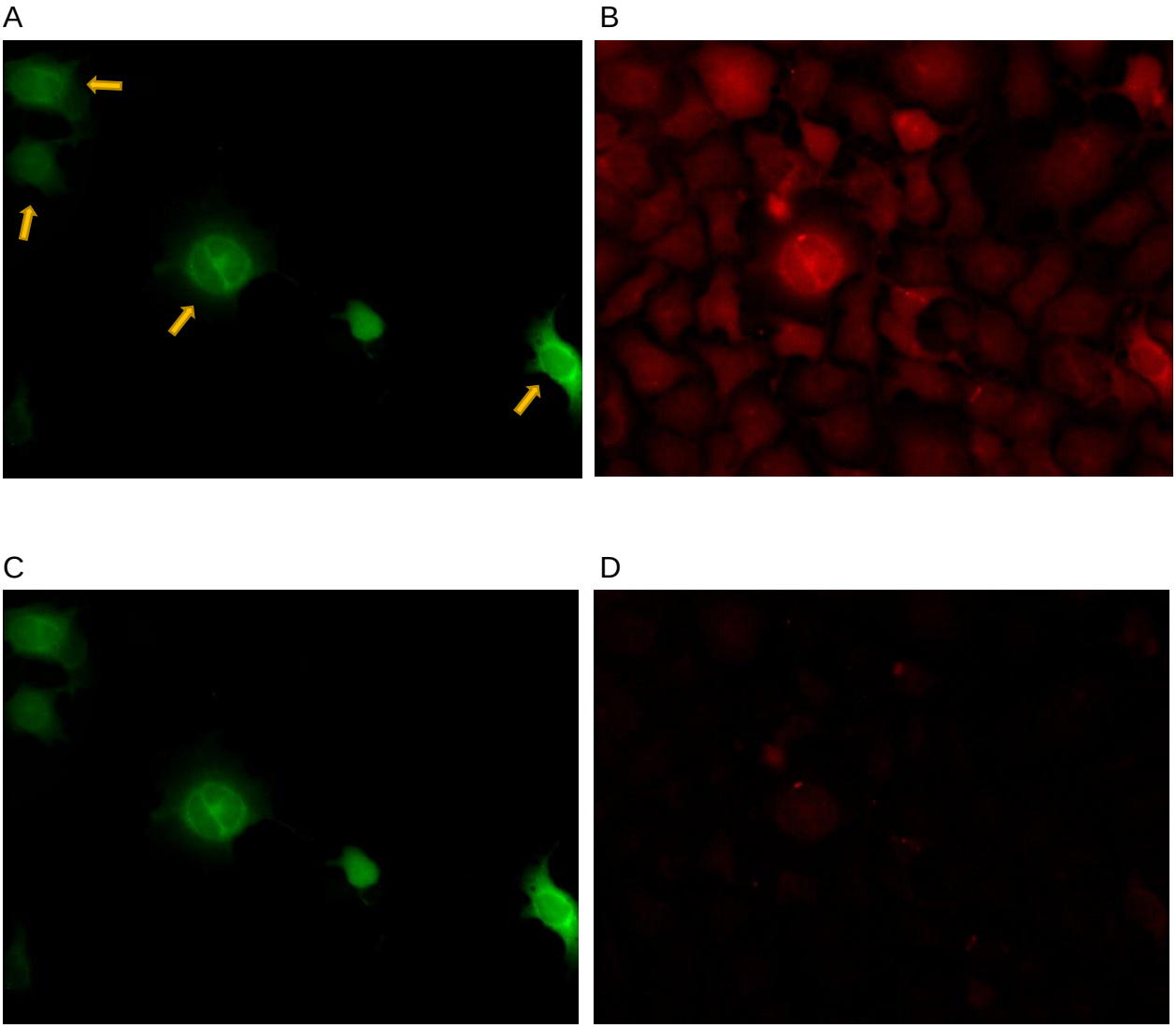

Figure 18: Representative photos of HEK cells transfected with mVenus_hDAT_PolyC1 utilized for FRET studies. Images of (A) mVenus and (B) ReAsH are recorded prior to bleaching ReAsH. Images of (C) mVenus and (D) ReAsH are recorded after bleaching ReAsH. These cells do not exhibit plasma membrane localization as seen by the diffuse fluorescence of mVenus. Cells with internal borders of bright fluorescence are selected for analysis, indicated by yellow arrows. ImageJ is used to quantify differences in fluorescence between (A) and (C). These values are reported in Figure 22.

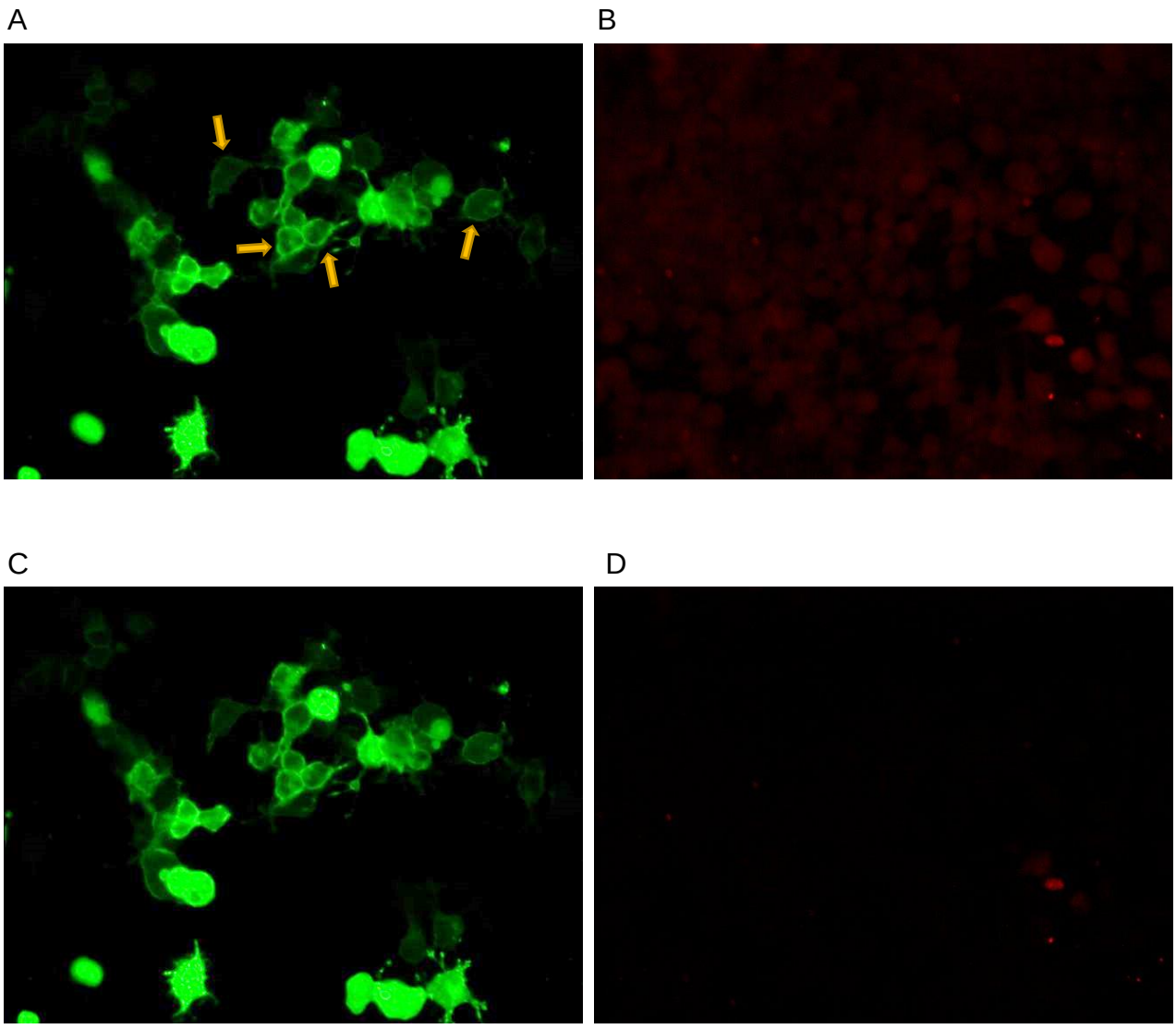

Figure 19: Representative photos of hDAT cells utilized for FRET studies. Images of (A) mVenus-$Ca_V1.2$ and (B) ReAsH are recorded prior to bleaching ReAsH. Images of (C) mVenus-$Ca_V1.2$ and (D) ReAsH are recorded after bleaching ReAsH. Cells with appropriate plasma membrane expression of mVenus-$Ca_V1.2$, represented by a distinct fluorescent border, are selected for analysis (indicated by yellow arrows). ImageJ is used to quantify differences in fluorescence between (A) and (C). These values are reported in Figure 22.

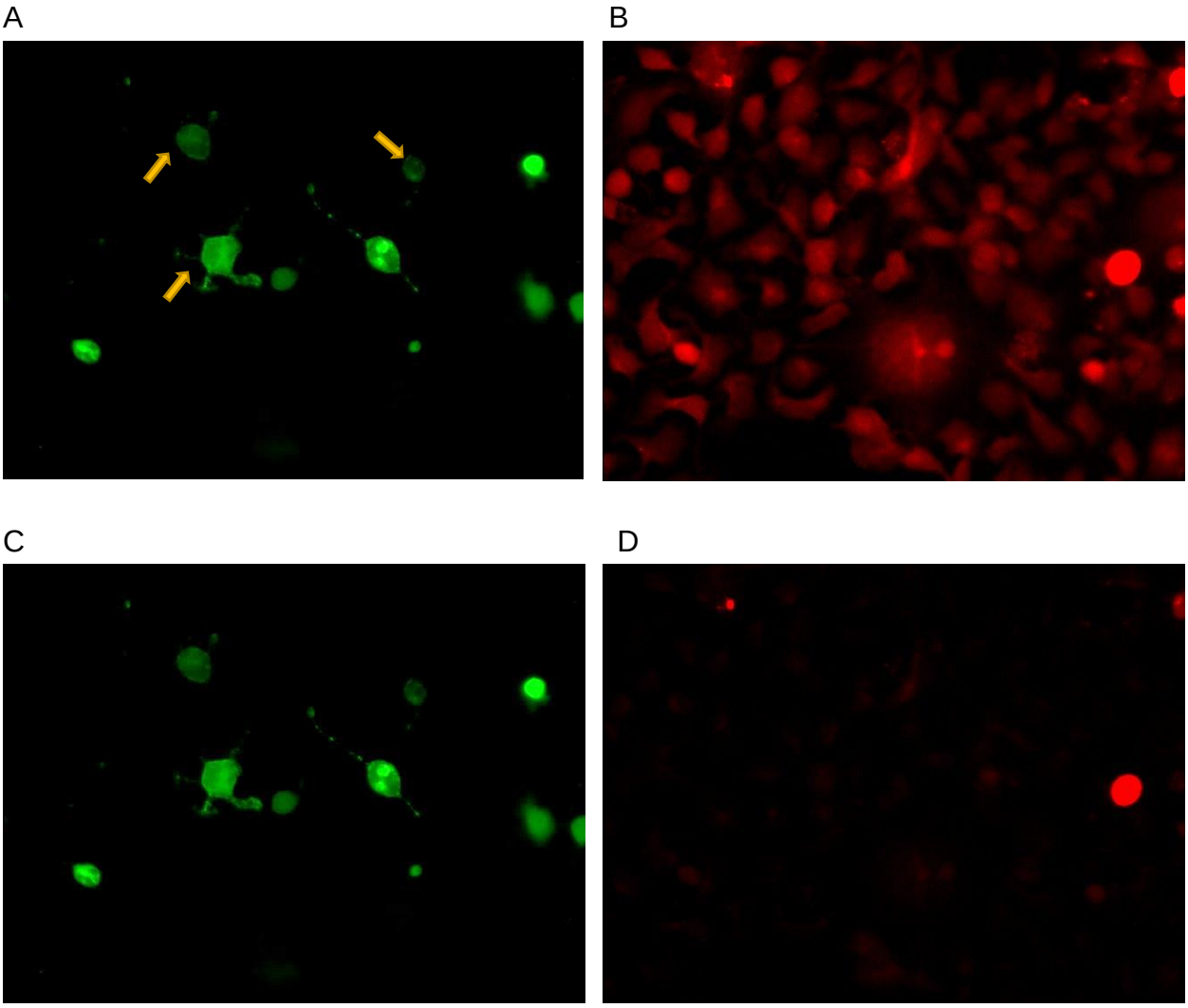

Figure 20: Representative photos of hDAT_PolyC1 cells utilized for FRET studies. Images of (A) mVenus-$Ca_v1.2$ and (B) ReAsH are recorded prior to bleaching ReAsH. Images of (C) mVenus-$Ca_v1.2$ and (D) ReAsH are recorded after bleaching ReAsH. Cells with appropriate plasma membrane expression of mVenus-$Ca_v1.2$, represented by a distinct fluorescent border, are selected for analysis (indicated by yellow arrows). ImageJ is used to quantify differences in fluorescence between (A) and (C). These values are reported in Figure 22.

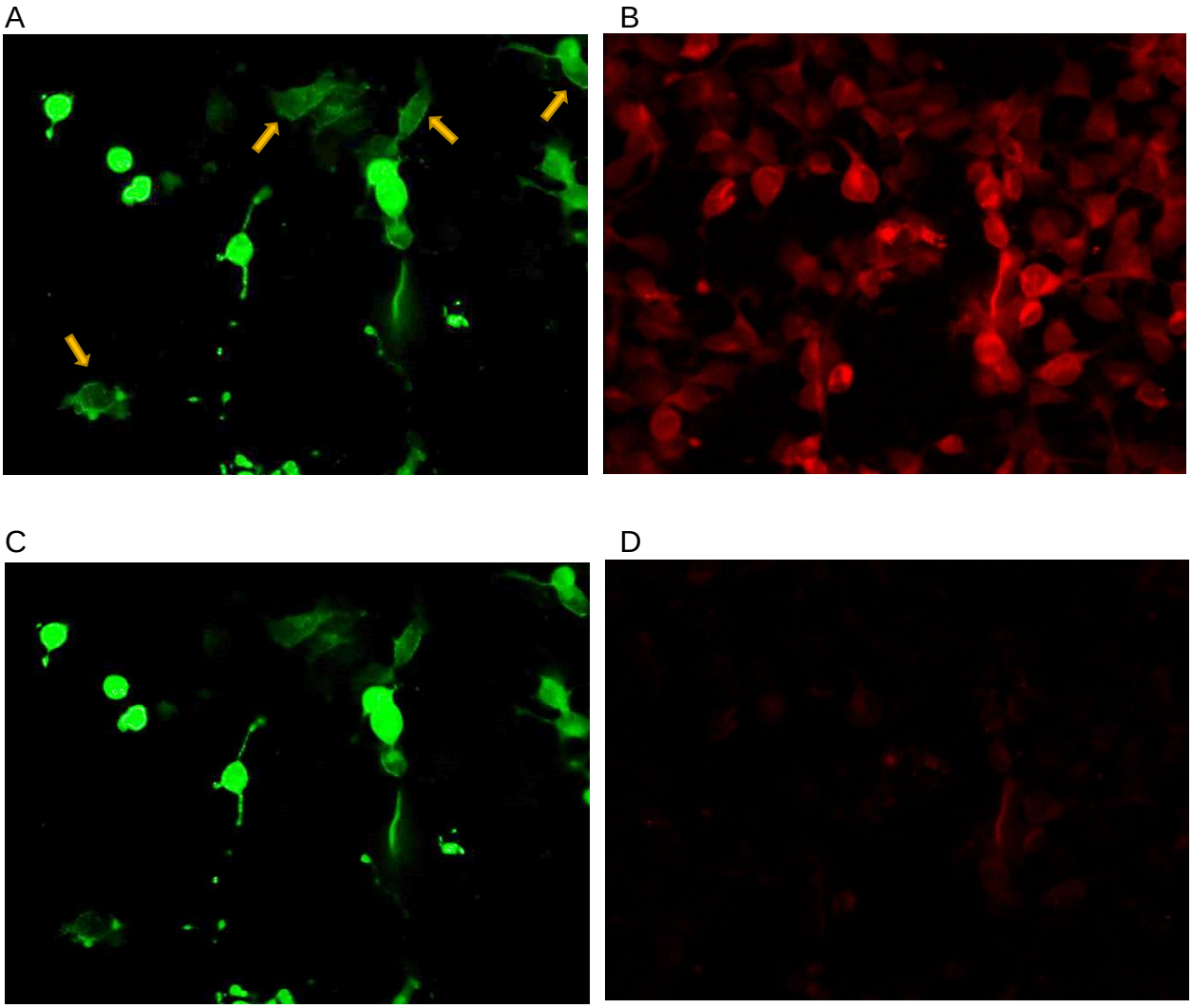

Figure 21: Representative photos of hDAT_PolyC2 cells utilized for FRET studies. Images of (A) mVenus-$Ca_v1.2$ and (B) ReAsH are recorded prior to bleaching ReAsH. Images of (C) mVenus-$Ca_v1.2$ and (D) ReAsH are recorded after bleaching ReAsH. Cells with appropriate plasma membrane expression of mVenus-$Ca_v1.2$, represented by a distinct fluorescent border, are selected for analysis (indicated by yellow arrows). ImageJ is used to quantify differences in fluorescence between (A) and (C). These values are reported in Figure 22.

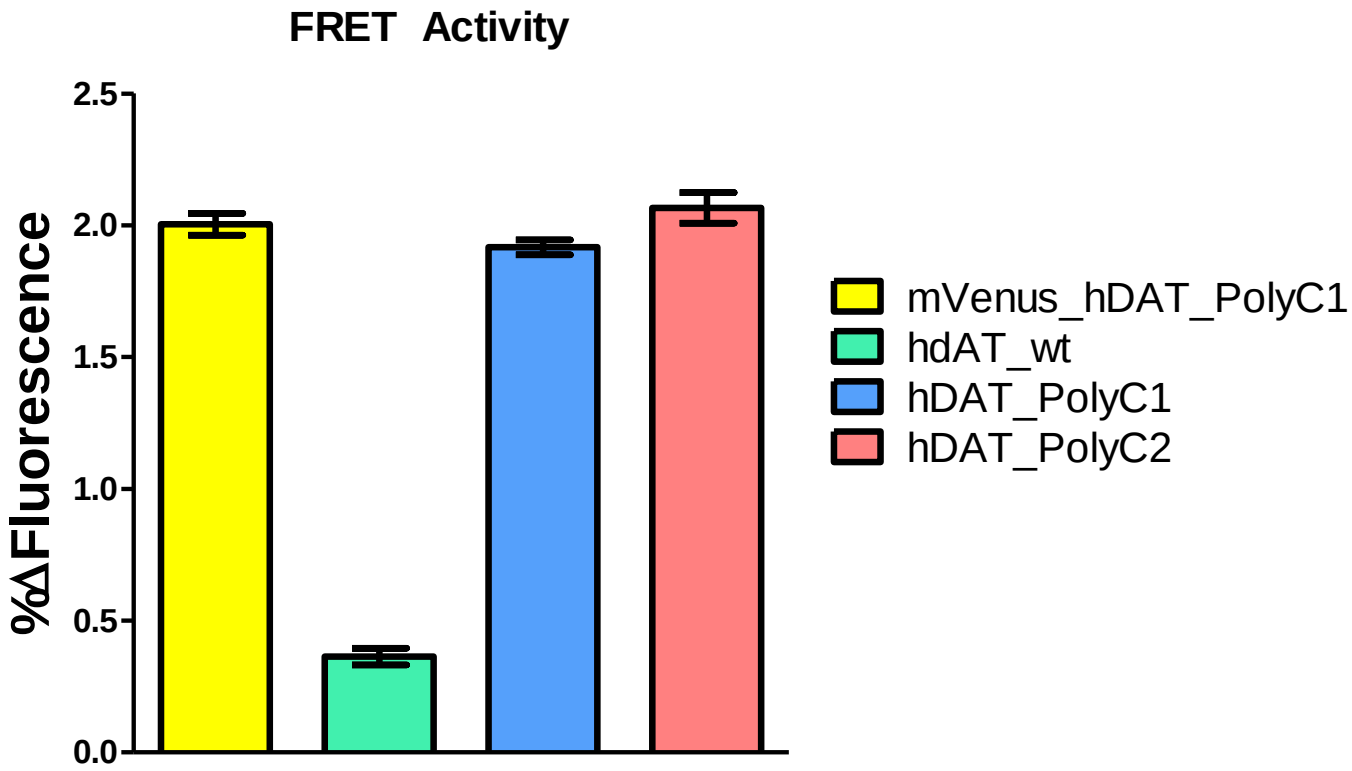

Figure 22: Average FRET data presented as percent change in fluorescence of mVenus after ReAsH bleaching. N per cell line = 38-66. One-way Anova did not show any statistical difference between the positive control, hDAT_PolyC1, and hDAT_PolyC2. There is a statistical difference between these three groups and hDAT, the negative control ($P<0.0001$, One-way Anova).

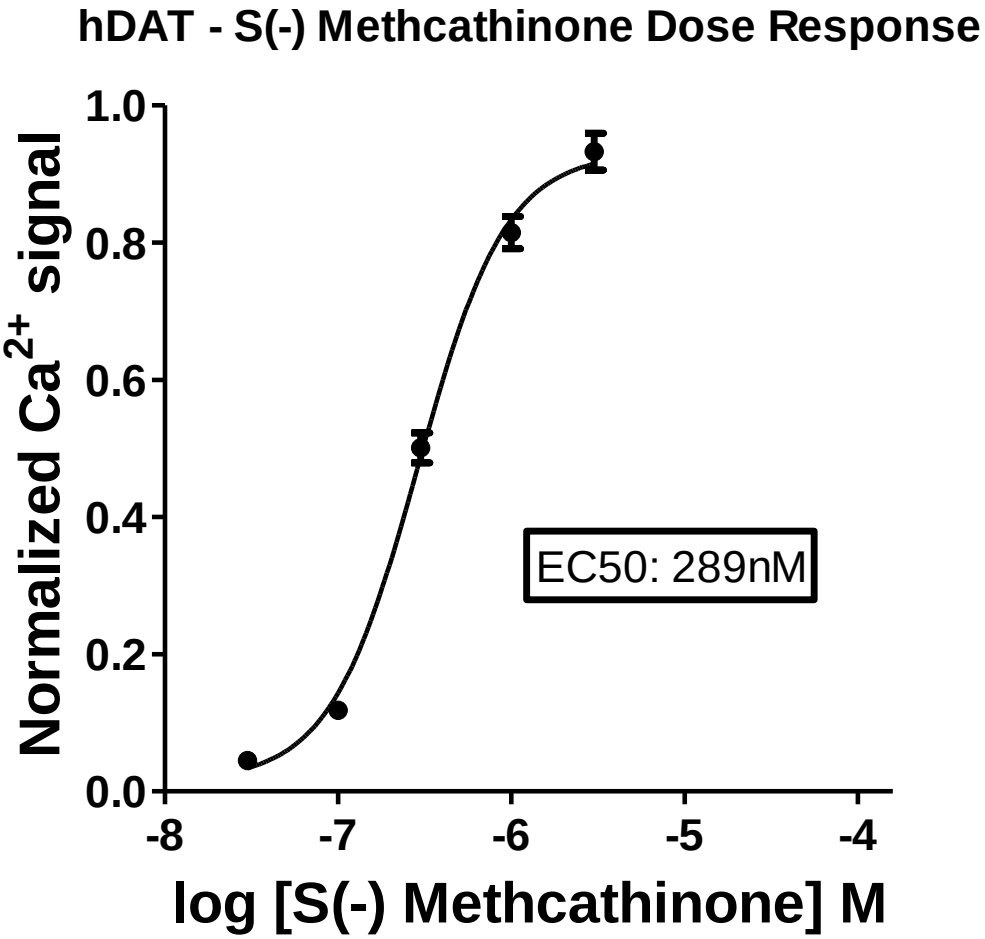

Figure 23: Dose versus response curve for S(-)methcathinone at hDAT utilizing Fura-2 binding of calcium. Calcium entry is mediated by $Ca_v1.2$. Data displayed as the mean with standard error values.

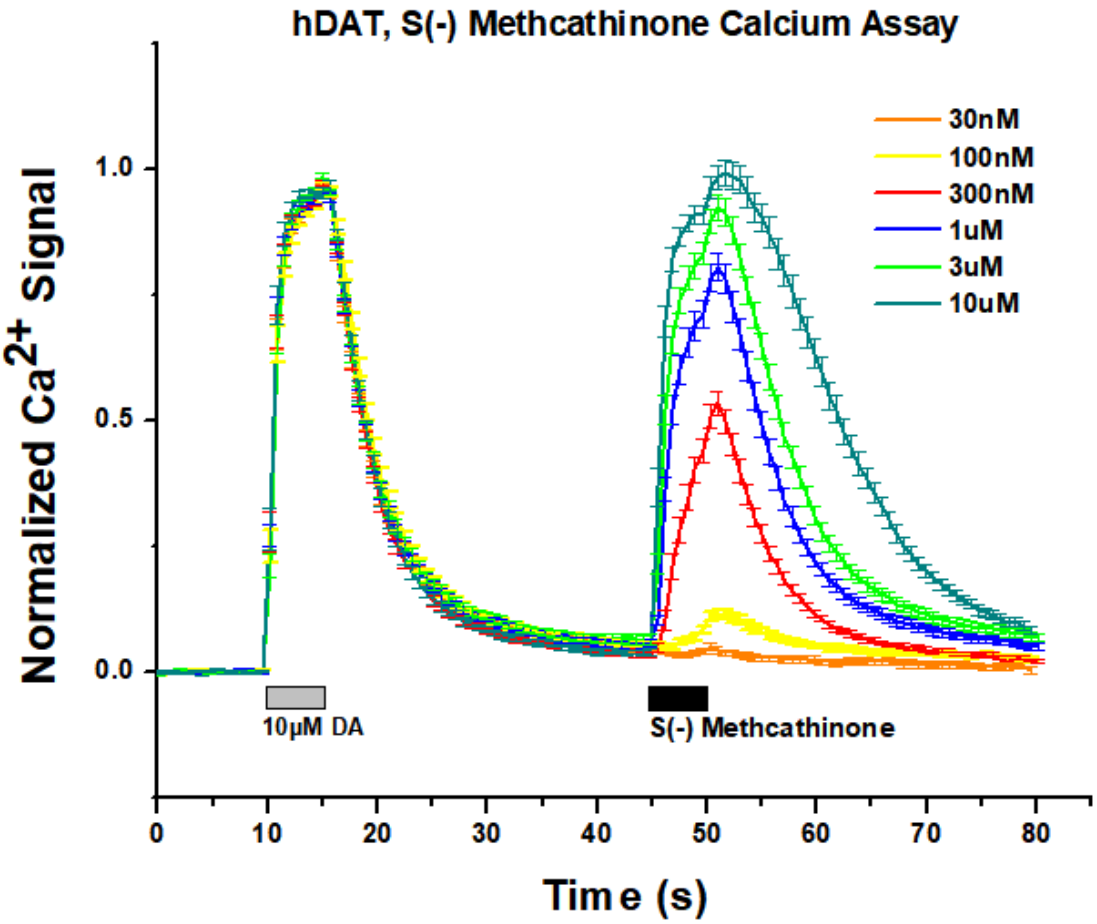

Figure 24: Cumulative calcium-fura-2 traces for S(-)methcathinone at hDAT. Each concentration is represented by the mean of all cells assayed with standard error values. Signal represents calcium-fura-2 binding mediated by $Ca_v1.2$. Bars directly beneath trace represent perfusion of the indicated solution.

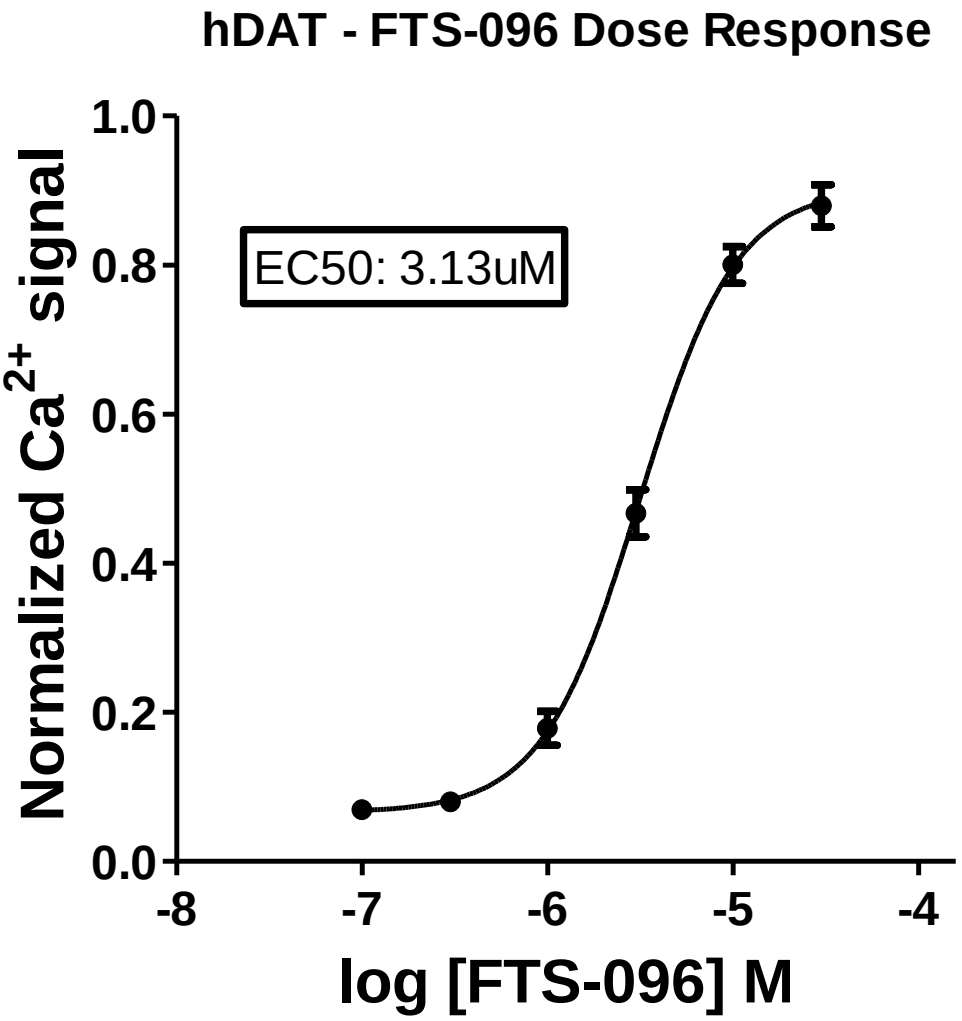

Figure 25: Dose versus response curve for FTS-096 at hDAT utilizing Fura-2 binding of calcium. Calcium entry is mediated by $Ca_V1.2$. Data displayed as the mean with standard error values.

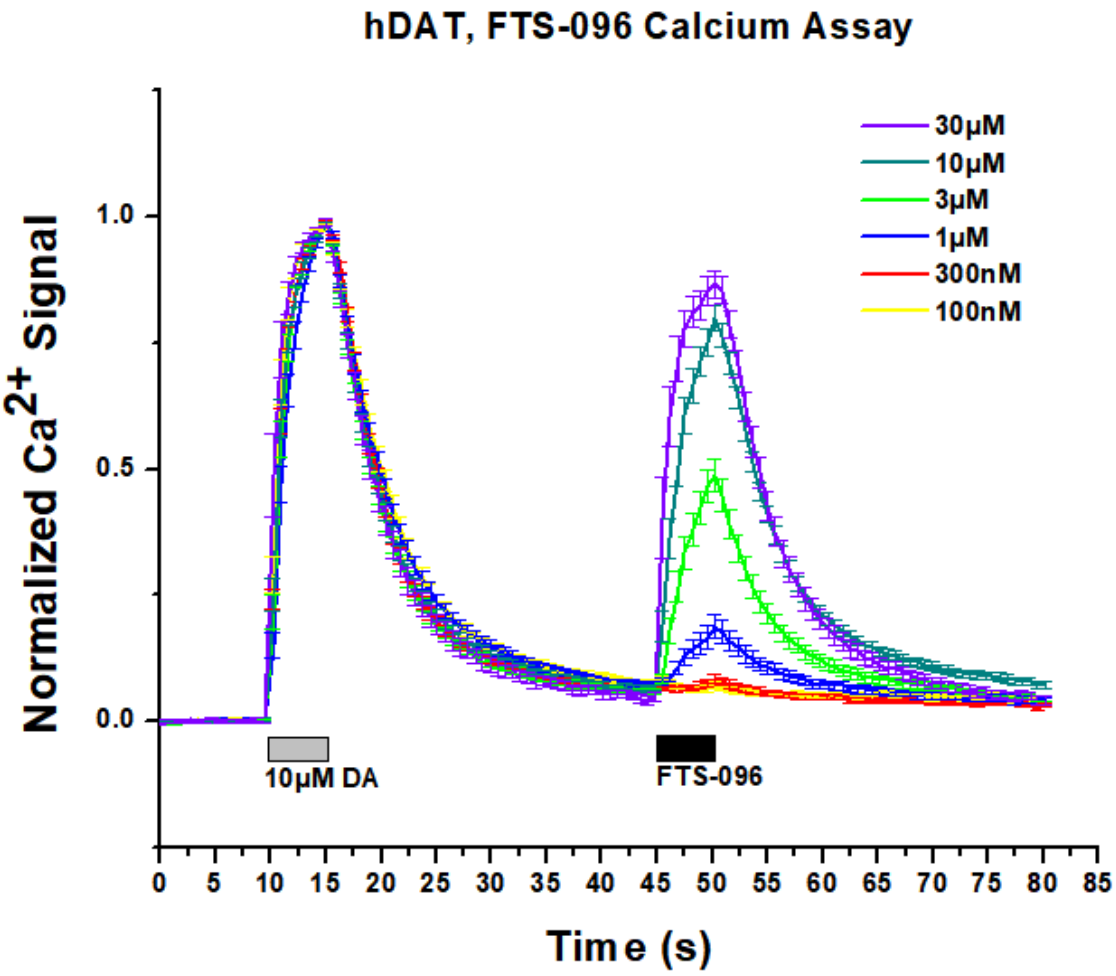

Figure 26: Cumulative calcium-fura-2 traces for FTS-096 at hDAT. Each concentration is represented by the mean of all cells assayed with standard error values. Signal represents calcium-fura-2 binding mediated by $Ca_v1.2$. Bars directly beneath trace represent perfusion of the indicated solution.

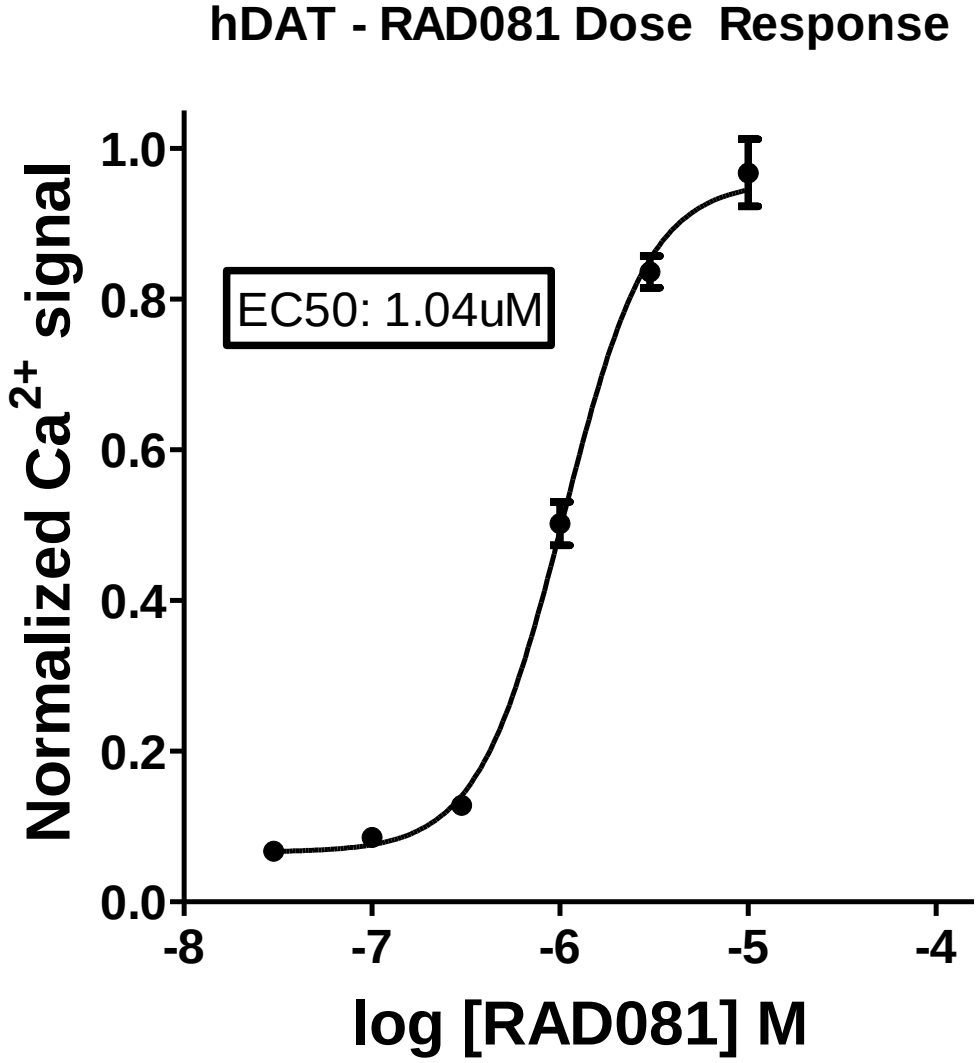

Figure 27: Dose versus response curve for RAD-081 at hDAT utilizing Fura-2 binding of calcium. Calcium entry is mediated by $Ca_V1.2$. Data displayed as the mean with standard error values.

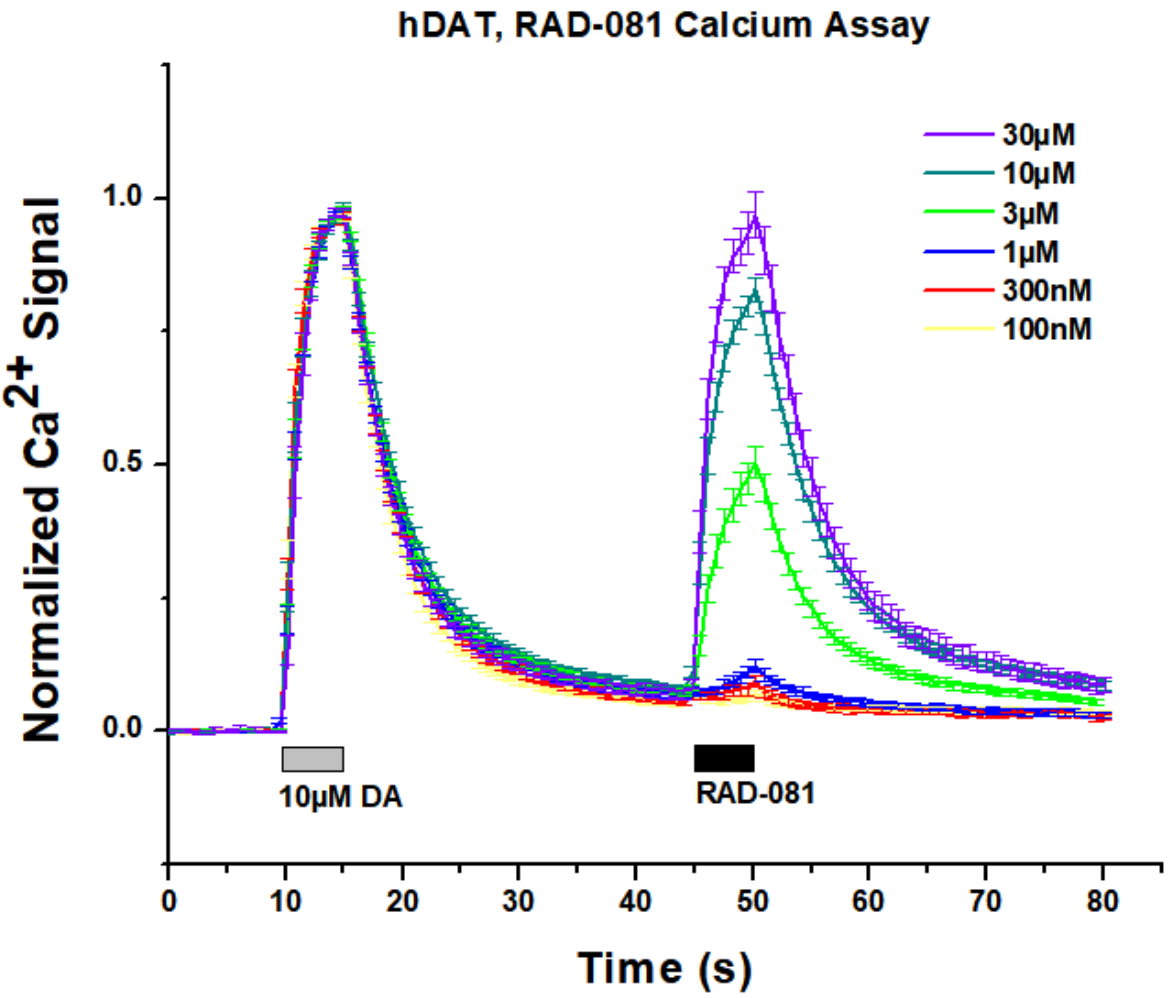

Figure 28: Cumulative calcium-fura-2 traces for RAD-081 at hDAT. Each concentration is represented by the mean of all cells assayed with standard error values. Signal represents calcium-fura-2 binding mediated by $Ca_v1.2$. Bars directly beneath trace represent perfusion of the indicated solution.

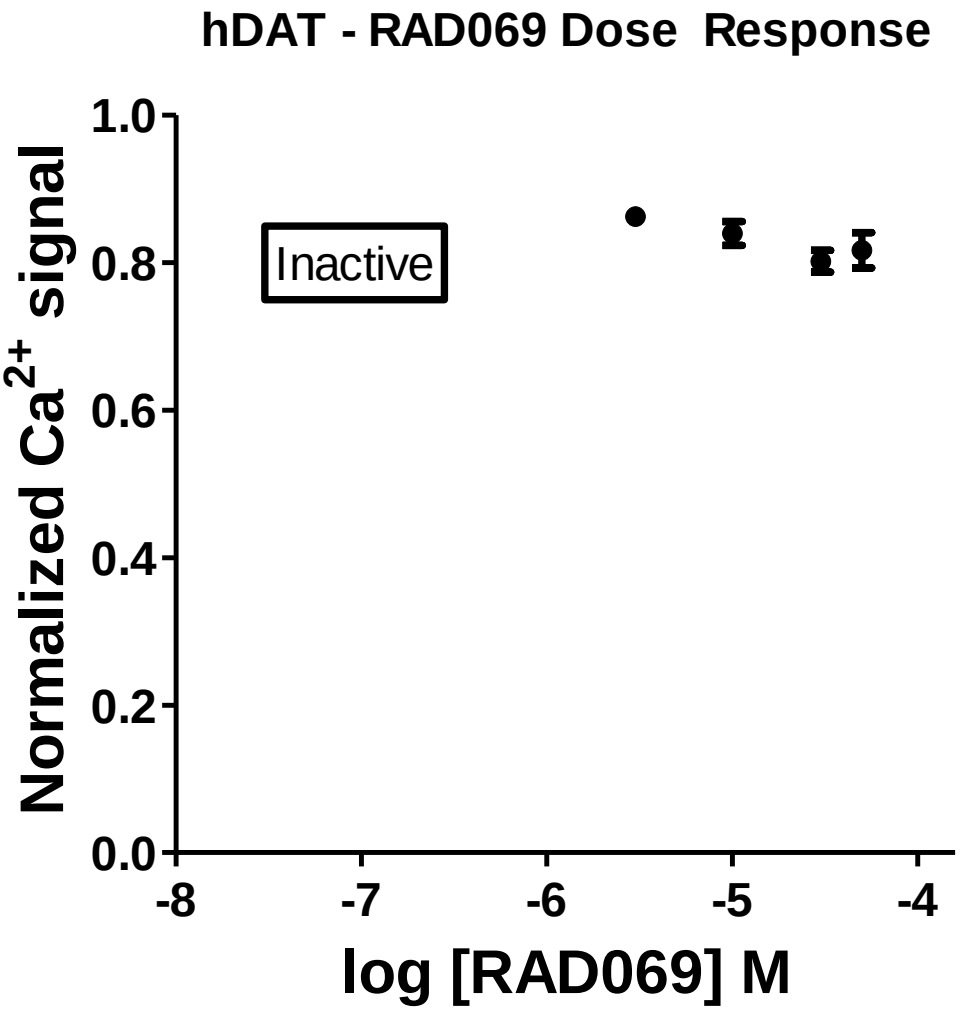

Figure 29: Dose versus response curve for RAD-069 at hDAT utilizing Fura-2 binding of calcium. Calcium entry is mediated by $Ca_V1.2$. Data displayed as the mean with standard error values.

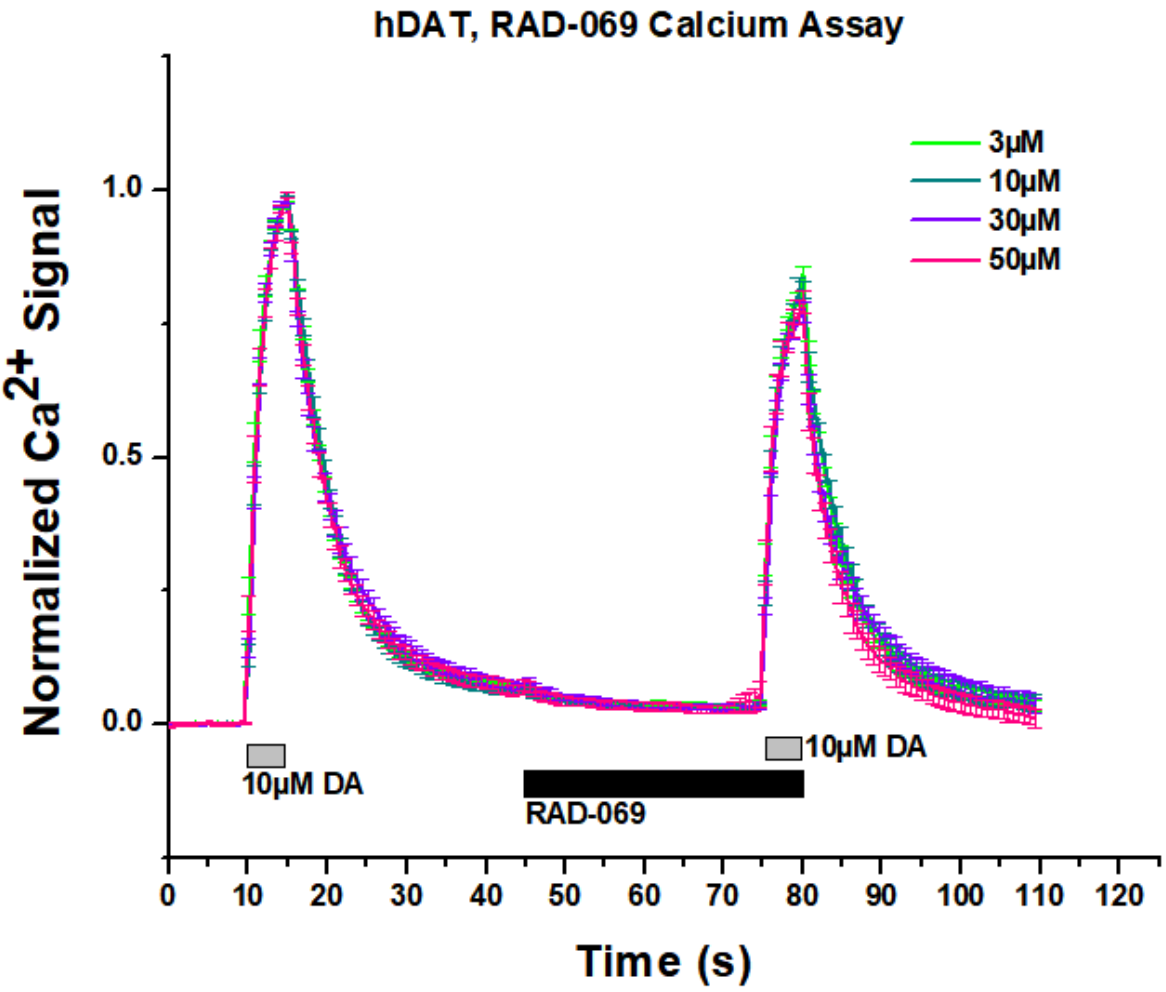

Figure 30: Cumulative calcium-fura-2 traces for RAD-081 at hDAT. Each concentration is represented by the mean of all cells assayed with standard error values. Signal represents calcium-fura-2 binding mediated by $Ca_V1.2$. Bars directly beneath trace represent perfusion of the indicated solution.

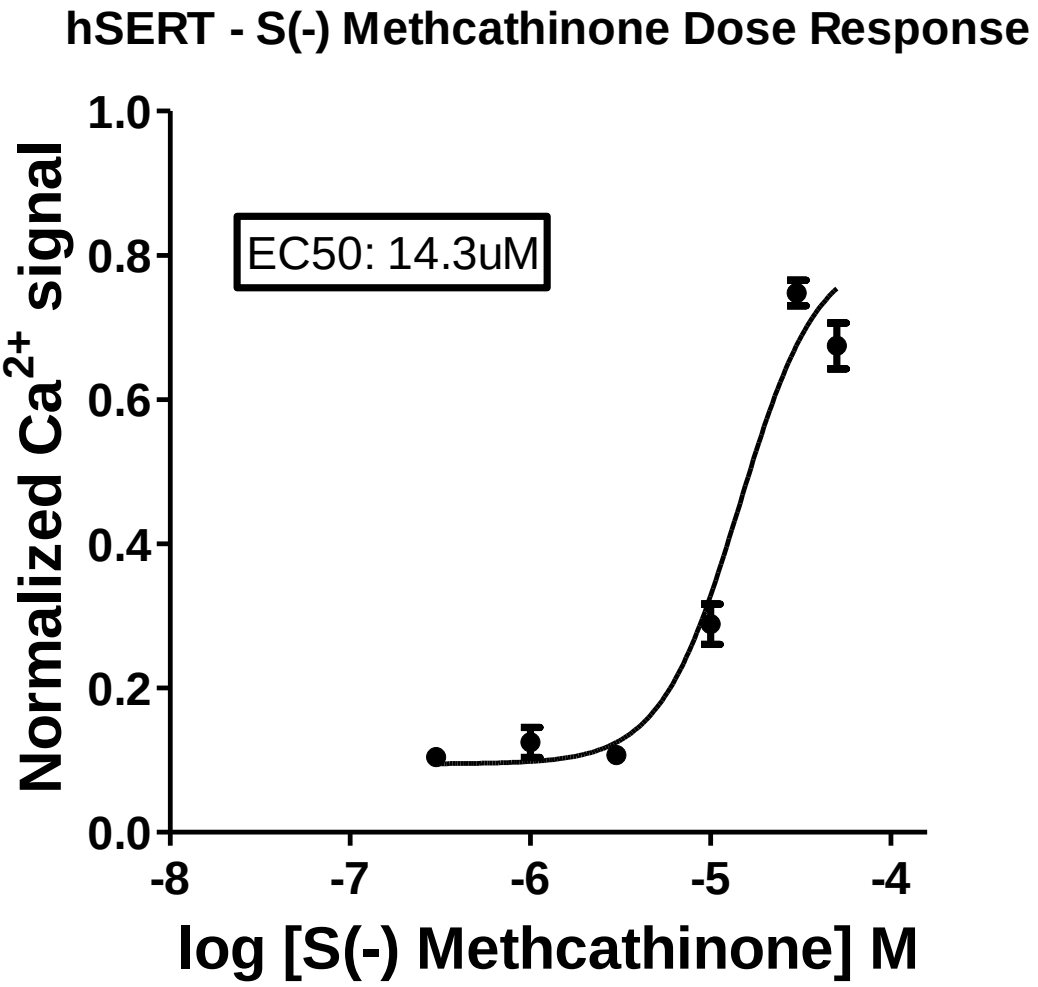

Figure 31: Dose versus response curve for S(-)methcathinone at hSERT utilizing Fura-2 binding of calcium. Calcium entry is mediated by $Ca_v1.2$. Data displayed as the mean with standard error values.

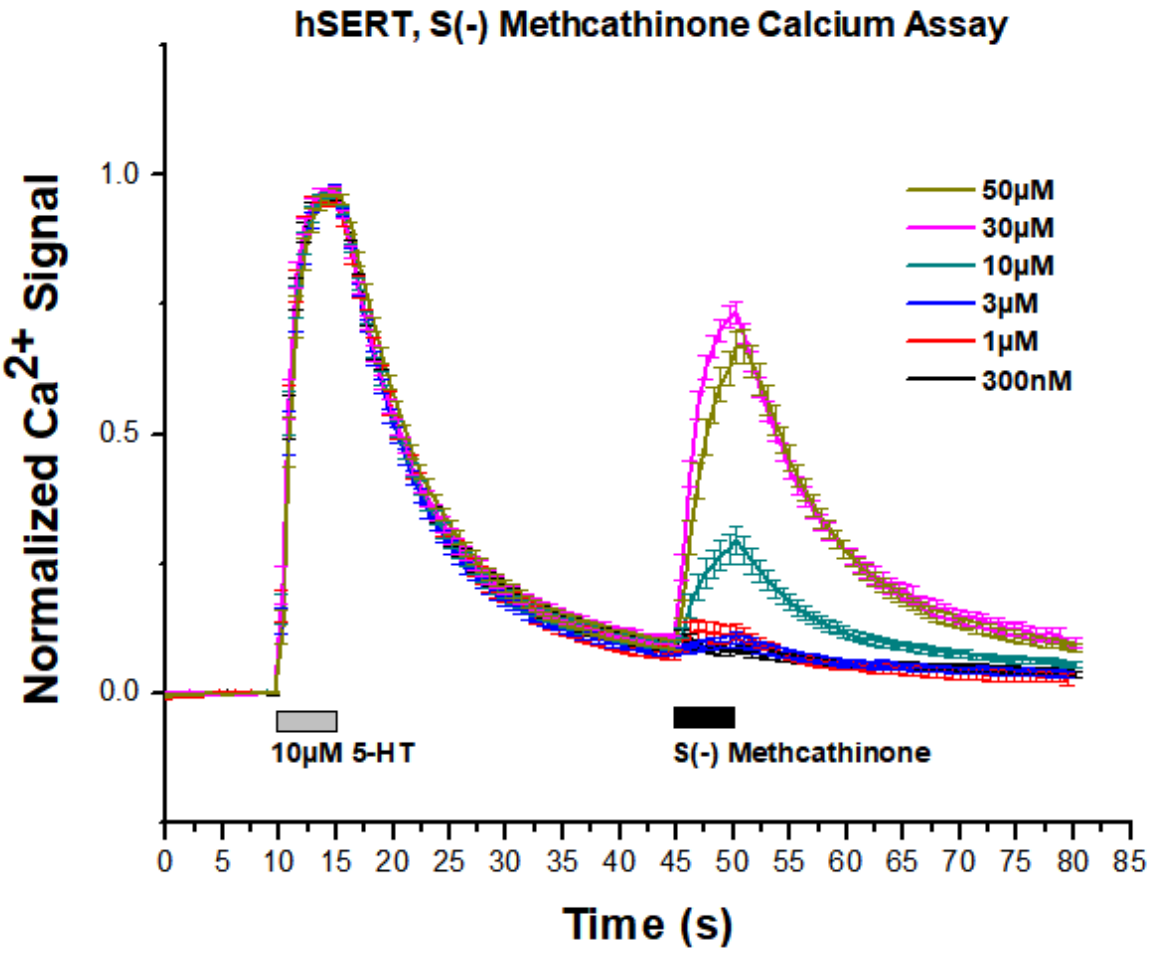

Figure 32: Cumulative calcium-fura-2 traces for S(-)methcathinone at hSERT. Each concentration is represented by the mean of all cells assayed with standard error values. Signal represents calcium-fura-2 binding mediated by $Ca_v1.2$. Bars directly beneath trace represent perfusion of the indicated solution.

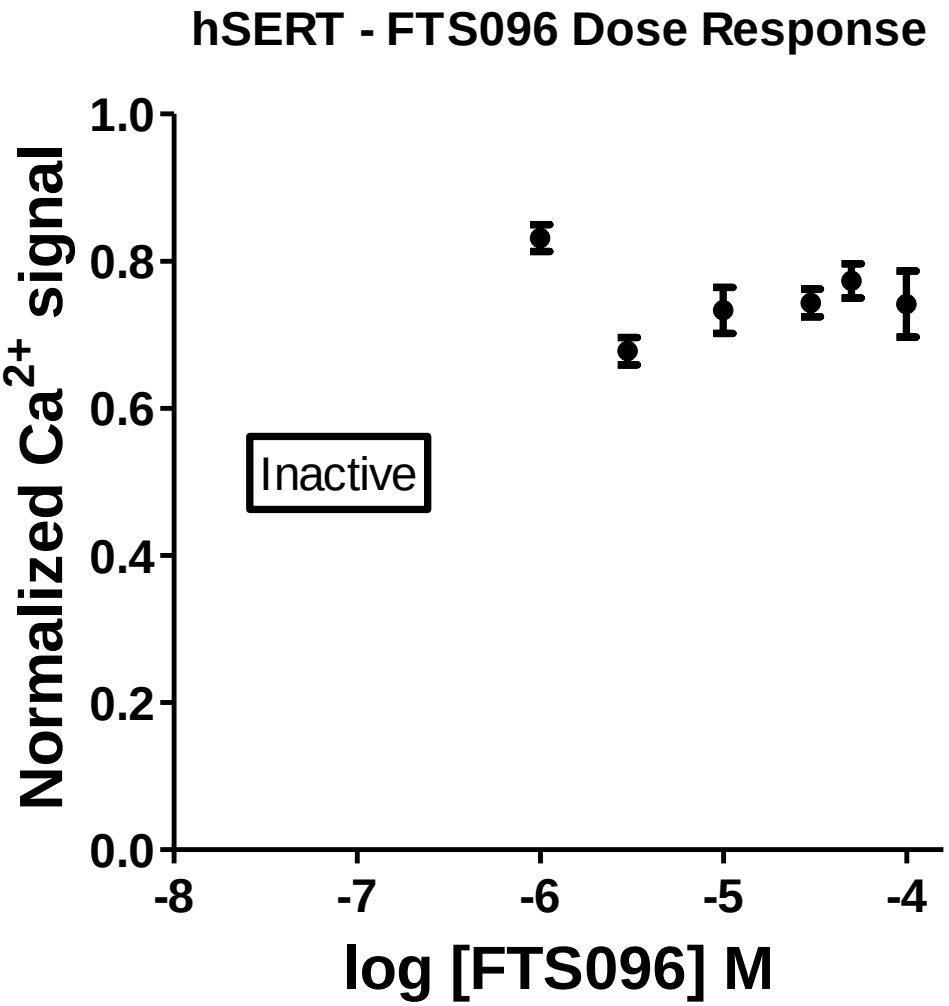

Figure 33: Dose versus response curve for FTS-096 at hSERT utilizing Fura-2 binding of calcium. Calcium entry is mediated by $Ca_v1.2$. Data displayed as the mean with standard error values.

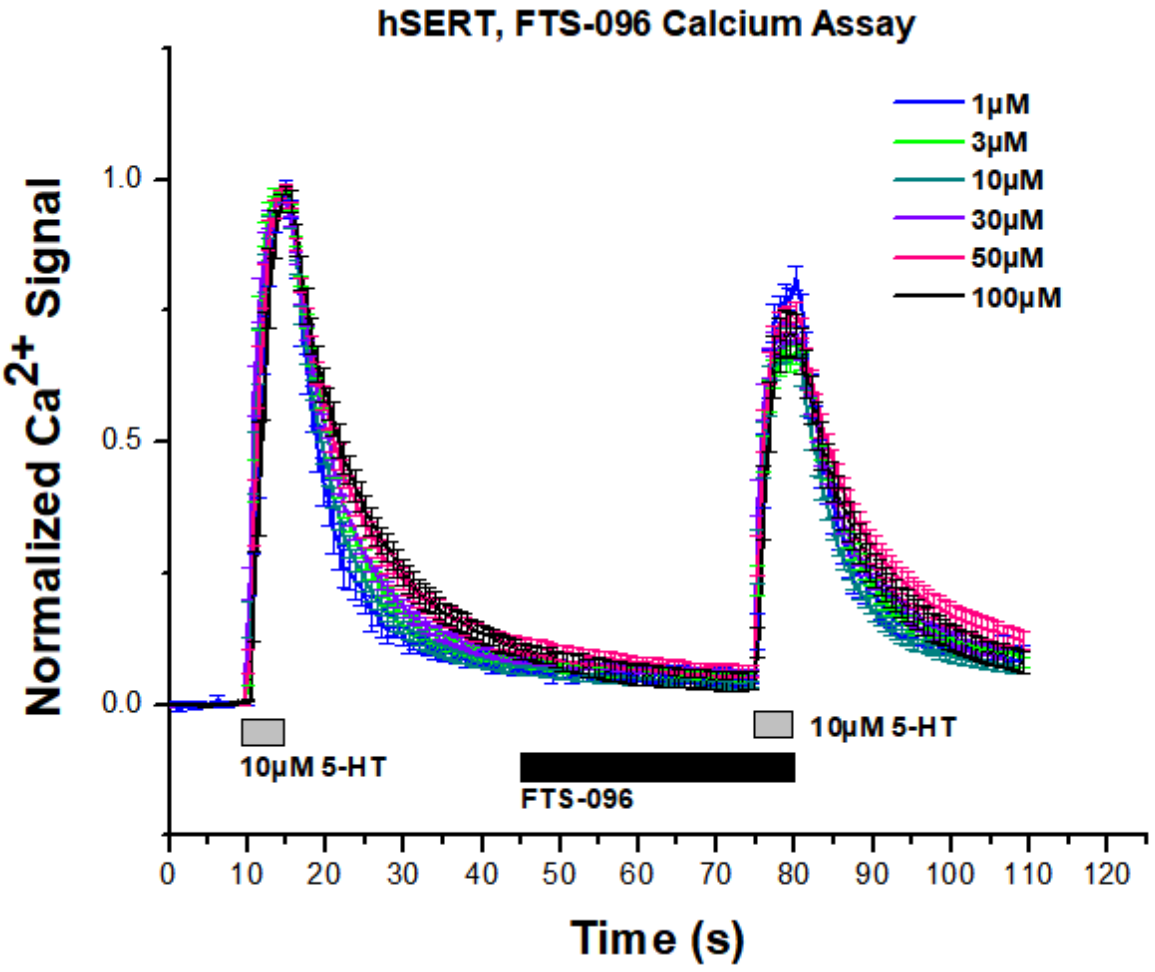

Figure 34: Cumulative calcium-fura-2 traces for FTS-096 at hSERT. Each concentration is represented by the mean of all cells assayed with standard error values. Signal represents calcium-fura-2 binding mediated by $Ca_v1.2$. Bars directly beneath trace represent perfusion of the indicated solution.

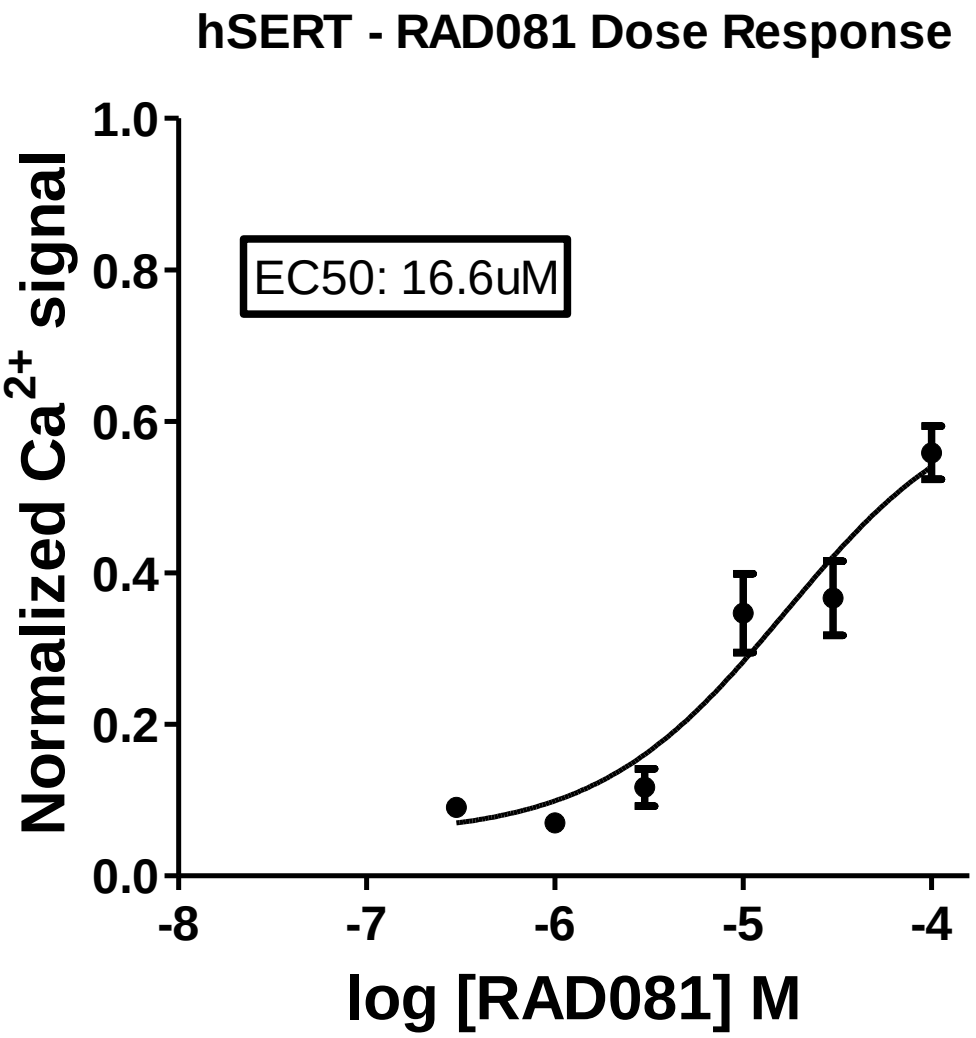

Figure 35: Dose versus response curve for RAD-081 at hSERT utilizing Fura-2 binding of calcium. Calcium entry is mediated by $Ca_v1.2$. Data displayed as the mean with standard error values.

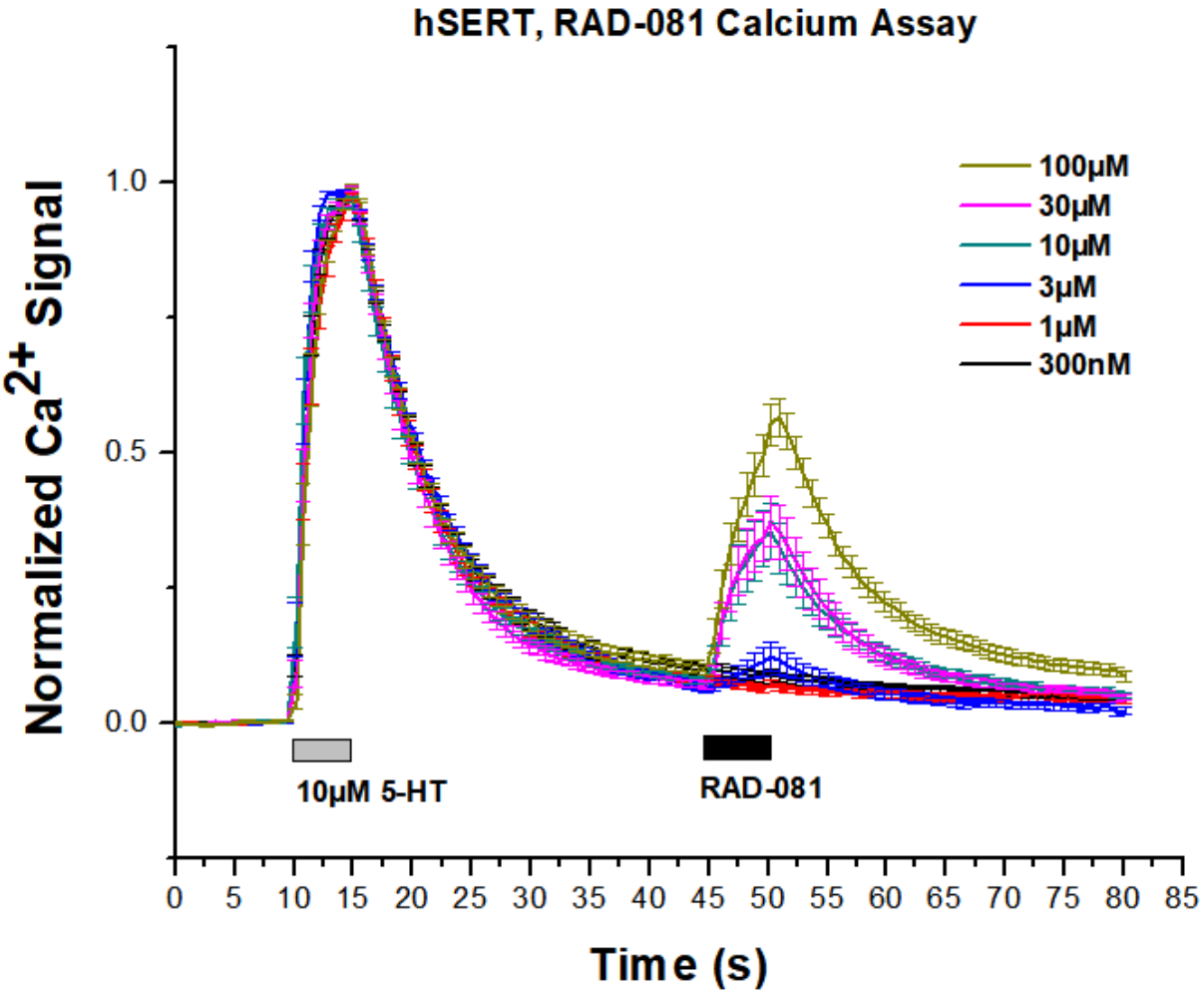

Figure 36: Cumulative calcium-fura-2 traces for RAD-081 at hSERT. Each concentration is represented by the mean of all cells assayed with standard error values. Signal represents calcium-fura-2 binding mediated by $Ca_V1.2$. Bars directly beneath trace represent perfusion of the indicated solution.

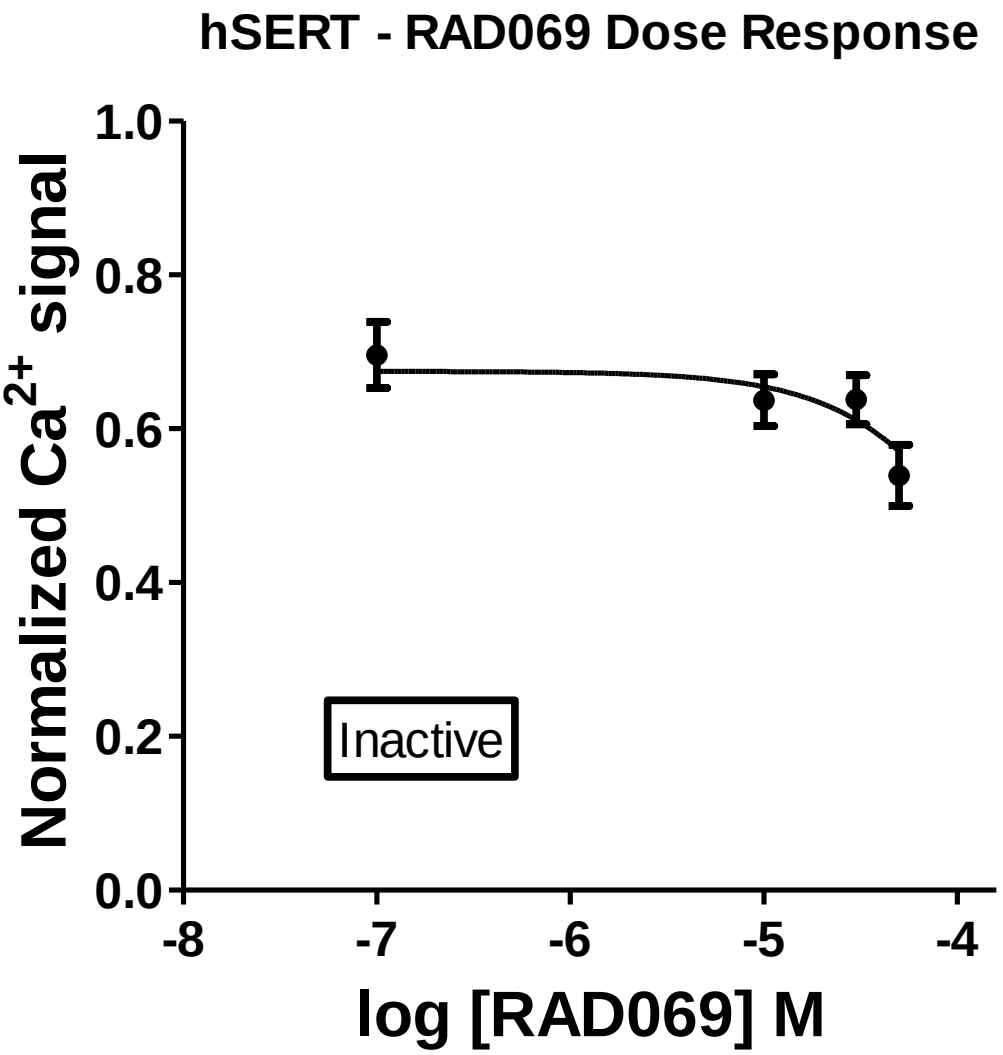

Figure 37: Dose versus response curve for RAD-0069 at hSERT utilizing Fura-2 binding of calcium. Calcium entry is mediated by $Ca_v1.2$. Data displayed as the mean with standard error values. Trials testing 10uM serotonin followed by a second pulse of 10uM serotonin were analyzed and placed above at x = -7 for comparison of experimental drug values to control as rundown of the serotonin signal is observed in these trials.

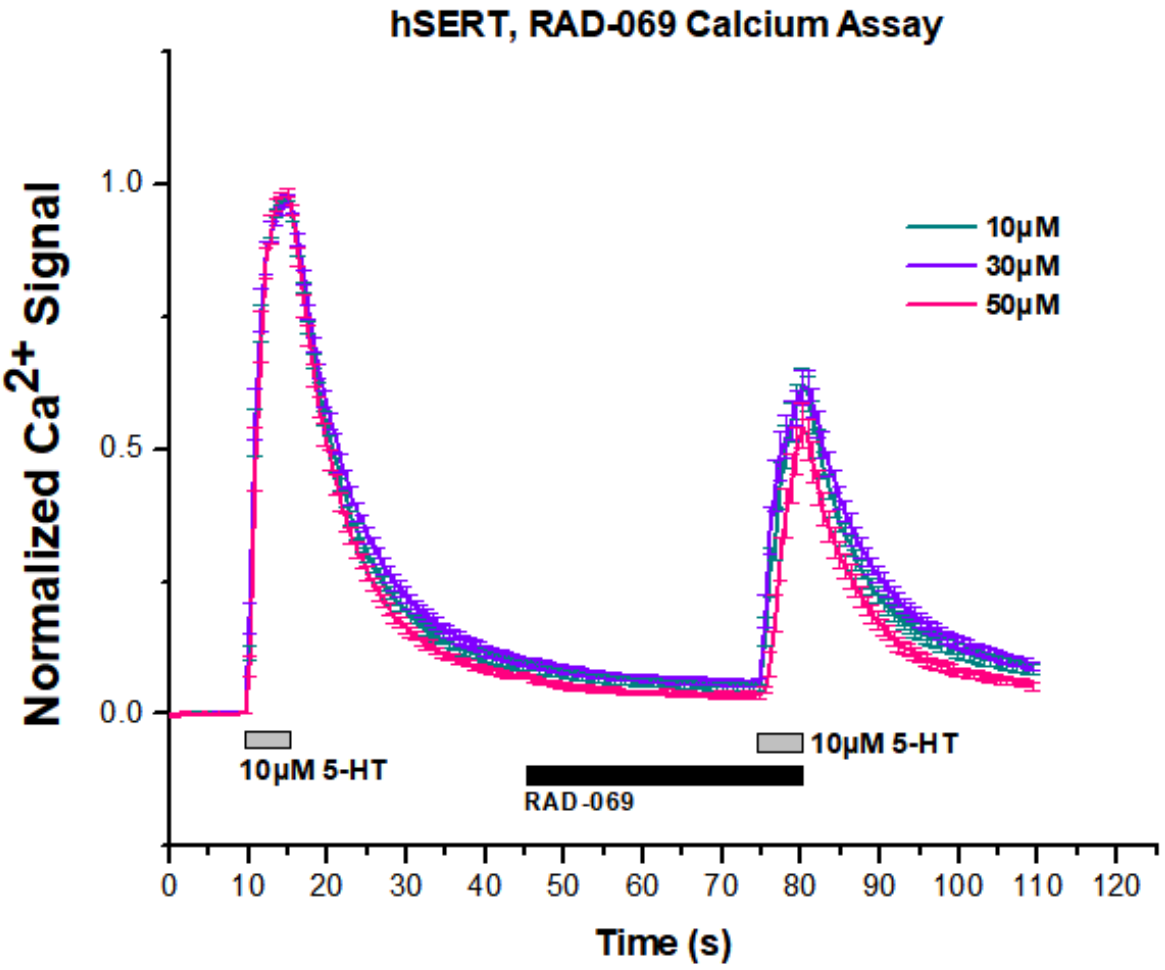

Figure 38: Cumulative calcium-fura-2 traces for RAD-069 at hSERT. Each concentration is represented by the mean of all cells assayed with standard error values. Signal represents calcium-fura-2 binding mediated by $Ca_V1.2$. Bars directly beneath trace represent perfusion of the indicated solution.

hDAT

Compound	EC50	Hill Slope	Maximum Efficacy Relative to 10µM Dopamine	N
FTS-096	3.13µM ± 0.29µM	1.666 ± 0.25	0.880 ± 0.028	20-43
S(-)methcathinone	289nM ± 19nM	1.714 ± 0.24	0.933 ± 0.028	32-53
RAD-081	1.04µM ± 0.06 µM	1.915 ± 0.22	0.967 ± 0.047	32-52
RAD-069	Inactive	--	--	25-44

Table 1: Fitting parameters for dose versus response curves for cathinone analogs at hDAT, displayed with ± standard error values. EC50 of FTS-096, RAD-081, and S(-)methcathinone are all statistically different from each other ($P<0.0001$, One-way Anova).

hSERT

Compound	EC50	Hill Slope	Maximum Efficacy Relative to 10µM Serotonin	N
FTS-096	Inactive	--	--	20-41
S(-)methcathinone	14.3µM ± 1.9µM	2.000*	0.748 ± 0.060	35-55
RAD-081	16.6µM ± 10µM	0.8751 ± 0.43	0.559 ± 0.035	21-39
RAD-069	Inactive	--	--	18-39

Table 2: Fitting parameters for dose versus response curves for cathinone analogs at hSERT, displayed with ± standard error values. EC50 of S(-)methcathinone and RAD-081 are not significantly different ($P<0.05$, Unpaired t test). *Hill Slope constrained to <2.000

DAT Selectivity

Compound	DAT Selectivity
FTS-096	>31.95
S(-)methcathinone	47.67
RAD-081	15.96

Table 3: DAT Selectivity is calculated as (hSERT EC50)/(hDAT EC50).

DISCUSSION

Previous studies have indicated that monoamine transporters and voltage-gated calcium channels can be electrically coupled in myotubes and in HEK cells. In these systems, substrate-induced current is sufficient to activate voltage-gated calcium channels and induce calcium influx (Cameron et al., 2015, Ruchala et al., 2014). Previous super resolution imaging using Structured Illumination Microscopy (SIM) technology and confocal imaging have suggested that while hDAT and $Ca_v1.2$ sort independently and occupy different regions of the plasma membrane, some colocalization exists (Harris, 2016). SIM super resolution microscopy is limited, however, to an approximately 100nm resolution limit, and protein-protein interactions such as hydrophobic interactions, hydrogen bonding, salt bridges, and π-stacking occur in the single-digit angstrom range (1 angstrom = 0.1nm) (Ferreira de Freitas & Schapira, 2017). To further put the scale into perspective, models suggest that $Ca_v1.2$ has a diameter of 9.0nm and hDAT has a diameter of 5.9nm (CalcTool, 2018). Clearly, direct protein-protein interactions occur in a range smaller than the threshold of super resolution. Taking into consideration the size of the proteins, super resolution can be suggestive of protein-protein interactions, but further biochemical analysis is needed to better solidify the relationship.

In the current study, fluorescent resonance energy transfer (FRET), which measures protein relationships at 10nm or less, is utilized to further define the

relationship of hDAT and $Ca_v1.2$ in live cells. Based on the FRET results, it is shown that compared to hDAT controls, the two mutants containing tetra-cysteine tags do undergo FRET and increase in fluorescence by 2% as compared to the negative control. Of note, this increase does represent a statistical difference from the control when running One-way Anova analysis. Interestingly, photobleaching studies in which both the FRET donor and acceptor are engineered to $Ca_v1.1$ have yielded FRET increases of 30% (Mahalingam, Perez et al., 2016). In comparison, the FRET value obtained in the hDAT/$Ca_v1.2$ experiments is less efficient. This result suggests several possibilities. For one, hDAT and Cav1.2 may in fact be colocalizing to just a small degree in the plasma membrane, as evidenced by prior super resolution (Harris, 2106). This small percentage of colocalization may reflect the small percentage of FRET. Second, the tetra-cysteine mutants may not be fully optimized for performing FRET.

Two factors are significant in promoting FRET, distance and relative fluorophore orientation. FRET studies which use two fluorescent proteins may experience distance issues in part due to the size of these proteins, approximately 4nm in diameter (CalcTool, 2018). Additionally, bulky fluorescent proteins can alter the function and trafficking of the protein under study (Polster, Ohrtman et al., 2012). The use of tetracysteine tags and ReAsH helps to limit this effect. The small tetracysteine tags used in the current study are comprised of 6 to 8 amino acid residues, most likely offering only minor changes to the normal protein conformation as compared to the effects of fused fluorescent proteins (Papadopoulos, Leuranguer et al., 2004, Polster et al., 2012). Based on the small percentage increase in fluorescence, it is also possible the relative distances between ReAsH and mVenus may be at or near the threshold

distance for FRET to occur. Variation in distance has been shown to alter FRET efficiency (Mahalingam et al., 2016). In addition to location of the fluorophores, orientation is important. Although this is more challenging to control and often computationally modeled, with its own limitations, (Loura, 2012), the synthesis and testing of additional locations of tetracysteine tags along the hDAT structure may yield better FRET efficiencies due to improved orientation.

Additionally, in the current study, it is apparent that the positive control, mVenus_hDAT_PolyC1 is not properly trafficking within the cell. Referring to Figure 18, it is clear that the fluorescence is diffuse and not well-localized to the membrane as seen in mVenus-Cav1.2 expressed in wild-type hDAT and hDAT_PolyC2 cells. The mVenus_hDAT_PolyC1 is likely trapped within the endoplasmic reticulum and ultimately undergoing cleavage in some manner. This could describe the diffuse fluorescence that is observed, which is similar to what is seen with soluble EGFP, the transfection marker in the calcium assay experiments. If such is the case, the low FRET efficiency of the positive control may be explained by the degradation of the protein, with a small proportion remaining intact in the ER at some point in time. An interesting comparison can be made between mVenus_hDAT_PolyC1 and hDAT_PolyC1. Based on hDAT_PolyC1 confocal images (Figure 13), this protein is strongly retained within the endoplasmic reticulum. These results suggest that the location of the tetracysteine tag on intracellular loop four may be interfering with targeting peptides and affecting trafficking mechanisms. Protein trafficking is highly reliant on sorting mechanisms guided by protein-innate targeting sequences, and disruption of these signals can lead to improper sorting or degradation (Bonifacino & Glick, 2004).

As opposed to utilizing mVenus_hDAT_PolyC1 in these experiments, engineering $Ca_v1.2$ to have both mVenus and the tetracysteine tag may prove to optimize the positive control. As previously mentioned, this was successfully achieved in studies concerning $Ca_v1.1$ (Mahalingam et al., 2016). The calcium channel is far larger than the dopamine transporter which could allow for better accommodation of bulky fluorophores, and it is known the fluorescent-tagging of the N-terminus of calcium channels has minimal effect on trafficking and function.

FRET has helped to further define the relationship between hDAT and $Ca_v1.2$ in HEK cells. Additional studies improving the positive control and testing alternative tetracysteine-tagged mutants will help to further optimize this experiment. The statistical difference between wild-type hDAT and the tetracysteine-tagged hDAT mutants is suggestive of possible interaction which brings these two proteins together in the low nanometer range between a subset of hDAT and $Ca_v1.2$ populations. Voltage-gated calcium channels have previously been shown to complex with other proteins in the membrane, such as $Ca_v1.2$ with β-adrenergic receptors in the mammalian heart, although specific interactions are yet to be determined and may involve other proteins (Davare, Avdonin et al., 2001). Additionally, N-type calcium channels are known to interact with SNARE protein complexes at the presynaptic terminal (Rettig et al., 1996, Sheng et al., 1994). Further, N-type calcium channels have been shown to interact directly with other membrane proteins, such as the opioid receptor ORL1, although the exact functional relationship is not fully understood (Corbani, Gonindard et al., 2004, Spampinato, Di Toro et al., 2002). Clearly, voltage-gated calcium channels interact with other proteins in a way to control function and/or regulation of processes. Given that

electrical coupling between monoamine transporters and $Ca_v1.2$ has been shown to occur in HEK cells (Cameron et al., 2015, Ruchala et al., 2014), a positive FRET result provides more evidence to support the concept of electrical coupling between the transporter and calcium channel. A similar relationship may occur in neurons, and immunostaining studies in neurons have shown that monoamine transporters and $Ca_v1.2$ channels are found on dendrites, soma, and axons (Eriksen, Rasmussen et al., 2009, Zhang, Fu et al., 2006). If the activity of the transporter can initiate calcium signals within neurons via $Ca_v1.2$ activation, the possible downstream effects are many and also dependent on the location on the neuron. For example, it has been shown that $Ca_v1.2$ activation on neuronal cell bodies and proximal dendrites regulates gene transcription through calmodulin (Bito, Deisseroth et al., 1996, Deisseroth, Heist et al., 1998) and calcineurin activation (Oliveria, Dell'Acqua et al., 2007). It is possible that there may be a link between monoamine transporter activity and gene regulation in neurons. Coupling of hDAT and $Ca_v1.2$ in vivo has not yet been studied and is a logical next step in further defining the role of these proteins in neurons.

The FRET results also have implications for the calcium assay itself. In conjunction with previous super resolution images, there is evidence that a subpopulation of dopamine transporters and calcium channels are colocalizing in the cell system utilized for the calcium assay. As previously described, there is a range of membrane potentials (approximately -30mV to -15mV) which activates $Ca_v1.2$ in this assay. Based on cross-comparisons between calcium signals generated with saturating substrate and I-V curves, it is evident that in this system the monoamine transporters are not depolarizing the membrane beyond approximately -15mV (Cameron et al.,

2015). This is shown by the inability of the system to activate $Ca_v2.2$. An important factor in electrical coupling in cells is the distance between the depolarization event and the target. In cells where tight coupling is essential, such as muscle cells and pace-making cells, voltage-channels and target proteins are mostly localized and form complexes, as seen with $Ca_v1.2$ and β-adrenergic receptors in cardiomyocytes (Davare et al., 2001). Similar functional arrangement in the calcium assay may result in excessive calcium channel activation, promoting a strong positive depolarization feedback that might compromise the utility of the method. As only a subpopulation of transporter and calcium channel appear to colocalize, it is possible that the system maintains greater control over how many calcium channels are activated in response to substrate-induced depolarization events, providing adequate sensitivity to produce reliable dose vs. response data for monoamine transporter substrates.

The relationship between monoamine transporters and voltage-gated calcium channels in HEK cells forms the foundation of the calcium assay, a quick and reliable tool for classifying the activity of compounds at hDAT, hSERT, and hNET. Legal and illegal drugs which interact with monoamine transporters are continually synthesized, and this tool provides an alternative method of pharmacological quantification which is quick, efficient, and does not require the use of animals. The current study of cathinone analogs adds to the growing set of drug data already collected utilizing this assay. Cathinones are known to exert similar stimulant effects as amphetamine, and as such have shown greater potency at the catecholamine transporters than at SERT (Bonano et al., 2015). High selectivity for DAT coupled with animal behavior studies, such as ICSS (Bonano et al., 2015) and locomotor activity with other functional assessments

(Marusich et al., 2014), have defined methcathinone, methamphetamine, MDPV, and α-PVP among many others as abuse liable.

The compounds under study relate to S(-)methcathinone, a potent CNS stimulant and DAT releaser, through removal and/or addition of methyl groups at the α-carbon. The structure completing the series relates to α-PPP due to the inclusion of a pyrrolidine group, which is found in a subset of known synthetic cathinones. Structural changes can affect binding affinity and cooperativity, which is described by the Hill slope. This concept is complex when applied to transporter mechanisms, as the protein binds different ligands (substrate and co-transport ions) and the transporter undergoes a multitude of conformational changes. Nonetheless, the Hill slope can provide insight to differences in affinity and transport. In comparing the Hill slope values in Tables 1 and 2, all range from 1.5-2 except for RAD-081 at hSERT, which has a Hill slope of 0.8751. This suggests that RAD-081 exhibits reduced cooperativity at hSERT in its transport process as compared to the other experimental conditions. The structural difference of RAD-081 may be influencing binding of itself or its cotransport ions at the binding pocket of hSERT, and possibly affecting the transport mechanism.

As described in the introduction, much research points to alterations of dopaminergic signaling as one of the primary factors in facilitating abuse and addiction. The compounds from the current study show greater preference for hDAT over hSERT as substrates (excluding RAD-069 as it is inactive at both), which in itself may be a significant finding. Compounds with comparatively higher hDAT potency to hSERT potency ratios are shown to have more abuse liability as previously mentioned. Other factors in this regard are significant, such as drug metabolism and ability to cross the

blood-brain barrier, but nonetheless determining a compound's pharmacodynamics at hDAT can help to screen and quickly identify potential culprits of psychostimulant abuse. Further, the addition of a methyl group to the α-carbon of S(-)methcathinone causes a shift in EC50 from approximately 300nM to 1uM in the calcium assay, making RAD-081 three times less potent than S(-)methcathinone at hDAT. Previous synaptosome release studies have shown that S(-)methcathinone releases dopamine with an EC50 of 15nM (Rothman et al., 2003). As results from the calcium assay and synaptosomal release/uptake studies have been strongly correlated (Solis et al., 2017), RAD-081 in this same release study would hypothetically yield an EC50 result around 45nM. When compared to dopamine-induced dopamine release in synaptosomes (EC50 = 90nM), RAD-081 would be essentially twice as potent as dopamine. Coupled with a high DAT to SERT ratio of 15.96, these results suggest that RAD-081 may have abuse potential. In comparison to S(-)methcathinone and RAD-081, FTS-096 is less potent at hDAT, suggesting that the α-methyl group is significant to binding and potency at the monoamine transporters. Interestingly, FTS-096 exhibits a DAT to SERT ratio of >31.95, suggesting that this compound may have higher abuse liability than RAD-081, although the DAT selectivity values for both are less than that of S(-)methcathinone (Table 3). Additional characterization studies are needed to further define this comparison.

The final compound of the study, RAD-069, is deemed inactive at both hDAT and hSERT, although at high concentration (50µM) there may be a weak blocking effect in hSERT. α-PPP is also weak at hSERT (3000nM in synaptosomes uptake inhibition), thus the structural change between the two compounds does not appear to influence

activity at SERT. Interestingly, α-PPP is a known uptake inhibitor at hDAT, and in comparison to RAD-069 it appears that the addition of a second methyl group to the α-carbon reduces potency as a DAT blocker.

Additionally, the potency of RAD-081 is significant from the standpoint of future synthesis of novel compounds and structural-activity relationship studies. The addition of the methyl group to the α-carbon removes the chiral center and generates a compound that is still more potent than dopamine. With this achiral backbone, compounds with modifications made to the β-carbon can be synthesized and characterized more efficiently. Methylphenidate, a well-known CNS stimulant and DAT inhibitor (Schweri, Skolnick et al., 1985) used to treat attention deficit hyperactivity disorder (Millichap, 1973), is one example of monoamine transporter ligands which are known to have functional groups extending from the β-carbon. It is possible that similar modifications to cathinones may produce compounds that are potent at the monoamine transporters, and continued use of the transporter-calcium channel coupling in the calcium assay will help to efficiently quantify the pharmacological effects of these potentially abusable compounds.

LIST OF REFERENCES

LIST OF REFERENCES

Ahlijanian MK, Westenbroek RE, Catterall WA (1990) Subunit structure and localization of dihydropyridine-sensitive calcium channels in mammalian brain, spinal cord, and retina. *Neuron* 4: 819-32

Banjaw MY, Miczek K, Schmidt WJ (2006) Repeated Catha edulis oral administration enhances the baseline aggressive behavior in isolated rats. *J Neural Transm (Vienna)* 113: 543-56

Baumann MH, Partilla JS, Lehner KR, Thorndike EB, Hoffman AF, Holy M, Rothman RB, Goldberg SR, Lupica CR, Sitte HH, Brandt SD, Tella SR, Cozzi NV, Schindler CW (2013) Powerful cocaine-like actions of 3,4-methylenedioxypyrovalerone (MDPV), a principal constituent of psychoactive 'bath salts' products. *Neuropsychopharmacology* 38: 552-62

Benarroch EE (2009) The locus ceruleus norepinephrine system: functional organization and potential clinical significance. *Neurology* 73: 1699-704

Berridge MJ, Lipp P, Bootman MD (2000) The versatility and universality of calcium signalling. *Nat Rev Mol Cell Biol* 1: 11-21

Bett WR (1946) Benzedrine sulphate in clinical medicine; a survey of the literature. *Postgrad Med J* 22: 205-18

Bito H, Deisseroth K, Tsien RW (1996) CREB phosphorylation and dephosphorylation: a Ca(2+)- and stimulus duration-dependent switch for hippocampal gene expression. *Cell* 87: 1203-14

Bjorklund A, Dunnett SB (2007) Dopamine neuron systems in the brain: an update. *Trends Neurosci* 30: 194-202

Bonano JS, Banks ML, Kolanos R, Sakloth F, Barnier ML, Glennon RA, Cozzi NV, Partilla JS, Baumann MH, Negus SS (2015) Quantitative structure-activity relationship analysis of the pharmacology of para-substituted methcathinone analogues. *Br J Pharmacol* 172: 2433-44

Bonifacino JS, Glick BS (2004) The mechanisms of vesicle budding and fusion. *Cell* 116: 153-66

Branch SY, Beckstead MJ (2012) Methamphetamine produces bidirectional, concentration-dependent effects on dopamine neuron excitability and dopamine-mediated synaptic currents. *J Neurophysiol* 108: 802-9

Broer S (2006) The SLC6 orphans are forming a family of amino acid transporters. *Neurochem Int* 48: 559-67

Cameron KN, Kolanos R, Solis E, Jr., Glennon RA, De Felice LJ (2013) Bath salts components mephedrone and methylenedioxypyrovalerone (MDPV) act synergistically at the human dopamine transporter. *Br J Pharmacol* 168: 1750-7

Cameron KN, Solis E, Jr., Ruchala I, De Felice LJ, Eltit JM (2015) Amphetamine activates calcium channels through dopamine transporter-mediated depolarization. *Cell Calcium* 58: 457-66

Catterall WA (2011) Voltage-gated calcium channels. *Cold Spring Harb Perspect Biol* 3: a003947

Catterall WA, Perez-Reyes E, Snutch TP, Striessnig J (2005) International Union of Pharmacology. XLVIII. Nomenclature and structure-function relationships of voltage-gated calcium channels. *Pharmacol Rev* 57: 411-25

Chang JM, Di Tommaso P, Taly JF, Notredame C (2012) Accurate multiple sequence alignment of transmembrane proteins with PSI-Coffee. *BMC Bioinformatics* 13 Suppl 4: S1

Chen NH, Reith ME, Quick MW (2004) Synaptic uptake and beyond: the sodium- and chloride-dependent neurotransmitter transporter family SLC6. *Pflugers Arch* 447: 519-31

Clapham DE (2007) Calcium signaling. *Cell* 131: 1047-58

Corbani M, Gonindard C, Meunier JC (2004) Ligand-regulated internalization of the opioid receptor-like 1: a confocal study. *Endocrinology* 145: 2876-85

Crow TJ (1973) Catecholamine-containing neurones and electrical self-stimulation. 2. A theoretical interpretation and some psychiatric implications. *Psychol Med* 3: 66-73

Curtis BM, Catterall WA (1984) Purification of the calcium antagonist receptor of the voltage-sensitive calcium channel from skeletal muscle transverse tubules. *Biochemistry* 23: 2113-8

Curtis BM, Catterall WA (1986) Reconstitution of the voltage-sensitive calcium channel purified from skeletal muscle transverse tubules. *Biochemistry* 25: 3077-83

Davare MA, Avdonin V, Hall DD, Peden EM, Burette A, Weinberg RJ, Horne MC, Hoshi T, Hell JW (2001) A beta2 adrenergic receptor signaling complex assembled with the Ca2+ channel Cav1.2. *Science* 293: 98-101

DeFelice LJ, Adams SV, Ypey DL (2001) Single-file diffusion and neurotransmitter transporters: Hodgkin and Keynes model revisited. *Biosystems* 62: 57-66

DeRuiter J, Hayes L, Valaer A, Clarke CR (1994) Methcathinone and designer analogues: synthesis, stereochemical analysis, and analytical properties. *J Chromatogr Sci* 32: 552-564

Deisseroth K, Heist EK, Tsien RW (1998) Translocation of calmodulin to the nucleus supports CREB phosphorylation in hippocampal neurons. *Nature* 392: 198-202

Di Biase V, Obermair GJ, Szabo Z, Altier C, Sanguesa J, Bourinet E, Flucher BE (2008) Stable membrane expression of postsynaptic CaV1.2 calcium channel clusters is independent of interactions with AKAP79/150 and PDZ proteins. *J Neurosci* 28: 13845-55

Dojindo Molecular Technologies, Inc. (2018) Fura-2 mechanism image. https://www.dojindo.com/store/p/545-Fura-2-AM.html

Dong H, Jiang Y, Triggle CR, Li X, Lytton J (2006) Novel role for K+-dependent Na+/Ca2+ exchangers in regulation of cytoplasmic free Ca2+ and contractility in arterial smooth muscle. *Am J Physiol Heart Circ Physiol* 291: H1226-35

Eriksen J, Rasmussen SG, Rasmussen TN, Vaegter CB, Cha JH, Zou MF, Newman AH, Gether U (2009) Visualization of dopamine transporter trafficking in live neurons by use of fluorescent cocaine analogs. *J Neurosci* 29: 6794-808

Ertel EA, Campbell KP, Harpold MM, Hofmann F, Mori Y, Perez-Reyes E, Schwartz A, Snutch TP, Tanabe T, Birnbaumer L, Tsien RW, Catterall WA (2000) Nomenclature of voltage-gated calcium channels. *Neuron* 25: 533-5

Ferreira de Freitas R, Schapira M (2017) A systematic analysis of atomic protein-ligand interactions in the PDB. *Medchemcomm* 8: 1970-1981

Fog JU, Khoshbouei H, Holy M, Owens WA, Vaegter CB, Sen N, Nikandrova Y, Bowton E, McMahon DG, Colbran RJ, Daws LC, Sitte HH, Javitch JA, Galli A, Gether U (2006) Calmodulin kinase II interacts with the dopamine transporter C terminus to regulate amphetamine-induced reverse transport. *Neuron* 51: 417-29

Galli A, Blakely RD, DeFelice LJ (1996) Norepinephrine transporters have channel modes of conduction. *Proc Natl Acad Sci U S A* 93: 8671-6

Galli A, DeFelice LJ, Duke BJ, Moore KR, Blakely RD (1995) Sodium-dependent norepinephrine-induced currents in norepinephrine-transporter-transfected HEK-293 cells blocked by cocaine and antidepressants. *J Exp Biol* 198: 2197-212

Giros B, Jaber M, Jones SR, Wightman RM, Caron MG (1996) Hyperlocomotion and indifference to cocaine and amphetamine in mice lacking the dopamine transporter. *Nature* 379: 606-12

Glennon RA, Dukat M (2017) Synthetic Cathinones: A brief overview of overviews with application to the forensic sciences. *Ann Forensic Res Anal* 4(2): 1040

Grynkiewicz G, Poenie M, Tsien RY (1985) A new generation of Ca2+ indicators with greatly improved fluorescence properties. *J Biol Chem* 260: 3440-50

Gu H, Wall SC, Rudnick G (1994) Stable expression of biogenic amine transporters reveals differences in inhibitor sensitivity, kinetics, and ion dependence. *J Biol Chem* 269: 7124-30

Gugelmann R, von Allmen M, Brenneisen R, Porzig H (1985) Quantitative differences in the pharmacological effects of (+)- and (-)-cathinone. *Experientia* 41: 1568-71

Guttmann E, Sargant W (1937) Observations on Benzedrine. *Br Med J* 1: 1013-5
Heal DJ, Smith SL, Findling RL (2012) ADHD: current and future therapeutics. *Curr Top Behav Neurosci* 9: 361-90

Harris AC, Unpublished Super Resolution Image (2016) VCU Department of Physiology and Biophysics

Heal DJ, Smith SL, Gosden J, Nutt DJ (2013) Amphetamine, past and present--a pharmacological and clinical perspective. *J Psychopharmacol* 27: 479-96

Heikkila RE, Orlansky H, Mytilineou C, Cohen G (1975) Amphetamine: evaluation of d- and l-isomers as releasing agents and uptake inhibitors for 3H-dopamine and 3H-norepinephrine in slices of rat neostriatum and cerebral cortex. *J Pharmacol Exp Ther* 194: 47-56

Hersch SM, Yi H, Heilman CJ, Edwards RH, Levey AI (1997) Subcellular localization and molecular topology of the dopamine transporter in the striatum and substantia nigra. *J Comp Neurol* 388: 211-27

Hoebel BG, Monaco AP, Hernandez L, Aulisi EF, Stanley BG, Lenard L (1983) Self-injection of amphetamine directly into the brain. *Psychopharmacology (Berl)* 81: 158-63

Hoglund PJ, Adzic D, Scicluna SJ, Lindblom J, Fredriksson R (2005) The repertoire of solute carriers of family 6: identification of new human and rodent genes. *Biochem Biophys Res Commun* 336: 175-89

Hyde JF, Browning E, Adams R (1928) Synthetic homologsof d,l-ephedrine. *J Am Chem Soc* 50: 2287

Ingram SL, Prasad BM, Amara SG (2002) Dopamine transporter-mediated conductances increase excitability of midbrain dopamine neurons. *Nat Neurosci* 5: 971-8

Ito R, Dalley JW, Robbins TW, Everitt BJ (2002) Dopamine release in the dorsal striatum during cocaine-seeking behavior under the control of a drug-associated cue. *J Neurosci* 22: 6247-53

Jacobs BL, Azmitia EC (1992) Structure and function of the brain serotonin system. *Physiol Rev* 72: 165-229

Jardetzky O (1966) Simple allosteric model for membrane pumps. *Nature* 211: 969-70

Jones SR, Gainetdinov RR, Jaber M, Giros B, Wightman RM, Caron MG (1998a) Profound neuronal plasticity in response to inactivation of the dopamine transporter. *Proc Natl Acad Sci U S A* 95: 4029-34

Jones SR, Gainetdinov RR, Wightman RM, Caron MG (1998b) Mechanisms of amphetamine action revealed in mice lacking the dopamine transporter. *J Neurosci* 18: 1979-86

Karpowicz RJ, Jr., Dunn M, Sulzer D, Sames D (2013) APP+, a fluorescent analogue of the neurotoxin MPP+, is a marker of catecholamine neurons in brain tissue, but not a fluorescent false neurotransmitter. *ACS Chem Neurosci* 4: 858-69

Kolanos R, Sakloth F, Jain AD, Partilla JS, Baumann MH, Glennon RA (2015) Structural Modification of the Designer Stimulant alpha-Pyrrolidinovalerophenone (alpha-PVP) Influences Potency at Dopamine Transporters. *ACS Chem Neurosci* 6: 1726-31

Koob G, Kreek MJ (2007) Stress, dysregulation of drug reward pathways, and the transition to drug dependence. *Am J Psychiatry* 164: 1149-59

Koob GF (2008) A role for brain stress systems in addiction. *Neuron* 59: 11-34

Koob GF, Volkow ND (2010) Neurocircuitry of addiction. *Neuropsychopharmacology* 35: 217-38

Krikorian AD (1984) Kat and its use: an historical perspective. *J Ethnopharmacol* 12: 115-78

Liu Y, Harding M, Pittman A, Dore J, Striessnig J, Rajadhyaksha A, Chen X (2014) Cav1.2 and Cav1.3 L-type calcium channels regulate dopaminergic firing activity in the mouse ventral tegmental area. *J Neurophysiol* 112: 1119-30

Loura LM (2012) Simple estimation of Forster Resonance Energy Transfer (FRET) orientation factor distribution in membranes. *Int J Mol Sci* 13: 15252-70

Ma H, Cohen S, Li B, Tsien RW (2012) Exploring the dominant role of Cav1 channels in signalling to the nucleus. *Biosci Rep* 33: 97-101

Madras BK (2017) The Growing Problem of New Psychoactive Substances (NPS). *Curr Top Behav Neurosci* 32: 1-18

Mahalingam M, Perez CF, Fessenden JD (2016) Fluorescence Resonance Energy Transfer-based Structural Analysis of the Dihydropyridine Receptor alpha1S Subunit Reveals Conformational Differences Induced by Binding of the beta1a Subunit. *J Biol Chem* 291: 13762-70

Mantle TJ, Tipton KF, Garrett NJ (1976) Inhibition of monoamine oxidase by amphetamine and related compounds. *Biochem Pharmacol* 25: 2073-7

Marusich JA, Antonazzo KR, Wiley JL, Blough BE, Partilla JS, Baumann MH (2014) Pharmacology of novel synthetic stimulants structurally related to the "bath salts" constituent 3,4-methylenedioxypyrovalerone (MDPV). *Neuropharmacology* 87: 206-13

McClernon FJ, Kozink RV, Lutz AM, Rose JE (2009) 24-h smoking abstinence potentiates fMRI-BOLD activation to smoking cues in cerebral cortex and dorsal striatum. *Psychopharmacology (Berl)* 204: 25-35

McGregor A, Roberts DC (1993) Dopaminergic antagonism within the nucleus accumbens or the amygdala produces differential effects on intravenous cocaine self-administration under fixed and progressive ratio schedules of reinforcement. *Brain Res* 624: 245-52

Miller HH, Shore PA, Clarke DE (1980) In vivo monoamine oxidase inhibition by d-amphetamine. *Biochem Pharmacol* 29: 1347-54

Millichap JG (1973) Drugs in management of minimal brain dysfunction. *Ann N Y Acad Sci* 205: 321-34

Mochida S, Sheng ZH, Baker C, Kobayashi H, Catterall WA (1996) Inhibition of neurotransmission by peptides containing the synaptic protein interaction site of N-type Ca2+ channels. *Neuron* 17: 781-8

Nanoprobes, Inc. (2006) ReAsH mechanism image. Localization and Role of HLA-G Nanoprobes E-News, Vol7, No 6

Nicosia N, Liccardo Pacula R, Kilmer B, Lundberg R, Chiesa J (2009) The economic cost of methamphetamine use in the United States. *RAND Corporation, MG-829-MPF/NIDA:* 1-171

Oliveria SF, Dell'Acqua ML, Sather WA (2007) AKAP79/150 anchoring of calcineurin controls neuronal L-type Ca2+ channel activity and nuclear signaling. *Neuron* 55: 261-75

Papadopoulos S, Leuranguer V, Bannister RA, Beam KG (2004) Mapping sites of potential proximity between the dihydropyridine receptor and RyR1 in muscle using a cyan fluorescent protein-yellow fluorescent protein tandem as a fluorescence resonance energy transfer probe. *J Biol Chem* 279: 44046-56

Perez-Reyes E, Kim HS, Lacerda AE, Horne W, Wei XY, Rampe D, Campbell KP, Brown AM, Birnbaumer L (1989) Induction of calcium currents by the expression of the alpha 1-subunit of the dihydropyridine receptor from skeletal muscle. *Nature* 340: 233-6

Polster A, Ohrtman JD, Beam KG, Papadopoulos S (2012) Fluorescence resonance energy transfer (FRET) indicates that association with the type I ryanodine receptor (RyR1) causes reorientation of multiple cytoplasmic domains of the dihydropyridine receptor (DHPR) alpha(1S) subunit. *J Biol Chem* 287: 41560-8

Rettig J, Heinemann C, Ashery U, Sheng ZH, Yokoyama CT, Catterall WA, Neher E (1997) Alteration of Ca2+ dependence of neurotransmitter release by disruption of Ca2+ channel/syntaxin interaction. *J Neurosci* 17: 6647-56

Rettig J, Sheng ZH, Kim DK, Hodson CD, Snutch TP, Catterall WA (1996) Isoform-specific interaction of the alpha1A subunits of brain Ca2+ channels with the presynaptic proteins syntaxin and SNAP-25. *Proc Natl Acad Sci U S A* 93: 7363-8

Reuter H (1979) Properties of two inward membrane currents in the heart. *Annu Rev Physiol* 41: 413-24

Robertson SD, Matthies HJ, Galli A (2009) A closer look at amphetamine-induced reverse transport and trafficking of the dopamine and norepinephrine transporters. *Mol Neurobiol* 39: 73-80

Robinson JB (1985) Stereoselectivity and isoenzyme selectivity of monoamine oxidase inhibitors. Enantiomers of amphetamine, N-methylamphetamine and deprenyl. *Biochem Pharmacol* 34: 4105-8

Rothman RB, Baumann MH, Dersch CM, Romero DV, Rice KC, Carroll FI, Partilla JS (2001) Amphetamine-type central nervous system stimulants release norepinephrine more potently than they release dopamine and serotonin. *Synapse* 39: 32-41

Rothman RB, Vu N, Partilla JS, Roth BL, Hufeisen SJ, Compton-Toth BA, Birkes J, Young R, Glennon RA (2003) In vitro characterization of ephedrine-related stereoisomers at biogenic amine transporters and the receptorome reveals selective actions as norepinephrine transporter substrates. *J Pharmacol Exp Ther* 307: 138-45

Ruchala I, Cabra V, Solis E, Jr., Glennon RA, De Felice LJ, Eltit JM (2014) Electrical coupling between the human serotonin transporter and voltage-gated Ca(2+) channels. *Cell Calcium* 56: 25-33

Rudnick G, Nelson PJ (1978) Platelet 5-hydroxytryptamine transport, an electroneutral mechanism coupled to potassium. *Biochemistry* 17: 4739-42

Sakloth F, Kolanos R, Mosier PD, Bonano JS, Banks ML, Partilla JS, Baumann MH, Negus SS, Glennon RA (2015) Steric parameters, molecular modeling and hydropathic interaction analysis of the pharmacology of para-substituted methcathinone analogues. *Br J Pharmacol* 172: 2210-8

Salamone JD, Correa M, Farrar A, Mingote SM (2007) Effort-related functions of nucleus accumbens dopamine and associated forebrain circuits. *Psychopharmacology (Berl)* 191: 461-82

Scholze P, Zwach J, Kattinger A, Pifl C, Singer EA, Sitte HH (2000) Transporter-mediated release: a superfusion study on human embryonic kidney cells stably expressing the human serotonin transporter. *J Pharmacol Exp Ther* 293: 870-8

Schweri MM, Skolnick P, Rafferty MF, Rice KC, Janowsky AJ, Paul SM (1985) [3H]Threo-(+/-)-methylphenidate binding to 3,4-dihydroxyphenylethylamine uptake sites in corpus striatum: correlation with the stimulant properties of ritalinic acid esters. *J Neurochem* 45: 1062-70

Seidel S, Singer EA, Just H, Farhan H, Scholze P, Kudlacek O, Holy M, Koppatz K, Krivanek P, Freissmuth M, Sitte HH (2005) Amphetamines take two to tango: an oligomer-based counter-transport model of neurotransmitter transport explores the amphetamine action. *Mol Pharmacol* 67: 140-51

Sheng ZH, Rettig J, Takahashi M, Catterall WA (1994) Identification of a syntaxin-binding site on N-type calcium channels. *Neuron* 13: 1303-13

Sitte HH, Huck S, Reither H, Boehm S, Singer EA, Pifl C (1998) Carrier-mediated release, transport rates, and charge transfer induced by amphetamine, tyramine, and dopamine in mammalian cells transfected with the human dopamine transporter. *J Neurochem* 71: 1289-97

Solis E, Jr., Partilla JS, Sakloth F, Ruchala I, Schwienteck KL, De Felice LJ, Eltit JM, Glennon RA, Negus SS, Baumann MH (2017) N-Alkylated Analogs of 4-

Methylamphetamine (4-MA) Differentially Affect Monoamine Transporters and Abuse Liability. *Neuropsychopharmacology* 42: 1950-1961

Solis E, Jr., Zdravkovic I, Tomlinson ID, Noskov SY, Rosenthal SJ, De Felice LJ (2012) 4-(4-(dimethylamino)phenyl)-1-methylpyridinium (APP+) is a fluorescent substrate for the human serotonin transporter. *J Biol Chem* 287: 8852-63

Sonders MS, Zhu SJ, Zahniser NR, Kavanaugh MP, Amara SG (1997) Multiple ionic conductances of the human dopamine transporter: the actions of dopamine and psychostimulants. *J Neurosci* 17: 960-74

Spampinato S, Di Toro R, Alessandri M, Murari G (2002) Agonist-induced internalization and desensitization of the human nociceptin receptor expressed in CHO cells. *Cell Mol Life Sci* 59: 2172-83

Springer D, Fritschi G, Maurer HH (2003) Metabolism of the new designer drug alpha-pyrrolidinopropiophenone (PPP) and the toxicological detection of PPP and 4'-methyl-alpha-pyrrolidinopropiophenone (MPPP) studied in rat urine using gas chromatography-mass spectrometry. *J Chromatogr B Analyt Technol Biomed Life Sci* 796: 253-66

Steinkellner T, Yang JW, Montgomery TR, Chen WQ, Winkler MT, Sucic S, Lubec G, Freissmuth M, Elgersma Y, Sitte HH, Kudlacek O (2012) Ca(2+)/calmodulin-dependent protein kinase IIalpha (alphaCaMKII) controls the activity of the dopamine transporter: implications for Angelman syndrome. *J Biol Chem* 287: 29627-35

Striessnig J, Pinggera A, Kaur G, Bock G, Tuluc P (2014) L-type Ca(2+) channels in heart and brain. *Wiley Interdiscip Rev Membr Transp Signal* 3: 15-38

Sulzer D, Chen TK, Lau YY, Kristensen H, Rayport S, Ewing A (1995) Amphetamine redistributes dopamine from synaptic vesicles to the cytosol and promotes reverse transport. *J Neurosci* 15: 4102-8

Teng L, Crooks PA, Dwoskin LP (1998) Lobeline displaces [3H]dihydrotetrabenazine binding and releases [3H]dopamine from rat striatal synaptic vesicles: comparison with d-amphetamine. *J Neurochem* 71: 258-65

Tsien RW, Lipscombe D, Madison DV, Bley KR, Fox AP (1988) Multiple types of neuronal calcium channels and their selective modulation. *Trends Neurosci* 11: 431-8

UN Document (1975) Studies on the chemical composition of khat. III. Investigations on the phenylalkylamine fraction. *United Nations Laboratory document MNAR/11/75, GE:* 75-1264

Volkow ND, Fowler JS, Wang GJ, Swanson JM (2004) Dopamine in drug abuse and addiction: results from imaging studies and treatment implications. *Mol Psychiatry* 9: 557-69

Volkow ND, Wang GJ, Fowler JS, Gatley SJ, Ding YS, Logan J, Dewey SL, Hitzemann R, Lieberman J (1996) Relationship between psychostimulant-induced "high" and dopamine transporter occupancy. *Proc Natl Acad Sci U S A* 93: 10388-92

Volkow ND, Wang GJ, Ma Y, Fowler JS, Wong C, Ding YS, Hitzemann R, Swanson JM, Kalivas P (2005) Activation of orbital and medial prefrontal cortex by methylphenidate in cocaine-addicted subjects but not in controls: relevance to addiction. *J Neurosci* 25: 3932-9

Volkow ND, Wang GJ, Telang F, Fowler JS, Logan J, Jayne M, Ma Y, Pradhan K, Wong C (2007) Profound decreases in dopamine release in striatum in detoxified alcoholics: possible orbitofrontal involvement. *J Neurosci* 27: 12700-6

Wadel K, Neher E, Sakaba T (2007) The coupling between synaptic vesicles and Ca2+ channels determines fast neurotransmitter release. *Neuron* 53: 563-75

Wise RA (1978) Catecholamine theories of reward: a critical review. *Brain Res* 152: 215-47

Yamashita A, Singh SK, Kawate T, Jin Y, Gouaux E (2005) Crystal structure of a bacterial homologue of Na+/Cl--dependent neurotransmitter transporters. *Nature* 437: 215-23

Yin HH, Ostlund SB, Knowlton BJ, Balleine BW (2005) The role of the dorsomedial striatum in instrumental conditioning. *Eur J Neurosci* 22: 513-23

Zhang H, Fu Y, Altier C, Platzer J, Surmeier DJ, Bezprozvanny I (2006) Ca1.2 and CaV1.3 neuronal L-type calcium channels: differential targeting and signaling to pCREB. *Eur J Neurosci* 23: 2297-310